Cold Atoms and Molecules

Yongkai Zhao

Submitted for the degree of Doctor of Philosophy

Heriot-Watt University

School of Engineering and Physical Sciences

August, 2012

Abstract

The ability to cool and trap atoms has revolutionized atomic and ultra-cold physics. Molecular physics is currently undergoing a similar transformation. This thesis aims to research a general cooling method that will be applicable to wide range of molecular and atomic species and other particles.

We studied the dynamics of molecules in optical fields, focusing in particular on exploring the molecular self-organisation phenomena in optical cavities to cool molecular ensembles to sub-mK temperatures.

Firstly, the general model of cavity cooling from atoms to molecules and the dynamics of a particle in a single cavity mode were discussed. We extended the existing cooling scheme for two-level atoms to an ensemble of multi-level molecules. Then we studied the spatial dynamics of molecules in the new parameter conditions, focusing in particular on exploring the molecular self-organisation phenomena in optical cavities to cool molecular ensembles to sub-mK temperatures. The scheme complements well with our present experimental work on the deceleration and focusing of cold molecules and can extend our present capability to simultaneously cool and trap a large cold molecular ensemble.

For simulation of a large ensemble of molecules, we proposed a new statistical model based on the Boltzmann equation beside the traditional discrete model and studied two solution methods. The comparison of the theory and numerical simulations between discrete model and statistical model showed a good agreement, which validated this new model.

We then explored the scaling laws with a view to the self-organization and cooling of a large ensemble of species. We studied the cooling of a CN molecular cloud of the density $10^{13}/cm^3$, with an initial temperature at 10 mK in an optical cavity. We found that more than a third of the molecules are stably trapped by the intracavity field and the final temperature is below 1mK. We discussed the scaling laws in the case when a large ensemble of species is involved. Finally we argue that cavity cooling using a far

off-resonant laser source can be a general cooling method that is applicable to any particles and studied the probability and conditions.

ACADEMIC REGISTRY
Research Thesis Submission

Name*:*	Yongkai Zhao		
School/PGI:	School of Engineering and Physical Sciences （EPS）		
Version: *(i.e. First, Resubmission, Final)*	First Submission	Degree Sought (Award **and** Subject area)	PhD

Declaration

In accordance with the appropriate regulations I hereby submit my thesis and I declare that:

1) the thesis embodies the results of my own work and has been composed by myself
2) where appropriate, I have made acknowledgement of the work of others and have made reference to work carriedout in collaboration with other persons
3) the thesis is the correct version of the thesis for submission and is the same version as any electronic versions submitted*.
4) my thesis for the award referred to, deposited in the Heriot-Watt University Library, should be madeavailable for loan or photocopying and be available via the Institutional Repository, subject to such conditions as the Librarian may require
5) I understand that as a student of the University I am required to abide by the Regulations of theUniversity and to conform to its discipline.

* *Please note that it is the responsibility of the candidate to ensure that the correct version of the thesis is submitted.*

Signature of candidate*:*	Yongkai Zhao	Date:	11-02-2013

Submission

Submitted By *(name in capitals):*	
Signature of Individual Submitting:	
Date Submitted:	

For Completion in Academic Registry

Received in the Academic Registry by *(name in capitals):*			
Method of Submission *(Handed in to Academic Registry; posted through internal/external mail):*			
*E-thesis Submitted (**mandatory for final theses from January 2009)***			
Signature:		Date:	

Acknowledgments

I would like to thank my supervisor, Dr Weiping Lu, for his insight, guidance, and continual support throughout the duration of this work. I have benefited greatly from his friendship, management and constant encouragement, and would appreciate his patience with my lasting writing up periods.

I gratefully acknowledges the former member of this research group, Dr. Guangjiong Dong, for his great encouragement, support and ideas during my study period even then he has graduated and moved to Hongkong.

My thanks also go to the UK SUPA for the provision of Scholarship. I would like to thank the staff in the physics department and school for their help and support during my PhD study period.

I would also like to acknowledge members of in Room 2.40, in particular Dr. Jianzhong Zhang, who gives me guidance when I feel not good. Neil McCulloch, Adam for their great help in smoothing English for my papers.

Thank all my friends includes Dr. Lei Yang, Tao Huang, Zhen Qiu and other guys in Edinburgh for sharing living experiences and help in daily life.

Finally, I have to express my gratitude to my families and would like to dedicate this thesis to them: my parents who give me constant support and encouragement; my wife Hongxia, who provided all her love, trust and support for my works over the years; and my son Yunxiang, who made me grow and comprehend the father's responsibility!

Contents

List of Publications

Journals

- Yongkai Zhao, Weiping Lu, Peter F. Barker, Guangjiong Dong, *Self-organisation and cooling of a large ensemble of particles in optical cavities*, Faraday Discussions, 142, 311-318 (2009).
- W. Lu and Y. Zhao, P. F. Barker, *Cooling molecules in optical cavities*, Physical Review A, 76, 013417-1-6 (2007).
- Zhihao Lan, Yongkai Zhao, Peter F. Barker, Weiping Lu, *Deceleration of molecules in a supersonic beam by the optical field in a low-finesse cavity*, Physical Review A, 81, 013419-1-5 (2010).

Conference Presentations

- Yongkai Zhao, Weiping Lu, Peter F. Barker, Guangjiong Dong, *Optical cavity cooling of a large ensemble of molecules*, 2009 Conference on Lasers and Electro-Optics (CLEO), 1-5, 2125-2126 (2009).
- Yongkai Zhao, Weiping Lu, Peter F. Barker, and Guangjiong Dong, *A statistical model for cooling atoms and molecules in optical cavities*, QEP-18 (2008).
- Yongkai Zhao, Weiping Lu, and Peter F. Barker, *Cooling of molecules in optical cavities*, CLEO/Europe-IQEC (2007).
- Zhihao Lan, Yongkai Zhao, Peter F. Barker, Weiping Lu, *Deceleration of a supersonic molecular beam in an optical cavity*, 2009 Conference on Lasers & Electro Optics & The Pacific Rim Conference on Lasers and Electro-Optics (CLEO/PACIFIC RIM), Shanghai, China (2009).

Chapter 1

General Introduction

1.1 Introduction

Recent advances in cooling and trapping atoms has revolutionized atomic and ultra-cold physics. The techniques to produce cold and trapped atoms have led to many scientific achievements, such as Bose-Einstein condensation [1.1], Fermi degeneracy [1.2], superfluidity in atomic vapors [1.3] and nonlinear atom optics [1.4]. Molecular physics is currently undergoing a similar development as effective methods for manipulating the motion of molecules are being put in place. In principle, all these experiments with atoms could be performed with molecules. Moreover, molecules offer a vast range of properties not available in atoms. Therefore, pursuing such investigations with cold trapped molecules would have more dramatic advances.

The capability of producing cold and ultra cold molecules may open up exciting applications in ultra-high resolution spectroscopy, tests of fundamental theories, ultracold photochemistry, dipolar gas, quantum control etc. In section 1.2, we present an introduction to these applications.

Several optical cooling methods have now been established for the creation of cold atoms over the last decades. Manipulation using tailored optical fields has proven to be an effective scheme, which has demonstrated unprecedented control over the external degrees of freedom of atoms and molecules. Besides the direct laser cooling schemes, considerable advances have been studied to produce cold molecular species in the mK regime. By the photoassociation method, various species of ultracold alkali molecules have been directly formed by ultracold atoms. Buffer-gas cooling, the collisional cooling method of atoms and molecules trapped in a magnetic potential, has been successfully implemented to produce cold paramagnetic molecules [1.104, 1.105].

The Stark deceleration scheme has been demonstrated to slow a beam of metastable CO or NH_3 molecules by using time-varying electrostatic fields [1.81, 1.106]. While these methods are quite general, additional techniques are required to produce large phase space densities below the mK regime. The cavity cooling scheme is one of the potential methods. In section 1.3, details of these techniques are introduced.

1.2 Applications of Cold Molecules

A molecule is broadly defined as a tightly or loosely bound collection of a small number of atoms, which is held together by the electromagnetic field of the constituent atoms, or even by applied external electromagnetic fields. Comparing with atoms, molecules are more interesting for several key differences:

First, molecules possess multiple rotational and vibrational degrees of freedom which are more complicated than atoms.

Second, unlike atoms, molecules are generally nonspherical. They carry a non-zero electric dipole moment, magnetic dipole moment and anisotropic short and long range electrostatic interaction. Therefore, the orientation of the molecular axis can be controlled with an electric or optical field.

In general, cold molecules are more interesting for many fundamental researches in physics compared to cold atoms. For example, simple diatomic molecules possess many more properties than atoms. The term "ultracold" generally refers to the temperature of molecules at sub-milliKelvin regime. Experiments with cold trapped molecules are being carried out by many research groups over the world in various areas of physics.

1.2.1 High resolution spectroscopy and quantum control

The cooled and trapped molecules provide an ideal platform for high resolution molecular spectroscopy. The spectroscopic measurements on molecules usually involve a single ro-vibrational state, and its precision is limited by photon-counting statistics. Cold molecules have slow moving velocities both in the moving frame and the laboratory frame, which allows long interaction times for the necessary measurements. On the other side, cold molecules have a narrow Doppler linewidth and a large population on the low rotational level which leads measurements with high photon counting rates [1.61]. These advantages can significantly increase the measurement's

statistical sensitivity level. A huge amount of accurate atomic and molecular data has been reported in the last two decades [1.8-1.12]. N. Vanhaecke et al. accurately studied the van der Waals coefficient in Cs2, and constructed the asymptotic ground state potential curves from two-color photoassociation (PA) spectroscopy [1.5]; C. Amiot presented the atomic radiative lifetime from molecular spectroscopy data [1.6].

The novel Feshbach spectroscopy is highly accurate in measuring near-threshold bound states in all systems that exhibit Feshbach resonances, which can populate any of the near-threshold bound molecular states with elaborate time-dependent magnetic fields, including those having high rotational energies [1.13-1.15]. N. R. Claussen et al. precisely measured the accurate spectroscopy of a Feshbach resonance in an ^{85}Rb Bose-Einstein condensate by the induced coherent atom-molecule oscillations [1.7]. Many meticulous experiments about Feshbach resonances have been done and more broad reviews of this technique and its applications are proposed in ref. [1.16-1.18].

High resolution quantum control in molecular systems with efficient population transfer among different quantum states or molecular wave packets is a new application of cold and ultracold molecules [1.19-1.22]. It will provide opportunities to study precisely controlled quantum chemistry. For ultracold molecules the external motional degree of freedom is effectively frozen out. By using highly stable optical fields in the form of phase-coherent pulse trains, coherent evolutions among different internal energy states can be precisely controlled. Molecular quantum wave packets, superpositions of quantum states in molecules, can be manipulated with phase-coherent femtosecond pulse trains. These ideas represent a new direction in quantum control of molecules with strong spectrally broad laser pulses.

1.2.2 Tests of fundamental physics

The transitions of cold molecules are only limited by the natural lifetimes of relevant molecular energy levels [1.12, 1.23]. It leads to very high precision studies of molecular structure and dynamics.The high-resolution capability is very useful for some stringent tests of fundamental physical laws and symmetries. Molecules can play a powerful role in the tests of the cosmological variation of the hyperfine structure constant α and the ratio of electron-to-proton mass m_e/m_p, while atoms generally lack transitions that can reveal it [1.24-1.29]. One example is the measurement of the Λ-doublet transitions of OH ground-state molecules in the microwave range [1.24, 1.30].

Another research area of cold molecules is the measurement of the electric dipole moment (EDM) of the electron. A non-zero EDM would imply a T-violation, i.e. an asymmetry with respect to time reversal [1.31-1.33]. When an external electric field is applied to an atom or molecule, a much larger internal effective electric field is felt by the unpaired electron which can be expressed by the product Q×P, where P is degree of the atomic or molecular polarizability induced by an external field and Q is a factor proportional to Z^3, with Z the nuclear charge [1.11]. The EDM measurement requires subjecting an electron to the highest electric field possible. The factor P of a typical atom is about 10^{-3} even when a very high external field is applied, while a typical diatomic molecule can be nearly completely polarized (P≈1) with a relatively modest external field. The internal fields in molecules can be orders of magnitude stronger than those in atoms. At the same time, the presence of internal molecular structure can allow a substantial reduction of many systematic errors. Therefore a heavy polar molecule is a good candidate forsensitive measurement. Enhanced population in low-lying levels and the narrow Doppler linewidth of cold molecules also improve detection sensitivity. Experiments aiming at determining the electron EDM are underway on P_bO [1.34-1.37] and Y_bF [1.38-1.40].

1.2.3 Ultracold chemistry and quantum degenerate chemistry

Research on chemistry at cold and ultralow temperatures has entered into a new era. When molecules are cooled to low temperatures, a number of phenomena, such as inelastic and reactive collisions, rotational and vibrational state changes, spin depolarization, become extremely state-selective. The molecules can be enhanced populated on specific ro-vibrational states [1.41-1.46]. This could be used for the efficient production of atoms or molecules with inverted populations of internal energy levels and potentially the development of new atomic or molecular lasers. When molecules are cooled to ultracold temperature, their dynamics are entirely determined by quantum effects. It allows the measurements of chemical reaction or collision rates at zero temperature, which can provide unique information about the role of tunneling, zero-point energy and quantum reflection effects.

Many research groups currently are trying to produce molecular BEC and degenerate Fermi gases since the achievement of a BEC of Feshbach molecules out of a degenerate atomic Fermi gas [1.47-1.50]. The region very close to a Feshbach

resonance has been investigated both in theory and in experiments. In the limit of weak interactions, many-body physics allows for the formation of fermionic pairs identifiable with Cooper pairs according to the Bardeen-Cooper-Schrieffer (BCS) theory which explains the occurrence of superconductivity and superfluidity [1.51]. BEC of Cooper pairs was observed by changing the magnetic field condition in the BCS [1.52-1.53] and the pairing energy gap has been detected [1.54-1.56]. Another phenomena of super chemistry has been proposed which is a stimulated Raman emission of molecules in a chemical reaction based on the dynamics of coupled atomic and molecular BEC [1.57].

1.2.4 Dipolar gases

Dipolar gases are a novel method to exhibit reaction and collision phenomena of ultracold particles with permanent electric dipole moments or electric dipole moment induced by an external electric field. The dominant atom-atom interaction is via the van der Waals potential varying as R^{-6}, with R their mutual distance. The polar molecules and other particles with dipole moment interact through long-range dipole-dipole interaction varying as R^{-3}, in addition to the van der Waals interaction. Such cold gases of ultracold atomic and molecular gases will lead to an entirely new regime of strong anisotropy interactions. The interaction between particles could be controlled either by external fields, or by using various geometries of the trapping configuration. Many research programmes have been proposed [1.58-1.60]. In particular, dipolar gases can be chosen to represent systems for many-body physics, and are suitable for modeling condensed matter phases.

1.3 Techniques for Creating Cold Molecules

Experiments forcreating cold atoms generally involve the following three steps [1.1, 1.61-1.63]. First, an ensemble of atoms ispre-cooled to a temperature in the Kelvin to milli-Kelvin range. The most common technique for this step is laser cooling. Once the temperature is low enough for trapping to be possible, atoms are placed into a trap. Finally, evaporative cooling or other schemes is used to bring atoms into the ultracold regime.

Near all currently-proposed methods for creations of ultracold molecules rely on the same three steps except photoassociation and Feshbach resonance. However, the technique of laser cooling usually is not suitable for molecules. Doppler cooling is a key

scheme in laser cooling that makes use of a velocity-dependent dissipative light force through the Doppler Effect to cool atoms [1.64]. The number of atomic species that can be cooled in this way is limited by the availability of a cycling transition in which many absorption and spontaneous emission cycles are required to reduce the momentum distribution of atoms in a thermal ensemble. This requirement also makes Doppler cooling of molecules generally not feasible because the absence of strict selection rules particularly between vibrational states precludes the existence of a single cycling transition [1.65].

Although proposals for laser cooling of certain molecules exist, and research on non-traditional laser cooling methods of molecules is being studied, a general laser cooling scheme of molecules is unlikely to become available in the near future [1.61, 1.66-1.67]. Therefore, an alternative cooling technique is necessary. A range of common techniques is introduced in the following sections.

1.3.1 Photo-association and Feshbach resonances

Photoassociation (PA) is a way that takes advantage of the success of laser cooling in atoms [1.8-1.10, 1.68]. It uses cold atoms as building blocks, and generally binds two atoms together to construct moleculeswith cold translational temperatures directly. However, the method is limited to the species range of alkali diatoms [1.69-1.75]. The molecule formed usually has a rather large internuclear distance between the bounded atoms, and locates on vibrational excited states just below the dissociation limit. With a variety of laser cooling schemes, the molecules can be transferred into their rotational-vibrational and electronic ground state.

The Feshbach resonance method is another way for creating ultracold molecules directly from ultracold atoms [1.53, 1.58, 1.76, 1.77]. A Feshbach resonance is a resonance of a many-body system in which a bound state is achieved if the coupling between an internal degree of freedom and the reaction coordinates which leads to dissociation vanishes. When a bound state is not formed, it is a shape resonance as the opposite situation [1.107]. This method becomes important in the study of Fermi gases. The molecules produced, limited to alkali dimers, have surprisingly long lifetimes, which allows formation of molecular BEC [1.78] and, molecular superfluid [1.79].

1.3.2 Stark and Zeeman deceleration

Stark deceleration is a general method which uses time varying inhomogeneous electric fields to slow down polar molecules from a room-temperature supersonic molecular beam [1.80-1.82].

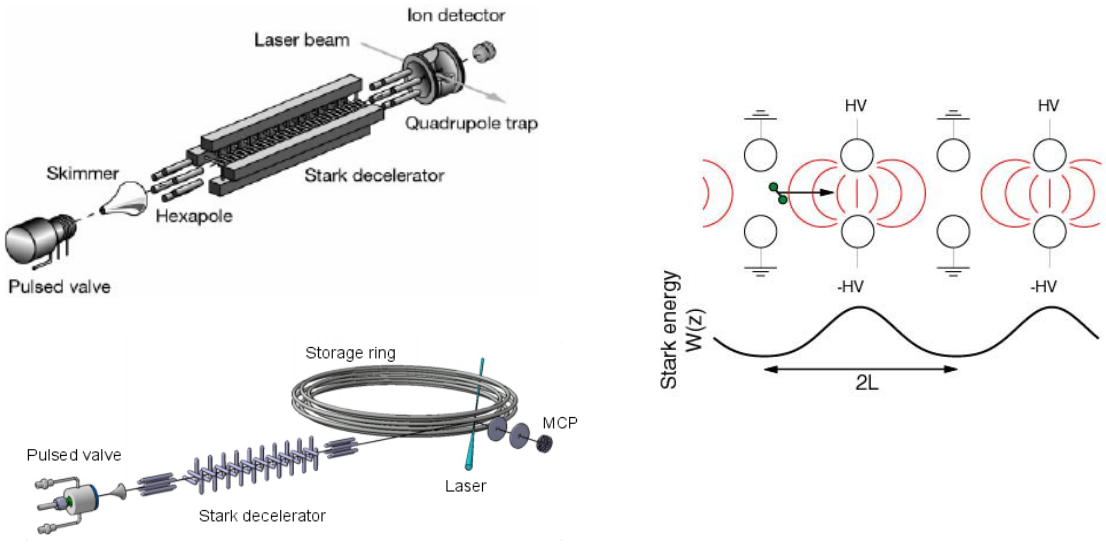

Figure1.1 Experiment setup and principle of Stark decelerator

A schematic view of their experimental setup is presented in Fig. 1.1 [1.83-1.84]. The Stark decelerator consists of an array of electric field stages. Each stage consists of two parallel cylindrical metal rods. One of the rods is connected to a positive potential and the other to a negative potential switched quickly. When a molecule in a quantum state with a positive Stark effect is moving through an electric field and approaching the region of maximum field strength, its Stark energy is increasing while its translational energy is being correspondingly reduced. To prevent the molecule from regaining the translational energy when it leaves the maximum region, the field is quickly switched off. The molecule thus ends up in a homogeneous, Filed-free region where its potential energy and kinetic energy both remain constant. In the stark decelerator setup, this process will repeat when the electric field of the next stage is switched on and the molecule keeps losing its kinetic energy. The exit of the experimental setup is normally equipped with an electrostatic storage ring or electrostatic quadrupole trap to trap the

slowed molecules. The technique is a simple and general way to produce small samples of milli-Kelvin-range cold polar molecules.

The Zeeman decelerator works under the similar principle but it uses the magnetic moment instead of electric moment of the molecules [1.84-1.85].

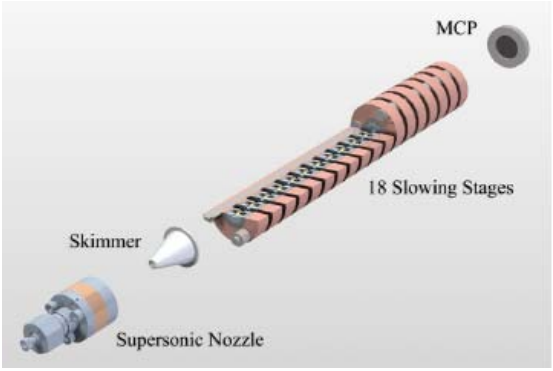

Figure 1.2 Zeeman decelerator experiment setup

1.3.3 Buffer gases cooling and other approaches

Buffer gas cooling is another general technique that has been developed for use in cooling paramagnetic atoms and molecules at ultracold temperatures [1.86-1.88].

This scheme allows the molecules of interest to be cooled through elastic collisions with a cold buffer gas inside a chamber. The buffer gas most commonly used in this sort of application is helium. If there are enough collisions between the buffer gas and the molecules of interest before the molecules hit the walls of the chamber and are gone, the buffer gas will sufficiently cool the ensemble [1.35, 1.61, 1.89-1.91]. There are several methods for introducing molecules into the buffer gas:

1. Laser ablation. As shown schematically in Fig. 1.3(a), an intense laser pulse illuminates a solid precursor target and heats up the surface to very high temperatures. As the result, the ablation products are ejected from the surface into the buffer gas. The unpredictability of its yield is the most important drawback of this method.

2. Capillary filing. A thin capillary connects the low-temperature buffer gas cell with a room-temperature gas supply, as shown in Fig. 1.3(b). The molecules are driven into the cell by the supply pressure. Only molecules with high vapour pressure can survive the trip along a thin cold channel without condensation or recombining.

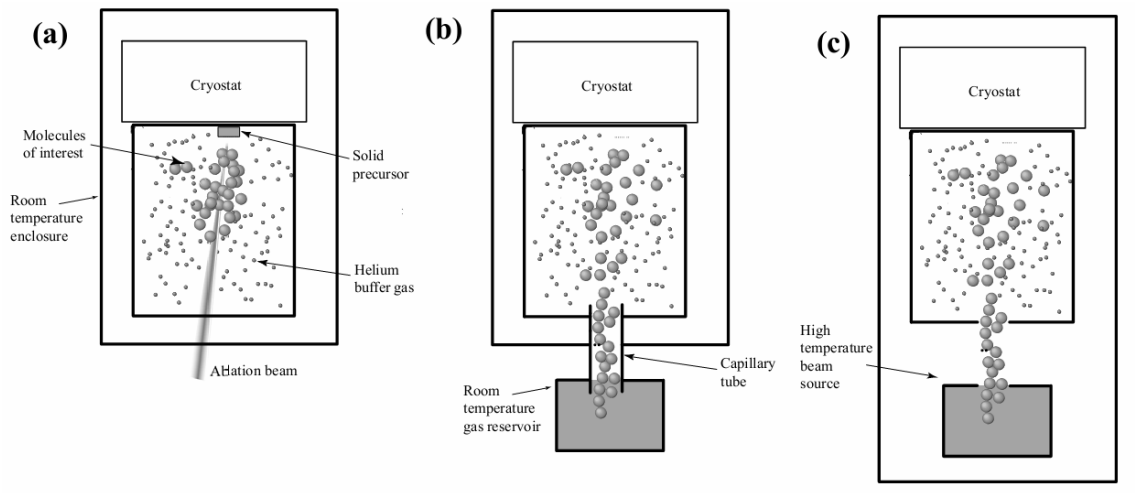

Figure 1.3Methods of loading molecules into cryogenic buffer gas cell

3. Beam loading. A molecular beam from a room-temperature source is injected into a cryogenic buffer gas cell. This is novel loading technique which can overcome the limitations of the previous two methods.

Buffer gas cooling can be applied to virtually any molecule, as long as the molecule is capable of surviving multiple collisions with low energy helium atoms, which most molecules are capable of doing. The final temperature is about a few hundred millikelvin, determined by the equilibrium vapour pressure of the buffer gas. It also can produce large number of cold molecule ensemble (5×10^{13} at 2K).

Some other methods to produce cold molecules have been proposed in recent years, such as Counter-rotating nozzle [1.92-1.93], phase space filtering [1.94], laser scoop [1.103], billiard-like collisions [1.95] and Stochastic cooling [1.96-1.97]. Stochastic cooling uses a measurement of the momentum followed by a corrective force to move small regions of the phase space towards zero momentum. Most of these methods are being currently studied to produce substantial numbers of cold molecules.

1.4 Cavity cooling

Cooling atoms within an optical cavity is a relatively new method, which was first proposed in 1997 by Horak et al. and has recently been demonstrated experimentally [1.98-1.102]. This scheme uses a cavity detuned from resonance to preferentially scatter blue shifted photons out of the cavity to extract energy from the atoms [1.98-1.99].

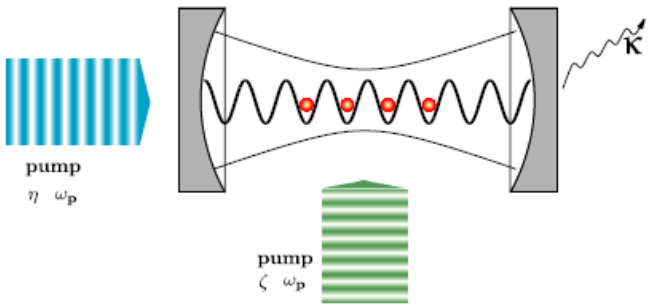

Figure 1.4 Set up of the cavity cooling

Cavity cooling does not require the particles to have a closed-cycling transition necessary for laser cooling. Therefore the method doesn't depend on the specific internal structure of the scattering species and can be applied for cooling any kind of polarizable particles including molecules. Since spontaneous emission plays little role in the cooling process, the lowest temperature that can be achieved in a cavity is determined by the cavity linewidth κ, i.e., $k_B T_C \approx \hbar\kappa$, which can be well below the Doppler cooling limit $k_B T_D \approx \hbar\gamma$.

The original configuration of the setup is a longitudinal pump where a laser is pumped through the mirror. In a good cavity, due to the finite response time of the cavity, there is a delay of the effect of the intracavity intensity on the particle dynamics and the delay will results in a force that cools the particle. Cavity cooling has been further studied beyond the single atom case [1.99-1.100] in which collective effects of many atoms are considered [1.101]. In 2002, Domokos proposed another configuration called transverse pump where the laser shines from the side instead of from the mirror. In this configuration on interesting phenomenon was found where a buildup of the intracavity intensity is accompanied by the self-organization of the particles in the cavity. This has led to the experimental demonstration of cooling 10^6 cesium atoms to a few μK [1.102].

The earlier research focused on the interesting dynamics such as self-organization from this special configuration and the considered number of particles is usually small (only hundreds of particles). Later on people (include us) begin to investigate the scaling characteristics of the system in order to cool a larger number of particles (10^{12}) which is more likely to be the real situation in experiment. Recently our

group has begun to use a continuous model which is based on the collisionless Boltzmann equation to numerically check the scaling results based on the discrete model. This works is an important step which puts forward the cavity cooling of larger number of particles toward the experimental realization.

1.5 References

[1.1] M.H. Anderson, J. R. Ensher, M. R. Matthews, C. E. Wieman, and E. A. Cornell, *Observation of Bose-Einstein condensation in a dilute atomic vapor*, Science, **269**, 198-201 (1995).

[1.2] B. de Marco, D. S. Jin, *Onset of Fermi degeneracy in a trapped atomic gas*, Science, **285**, 1703-1706 (1999).

[1.3] R. Onofrio, C. Raman, J. M. Vogels, J. Abo-Shaeer, A. P. Chikkatur, and W. Ketterle, *Observation of superfluid flow in a Bose-Einstein condensed gas*, Physical Review Letters, 85, 2228-2231 (2000).

[1.4] S. Inouye, T. Pfau, S. Gupta, A. P. Chikkatur, A. Gorlitz, D. E. Pritvhard, and W. Ketterle, *Phase-coherent amplification of atomic matter waves*, Nature (London), 402, 641-644 (1999).

[1.5] N. Vanhaecke, Ch. Lisdat, B. T'Jampens, D. Comparat, A. Crubellier, and P. Pilleta, *Accurate asymptotic ground state potential curves of Cs_2 from two-colour photoassociation*, The European Physical Journal D, **28**, 351-360 (2004).

[1.6] C. Amiot, O. Dulieu, R. F. Gutterres, and F. Masnou-Seeuws, *Determination of $Cs_2\, 0_g^-\, (P_{3/2})$ potential curve and of C_s 6 $P_{1/2,3/2}$ atomic ragiative lifetimes from photoassociation spectroscopy*, Physical Review A, **66**, 052506 (2002).

[1.7] N. R. Claussen, S. J. J. M. F. Kokkelmans, S. T. Thompson, E. A. Donley, E. Hodby, and C. E. Wieman, *Very-high-precision bound-state spectroscopy near a ^{85}Rb Feshbach resonance*, Physical Review A, **67**, 060701 (2003).

[1.8] J. Weiner, V. S. Bagnato, S. Zilio, and P. S. Julienne, *Experiments and theory in cold and ultracold collisions*, Reviews of Modem Physics, **71**, 1-81 (1999).

[1.9] W. C. Stwalley and H. Wang, *Photoassociation of Ultracold Atoms: A New Spectroscopic Technique*, Journal of Molecular Spectroscopy, **195**, 194-228 (1999).

[1.10] K. M. Jones, E. Tiesinga, P. D. Lett, and P. S. Julienne, *Ultracold photoassociation spectroscopy: Long-range molecules and atomic scattering*, Reviews of Modern Physics, **78**, 483-535 (2006).

[1.11] O. Dulieu and C. Gabbanini, *The formation and interactions of cold and ultracold molecules: new challenges for interdisciplinary physics*, Reports on Progress in Physics, **72**, 086401-1-35 (2009).

[1.12] L. D. Carr, D. DeMille, R. V. Krems, and J. Ye, *Cold and Ultracold Molecules: Science, Technology, and Applications*, New Journal of Physics, 11, 055409-1-87 (2009).

[1.13] Ph. Courteille, R. S. Freeland, D. J. Heinzen, F. A. van Ableelen, and B. J. Verhaar, *Observation of a Feshbach Resonance in Cold Atom Scattering*, Physical Review Letters, 81, 69-72 (1998).

[1.14] M. Mark, F. Ferlaino, S. Knoop, J. G. Danzl, T. Kraemer, C. Chin, H. C. Nagerl, and R. Grimm, *Spectroscopy of ultracold trapped cesium Feshbach molecules*, Physical Review A, 76, 042514-1-14 (2007).

[1.15] F. Schwarz, T.-O. Muller, and H. Friedrich, *Near-threshold Feshbach resonances in interatomic collisions and spectra*, Physical Review A, 85, 052703-1-9 (2012).

[1.16] T. Schuster, R. Scelle, A. Trautmann, S. Knoop, M. K. Oberthaler, M. M. Haverhals, M. R. Goosen, S. J. J. M. F. Kokkelmans, and E. Tiemann, *Feshbach spectroscopy and scattering properties of ultracold Li+Na mixtures*, Physical Review A, 85, 042721-1-8 (2012).

[1.17] O. Dulieu, M. Raoult, and E. Tiemann, *Cold Molecules: a chemistry kitchen for physicists*, Journalof Physics B: Atomic, Molecular and Optical Physics, 39 (2006).

[1.18] C. Trefzger and Y. Castin, *Impurity in a Fermi sea on a narrow Feshbach resonance: A variational study of the polaronic and dimeronic branches*, Physical Review A, 85, 053612-1-22 (2012).

[1.19] C. J. Bardeen, V. V. Yakovlev, K. R. Wilson,S. D. Carpenter, P. M. Weber, W. S. Warren, *Feedback quantum control of molecular electronic population transfer*, Chemical Physics Letters, 280, 151–158 (1997).

[1.20] B. Kohler, V. V. Yakovlev, J. Che, J. L. Krause, M. Messina, K. R. Wilson, N. Schwentner, R. M. Whitnell, and Y. Yan, *Quantum Control of Wave Packet Evolution with Tailored Femtosecond Pulses*, Physical Review Letters, 74, 3360-3363 (1995).

[1.21] A. Pe'er, E. A. Shapiro, M. C. Stowe, M. Shapiro, and J. Ye,*Precise control of molecular dynamics with a femtosecond frequency comb*, Physical Review Letters, 98, 113004-1-4 (2007).

[1.22] E. A. Shapiro, A. Pe'er, J. Ye, and M. Shapiro, *Piecewise Adiabatic Population Transfer in a Molecule via aWave Packet*, Physical Review Letters, 101, 023601-1-4 (2008).

[1.23] S. Y. T. van de Meerakker, N. Vanhaecke, M. P. J. van der Loo, G. C. Groenenboom, and G. Meijer, *Direct Measurement of the Radiative Lifetime of Vibrationally Excited OH Radicals*, Physical Review Letters, 95, 013003-1-4 (2005).

[1.24] E. R. Hudson, H. J. Lewandowski, B. C. Sawyer, and J. Ye, *Cold Molecule Spectroscopy for Constraining the Evolution of the Fine Structure Constant*, Physical Review Letters, 96, 143004-1-4 (2006).

[1.25] D. DeMille, S. B. Cahn, D. Murphree, D. A. Rahmlow, and M. G. Kozlov, *Using molecules to measure nuclear spin–dependent parity violation*, Physical Review Letters, 100,023003-1-4 (2008).

[1.26] M. J. Thorpe and J. Ye, *Cavity-enhanced direct frequency comb spectroscopy*, Applied Physics B, 91, 397-414 (2008).

[1.27] M. J. Thorpe, F. Adler, K. C. Cossel, M. H.G. de Miranda, J. Ye, *Tomography of a supersonically cooled molecular jet using cavity-enhanced direct frequency comb spectroscopy*, Chemical Physics Letters, 468, 1-8 (2009).

[1.28] J. Aldegunde, B. A. Rivington, P. S. Zuchowski, and J. M. Hutson, *Hyperfine energy levels of alkali-metal dimers: ground-state polar molecules in electric and magnetic fields*, Physical Review A, 78, 033434-1-8 (2008).

[1.29] S. Schiller, *Hydrogenlike Highly Charged Ions for Tests of theTime Independence of Fundamental Constants*, Physical Review Letters, 98, 180801-1-4 (2007).

[1.30] B. Lev, E. Meyer, E. R. Hudson, B. C. Sawyer, J. L. Bohn, and J. Ye, *OH hyperfine ground state-from precision measurement to molecular qubits*, Physical Review A, 74, 061402-1-4 (2006).

[1.31] I. B. Khriplovich and S. K. Lamoreaux. *CP Violation without Strangeness, Electric Dipole Moments of Particles, Atoms, and Molecules*, Springer, New York (1997).

[1.32] L. R. Hunter, D. Krause, D. J. Berkeland, and M. G. Boshier, *Precise measurement of the Stark shift of the lithium D1 line*, Physical Review A, 44, 61401-6143 (1991).

[1.33] D. DeMille, F. Bay, S. Bickman, D. Kawall, D. Krause, S. E. Maxwell, and L. R. Hunter, *Investigation of PbO as a system for measuring the electric dipole moment of the electron*, Physical Review A, 61, 052507-1-8 (2000).

[1.34] D. Kawall, F. Bay, S. Bickman, Y. Jiang, and D. DeMille, *Precision Zeeman-Stark Spectroscopy of the Metastable a(1)[$^3\Sigma^+$] State of PbO*, Physical Review Letters, 92,133007-1-4 (2004).

[1.35] D. Egorov, J. D. Weinstein, D. Patterson, B. Friedrich, and J. M. Doyle, *Spectroscopy of laser-ablated buffer-gas-cooled PbO at 4 K and the prospects*

for measuring the electric dipole moment of the electron, Physical Review A, 63, 030501-1-4 (2001).

[1.36] D. Kawall, Y. V. Gurevich, C. Cheung, S. Bickman, Y. Jiang, and D. DeMille, *Stark-modulation spectroscopy of the B(1)[^{3}II] state of PbO*, Physical Review A, 72, 064501-1-4 (2005).

[1.37] S. Bickman, P. Hamilton, Y. Jiang, and D. DeMille, *Preparation and detection of states with simultaneous spin alignment and molecular orientation in PbO*, Physical Review A, 80, 023418-1-16 (2009).

[1.38] J. J. Hudson, B. E. Sauer, M. R. Tarbutt, and E. A. Hinds, *Measurement of the Electron Electric Dipole Moment Using YbF Molecules*, Physical Review Letters, 89, 023003-1-4 (2002).

[1.39] M. R. Tarbutt, H. L. Bethlem, J. J. Hudson, V. L. Ryabov, V. A. Ryzhov, B. E. Sauer, G. Meijer, and E. A. Hinds, *Slowing Heavy, Ground-State Molecules using an Alternating Gradient Decelerator*, Physical Review Letters, 92, 173002-1-4 (2004).

[1.40] M. R. Tarbutt, J. J. Hudson, B. E. Sauer, and E. A. Hinds, *Prospects for measuring the electric dipole moment of the electron using electrically trapped polar molecules*, Faraday Discussions, 142, 37-56 (2009).

[1.41] R. V. Krems, *Molecules near absolute zero and external field control of atomic and molecular dynamics*, International Reviews in Physical Chemistry, 24, 99-118 (2005).

[1.42] N. Balakrishnan and A. Dalgarno, *Chemistry at ultracold temperatures*, Chemical Physics Letters, 341, 652-656 (2001).

[1.43] E. Bodo, F. A. Gianturco, N. Balakrishnan, and A. Dalgarno, *Chemical reactions in the limit of zero kinetic energy: virtual states and Ramsauer minima in $F+H_2 \rightarrow HF+H$*, Journal of Physics B: Atomic, Molecular and Optical Physics, 37, 3641-3648 (2004).

[1.44] P. F. Weck and N. Balakrishnan, *Chemical reactivity of ultracold polar molecules: investigation of H + HCl and H + DCl collisions*, The European Physical Journal D, 31, 417-421 (2004).

[1.45] P. F. Weck and N. Balakrishnan, *Quantum dynamics of the $Li+HF \rightarrow H+LiF$ reaction at ultralow temperatures*, The Journal of Chemical Physics, 122, 154309-1-7 (2005).

[1.46] R. V. Krems and A. Dalgarno, *Electronic and rotational energy transfer in F + H_2 collisions at ultracold temperatures*. The Journal of Chemical Physics, 117, 118-123 (2002).

[1.47] S. J. J. M. F. Kokkelmans, G. V. Shlyapnikov, and C. Salomon, *Degenerate atom-molecule mixture in a cold Fermi gas*, Physical Review A, 69, 031602-1-4 (2004).

[1.48] S. Durr, T. Volz, A. Marte, and G. Rempe, *Observation of Molecules Produced from a Bose-Einstein Condensate*, Physical Review Letters, 92, 020406-1-4 (2004).

[1.49] K. M. O'Hara, S. L. Hemmer, M. E. Gehm, S. R. Granade, J. E. Thomas, *Observation of a Strongly Interacting Degenerate Fermi Gas of Atoms*, Science, 298, 2179-2182 (2002).

[1.50] J. E. Williams, T. Nikuni, N. Nygaard, and C. W. Clark, *Atom-molecule equilibration in a degenerate Fermi gas with resonant interactions*, Journal of Physics B: Atomic, Molecular and Optical Physics, 37, L351-L357 (2004).

[1.51] J. Bardeen, L. N. Cooper, and J. R. Schrieffer, *Theory of Superconductivity*, Physical Review, 108, 1175-1204 (1957).

[1.52] M.W. Zwierlein, C. A. Stan, C. H. Schunck, S.M. F. Raupach, A. J. Kerman, and W. Ketterle, *Condensation of Pairs of Fermionic Atoms near a Feshbach Resonance*, Physical Review Letters, 92, 120403-1-4 (2004).

[1.53] C. A. Regal, M. Greiner, and D. S. Jin, *Lifetime of Molecule-Atom Mixtures near a Feshbach Resonance in ^{40}K*, Physical Review Letters, 92, 083201-1-4 (2004).

[1.54] C. Chin and R. Grimm, *Thermal equilibrium and efficient evaporation of an ultracold atom-molecule mixture*, Physical Review A, 69, 033612-1-6 (2004).

[1.55] M. Greiner, C. A. Regal, and D. S. Jin, *Probing the Excitation Spectrum of a Fermi Gas in the BCS-BEC Crossover Regime*, Physical Review Letters, 94, 070403-1-4 (2005).

[1.56] G. B. Partridge, K. E. Strecker, R. I. Kamar, M. W. Jack, and R. G. Hulet, *Molecular Probe of Pairing in the BEC-BCS Crossover*, Physical Review Letters, 95, 020404-1-4 (2005).

[1.57] D. J. Heinzen, R. Wynar, P. D. Drummond and K. V. Kheruntsyan, *Superchemistry: Dynamics of Coupled Atomic and Molecular Bose-Einstein Condensates*, Physical Review Letters, 84, 5029-5033 (2000).

[1.58] M. A. Baranov, *Theoretical progress in many-body physics with ultracold dipolar gases*, Physics Reports, 464, 71-111 (2008).

[1.59] M. Lewenstein, A. Sanpera, V. Ahufinger, B. Damski, A. Sen (de), and U. Sen, *Ultracold atomic gases in optical lattices: mimicking condensed matter physics and beyond*, Advances in Physics, 56, 243-379 (2007).

[1.60] G. Pupillo, A. Micheli, H. P. Buchler, and P. Zoller, *Condensed Matter Physics with Cold Polar Molecules*, arXiv:0805.1896v1[cond-mat.other] (2008).

[1.61] D. M. Egorov, *Buffer-Gas Cooling of Diatomic Molecules*, Thesis (2004).

[1.62] C. C. Bradley, C. A. Sackett, J. J. Tollett, and R. G. Hulet, *Evidence of Bose-Einstein Condensation in an Atomic Gas with Attractive Interactions*, Physical Review Letters, 75, 1687-1691 (1995).

[1.63] K. B. Davis, M. O. Mewes, M. R. Andrews, N. J. van Druten, D. S. Durfee, D. M. Kurn, and W. Ketterle, *Bose-Einstein Condensation in a Gas of Sodium Atoms*, Physical Review Letters, 75, 3969-3974 (1995).

[1.64] S. Chu, L. Hollberg, J. E. Bjorkholm, A. Cable, and A. Ashkin, *Three-Dimensional Viscous Confinement and Cooling of Atoms by Resonance Radiation Pressure*, Physical Review Letters, 55, 48-53 (1985).

[1.65] G. Herzberg. *Molecular Spectra and Molecular Structure*, 2nd edition, reprint w/corrections, Krieger, Malabar (1989)。

[1.66] V. Vuletic and S. Chu, *Laser cooling of atoms, ions, or molecules by coherent scattering*, Physical Review Letters, 84, 3787-3790 (2000).

[1.67] M. D. Di Rosa, *Laser-cooling molecules: Concept, candidates, and supporting hyperfine-resolved measurements of rotational lines in the A–X(0,0) band of CaH*, The European Physical Journal D, 31, 395-402 (2004).

[1.68] J. T. Bahns, P. L. Gould, W. C. Stwalley, *Formation of cold (T<1K) molecules*, Advances in Atomic, Molecular, and Optical Physics, 42, 171-224 (2000).

[1.69] D. Comparat, C. Drag, A. Fioretti, O. Dulieu, and P. Pillet, *Photoassociative Spectroscopy and Formation of Cold Molecules in Cold Cesium Vapor: Trap-Loss Spectrum versus Ion Spectrum*. Journal of Molecular Spectroscopy, 195, 229-235 (1999).

[1.70] C. M. Dion, C. Drag, O. Dulieu, B. L. Tolra, F. Masnou-Seeuws, and P. Pillet, *Resonant coupling in the formation of ultracold ground state molecules via photoassociation*, Physical Review Letters, 86, 2253-2256 (2001).

[1.71] A. Fioretti, D. Comparat, A. Crubellier, O. Dulieu, F. Masnou-Seeuws, and P. Pillet, *Formation of Cold Cs_2 Molecules through Photoassociation*, Physical Review Letters, 80, 4402-4405 (1998).

[1.72] C. Gabbanini, A. Fioretti, A. Lucchesini, S. Gozzini, and M. Mazzoni, *Cold rubidium molecules formed in a magneto-optical trap*, Physical Review Letters, 84, 2814-2817 (2000).

[1.73] A. N. Nikolov, J. R. Ensher, E. E. Eyler, H. Wang, W. C. Stwalley, and P. L. Gould, *Efficient production of ground-state potassium molecules at sub-mK temperatures by two-step photoassociation*, Physical Review Letters, 84, 246-249 (2000).

[1.74] J. P. Shaffer, W. Chalupczak, and N. P. Bigelow, *Highly excited states of ultracold molecules: Photoassociative spectroscopy of Na_2*, Physical Review Letters, 83, 3621-3624 (1999).

[1.75] T. Takekoshi, B. Patterson, and R. J. Knize, *Optical trapping of ultracold molecules*, Abstracts of Papers of the American Chemical Society, 220, 199-200 (2000).

[1.76] K. Xu, T. Mukaiyama, J. R. Abo-Shaeer, J. K. Chin, D. E. Miller, and W. Ketterle, *Formation of quantum-degenerate sodium molecules*, Physical Review Letters, 91, 210402-1-4 (2003).

[1.77] K. E. Strecker, G. B. Partridge, and R. G. Hulet, *Conversion of an atomic Fermi gas to a long-lived molecular Bose gas*, Physical Review Letters, 91, 080406-1-4 (2003).

[1.78] M.W. Zwierlein, C. A. Stan, C. H. Schunck, S.M. F. Raupach, S. Gupta, Z. Hadzibabic, and W. Ketterle, *Observation of Bose-Einstein Condensation of Molecules*, Physical Review Letters, 91, 250401-1-4 (2003).

[1.79] L. Radzihovsky, J. Park, and P. B. Weichman, *Superfluid Transitions in Bosonic Atom-Molecule Mixtures near a Feshbach Resonance*, Physical Review Letters, 92, 160402-1-4 (2004).

[1.80] S. Y. T. van de Meerakker, R. T. Jongma, H. L. Bethlem, and G. Meijer, *Accumulating NH radicals in a magnetic trap*, Physical Review A, 64, 041401-1-4 (2001).

[1.81] H. L. Bethlem, G. Berden, and G. Meijer, *Decelerating neutral dipolar molecules*, Physical Review Letters, 83, 1558-1561 (1999).

[1.82] H. L. Bethlem, G. Berden, F. M. H. Crompvoets, R. T. Jongma, A. J. A. van Roij, and G. Meijer, *Electrostatic trapping of ammonia molecules*, Nature, 406, 491-494 (2000).

[1.83] H. L. Bethlema and G. Meijerbcd, *Production and application of translationally cold molecules*, International Reviews in Physical Chemistry, 22, 73-128 (2003).

[1.84] N. Vanhaecke, U. Meier, M. Andrist, B. H. Meier, and F. Merkt, *Multistage Zeeman deceleration of hydrogen atoms*, Physical Review A, 75, 031402-1-4 (2007).

[1.85] E. Narevicius, A. Libson, C. G. Parthey, I. Chavez, J. Narevicius, U. Even, and M. G. Raizen, *Stopping supersonic oxygen with a series of pulsed electromagnetic coils: A molecular coilgun*, Physical Review A, 77, 051401-1-4 (2008).

[1.86] J. D. Weinstein, R. deCarvalho, T. Guillet, B. Friedrich, and J. M. Doyle, *Magnetic trapping of calcium monohydridemolecules atmillikelvin temperatures*, Nature, 395, 148-150 (1998).

[1.87] D. J. Larson, J. C. Bergquist, J. J. Bollinger, W. M. Itano, and D. J. Wineland, *Sympathetic Cooling of Trapped Ions: A Laser-Cooled Two-Species Nonneutral Ion Plasma*, Physical Review Letters, 57, 70-73 (1986).

[1.88] C. J. Myatt, E. A. Burt, R. W. Ghrist, E. A. Cornell, and C. E. Wieman, *Production of Two Overlapping Bose-Einstein Condensates by Sympathetic Cooling*, Physical Review Letters, 78, 586-589 (1997).

[1.89] M. Stoll, J. M. Bakker, T. C. Steimle, G. Meijer, and A. Peters, *Cryogenic buffer-gas loading and magnetic trapping of CrH and MnH molecules*, Physical Review A, 78, 032707-1-8 (2008).

[1.90] D. Egorov, W. C. Campbell, B. Friedricha, S. E. Maxwell, E. Tsikata, L. D. van Buuren, and J. M. Doyleb, *Buffer-gas cooling of NH via the beam loaded buffer-gas method*, The European Physical Journal D, 31, 307-311 (2004).

[1.91] S. E. Maxwell, N. Brahms, R. deCarvalho, D. R. Glenn, J. S. Helton, S.V. Nguyen, D. Patterson, J. Petricka, D. DeMille, and J. M. Doyle, *High-Flux Beam Source for Cold, Slow Atoms or Molecules*,Physical Review Letters, 95, 173201-1-4 (2005).

[1.92] M. Gupta and D. Herschbach, *Slowing and Speeding Molecular Beams by Means of a Rapidly Rotating Source*, The Journal of Physical Chemistry A, 105, 1626-1637 (2001).

[1.93] B. S. Zhao, M. Castillejo, D. S. Chung, B. Friedrich, and D. Herschbach, *Cool pulsed molecular microbeam*, Review of Scientific Instruments, 75, 146-150 (2004).

[1.94] S. A. Rangwala, T. Junglen, T. Rieger, P. W. H. Pinkse, and G. Rempe, *Continuous source of translationally cold dipolar molecules*, Physical Review A, 67, 043406-1-4 (2003).

[1.95] M. S. Elioff, J. J. Valentini, D. W. Chandler, *Cooling NO Molecules via "Billiard-like" Collisions with Argon*, Science, 302, 1940-1943 (2003).

[1.96] A. A. Mikhailichenko and M. S. Zolotorev, *Optical Stochastic Cooling*, Physical Review Letters, 71, 4146-4149 (1993).

[1.97] M. G. Raizen, J. Koga, B. Sundaram, Y. Kishimoto, H. Takuma, and T. Tajima, *Stochastic cooling of atoms using lasers*, Physical Review A, 58, 4757-4760 (1998).

[1.98] P. Horak, G. Hechenblaikner, K. M. Gheri, H. Stecher, and H. Ritsch, *Cavity-Induced Atom Cooling in the Strong Coupling Regime*, Physical Review Letters, 79, 4974-4977 (1997).

[1.99] V. Vuletic and S. Chu, *Laser Cooling of Atoms, Ions, or Molecules by Coherent Scattering*, Physical Review Letters, 84, 3787-3790 (2000).

[1.100] P. Maunz, T. Puppe, I. Schuster, N. Syassen, P. W. H. Pinkse, and G. Rempe, *Cavity cooling of a single atom*, Nature, 428, 50-52 (2004).

[1.101] P. Domokos and H. Ritsch, *Collective Cooling and Self-Organization of Atoms in a Cavity*, Physical Review Letters, 89, 253003-1-4 (2002).

[1.102] H. W. Chan, A. T. Black, and V. Vuletic, *Observation of Collective-Emission-Induced Cooling of Atoms in an Optical Cavity*, Physical Review Letters, 90, 063003-1-4 (2003).

[1.103] B. Friedrich, *Slowing of supersonically cooled atoms and molecules by time-varying nonresonant induced dipole forces*, Physical Review A, 61, 025403-1-4 (2000).

[1.104] R. de Carvalho, J. M. Doyle, B. Friedrich, T. Guillet, J. Kim, D. Patterson, and J. D. Weinstein, *Buffer-gas loaded magnetic traps for atoms and molecules: A primer*, The European Physical Journal D, 7, 289-309 (1999).

[1.105] J. K. Messer and F. C. Delucia, *Measurement of Pressure-Broadening Parameters for the Co-He System at 4K*, Physical Review Letters, 53, 2555-2558 (1984).

[1.106] H. L. Bethlem, F. M. H. Crompvoets, R. T. Jongma, S. Y. T. van de Meerakker, and G. Meijer, *Deceleration and trapping of ammonia using time-varying electric fields*, Physical Review A, 65, 053416-1-20 (2002).

[1.107] Panel on Atomic, Molecular, and Optical Physics Physics Survey Committee, Board on Physics and Astronomy, National Research Council. *Atomic, Molecular, and Optical Physics*, National Academic Press (1986).

Chapter 2

Cavity Cooling of atoms

2.1 Introduction

In this chapter, the theoretical descriptions of the cavity cooling are introduced. Cooling atoms with an optical cavity is a relatively new method, which has recently been demonstrated experimentally [2.1-2.5]. This scheme uses a cavity detuned from resonance to preferentially scatter blue shifted photons out of the cavity to extract energy from the atoms. It does not depend on the specific internal structure of the scattering species and can be applied to any polarizable particles including molecules.

In spite of recent prolific activity in the fields of cavity QED and cavity cooling, the present understanding of the dynamics of the atom-field interaction in a cavity is largely limited to a single atom. When an ensemble is placed in a cavity, different atoms are coupled by their interaction with the common intracavity field. This field-mediated atom-atom interaction leads to significant modification to the dynamics of a single atom, and experimental and theoretical work suggest a nontrivial scaling with the number of atoms [2.6].

More recent studies have shown that spatial self-organization of atoms in a cavity occurs when the detuned pump light is send into the cavity from the side instead of directly [2.4, 2.8]. This phenomenon can reduce or eliminate the undesirable atom-atom correlation [2.9]. It has demonstrated significant enhancement of the cooling process through the collective dynamics of many body species.

In section 2.2, the general cavity cooling model is theoretically discussed. In section 2.3, we utilize the classical theory to derive the numerical solution of a single two-level atom in a single cavity mode. In section 2.4, the atom-atom interaction in an

optical cavity is presented. In section 2.5, the theoretical model of atomic self-organization is studied.

2.2 Basic Model of Cavity QED

Cavity-cooling has so far been studied almost exclusively in the strong atom-field coupling regime in which the refractive index changes induced by atoms are significant.

The schematic sketch of the basic cavity cooling system is shown in Fig. 2.1, according to the work of Peter Domokos and Helmut Ritsch [2.10]. There are N two-level center-of-mass (CM) atoms with transition frequency ω_A, which are able to be strongly coupled to M modes of a high-finesse optical cavity with frequencies $\omega_m \approx \omega_c$ for all modes m =1 ... M.

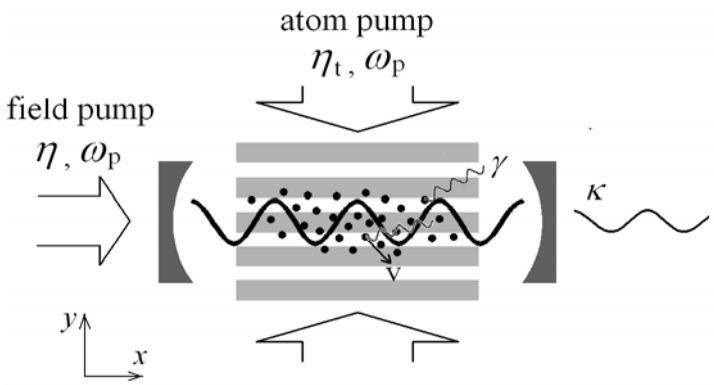

Fig. 2.1 Schematic representation of the system composed of many atoms coupled to a multimode cavity.

In general, the system is driven by two coherent laser fields. One field is directly injected into the cavity through one of its mirrors, yielding an effective pump strength η_m for the m_{th} mode. The second driving laser field impinges on the atoms from the side with spatially dependent pump strength η_t. There is an efficient scattering of photons into the cavity due to the dipole coupling between the pump field and the atoms. For simplicity the two pump lasers are set to have the same frequency ω_p. The pump-atom red detuning is defined as $\Delta_A = \omega_p - \omega_A$.

There are two dissipation channels to take into account. First, the atoms spontaneously emit into free space other than the cavity modes with a rate 2γ. Second, cavity photons decay with a rate 2κ via the output coupler mirror of the cavity.

In addition to the coherent pumping and dissipations, the system is subject to incoherent damping that is due to the atom-light coupling. We firstly discuss the interaction between atom and optical field.

2.2.1 Interaction between a two-level atom and single mode optical field

The simplest and most important model of an atom includes only the ground (lower) state $|g\rangle$ and excited (upper) state $|e\rangle$ of an optical transition. This concept of "two-level atom" is often used to describe its interaction with the electromagnetic field in detail and obtain analytic solutions [2.11]. A two-level atom in an optical field is depicted in Fig. 2.2 according to the condition of our general model.

This dipole interaction has two effects: (1) when the field is off-resonant with the atomic transitions, the dominant effect is that the atomic energy levels undergo an energy shift; (2) when the field is near-resonant with an atomic transition, the dominant effect is transitions between atomic levels [2.2].

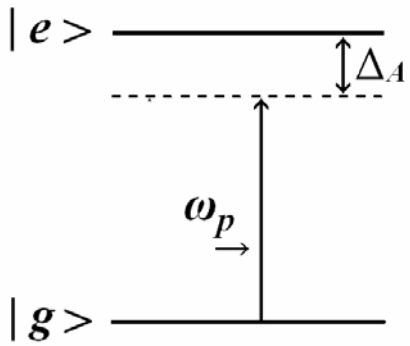

Fig. 2.2 A two-level atom in an optical field with frequency ω_p. The detuning is Δ_A

Following standard quantum optics techniques and approximations, the total Hamiltonian for the combined system of the optical field and the two-level atom can be written as

$$H = H_{\text{atom}} + H_{\text{field}} + H_{\text{int}} \tag{2.1}$$

where H_{atom}, H_{field} and H_{int} are respectively the Hamiltonian of the two-level atom, the optical field, and the interaction between the atom and the optical field.

In the optical field, the atom is stimulated from the ground state to the excited state by absorbing a photon with frequency ω_p, and when in the excited state, it emits a photon with the same frequency through the spontaneous process.

In treating two-level atoms the Pauli atomic raising operator $\sigma_+ = |e\rangle\langle g|$ and lowering operator $\sigma_- = |g\rangle\langle e|$ are handy for representing these transitions caused by interaction energy. They are conveniently written in terms of Pauli Spin Matrices.

The kinematic velocity of the atom is assumed as v. Due to the Doppler effect, the frequency of the emitted photon from the atom in the laboratory frame is $(\omega_A + \mathrm{k}\cdot\mathrm{v})(1-\mathrm{v}^2/c^2)^{-1/2}$, where k is the wave vector of the optical field. In typical atom physics experiments, $|\mathrm{v}| << c$, therefore, the relativistic effect can be neglected. The atomic Hamiltonian H_{atom} can be given by

$$H_{atom} = \frac{\hat{p}^2}{2m} + \hbar(\omega_A + \mathbf{k}\cdot\mathbf{v})\sigma_+\sigma_- \tag{2.2}$$

where $\hat{p}$ is the CM momentum of the atom operator, m is the mass. When the light field is red detuned, k is less than k_A, the term of $\mathbf{k}\cdot\mathbf{v}$ can be neglected as well.

The Hamiltonian of a single mode light field with frequency ω_p is

$$H_{field} = \hbar\omega_p(a^\dagger a + 1/2) \tag{2.3}$$

where $a^\dagger$ and a are the creation and annihilation operators for a photon in the field with energy $\hbar\omega_p$, $a^\dagger a$ is called the number operator.

The electric dipole approximation is generally adopted to deal the interaction Hamiltonian H_{int}. The dipole approximation assumes the wavelength of the light field is much greater than the size of the atom, and the position $\mathbf{r}$ of the atomic nucleus is concerned rather than the location of the electron. The field is approximated as a constant over the dimensions of the atom.

H_{int} in the dipole approximation is

$$H_{\text{int}} = -\,\mathbf{d}\cdot\mathbf{E}(\mathbf{r}) \tag{2.4}$$

where

$$\mathbf{d} = \mathrm{e}\mathbf{r} \tag{2.5}$$

is the dipole moment operator of the atom. The two-level atom does not have a dipole moment when it is in the ground and excited states. The dipole operator which is real can be given as

$$\mathbf{d} = \mathbf{d}_{eg} * \sigma_+ + \mathbf{d}_{eg}\, \sigma_- = \mathbf{d}_{eg}(\sigma_+ + \sigma_-) \tag{2.6}$$

The quantized electric field operator at position **r** for the plane-wave mode with wavevector **k**, frequency ω_p and linear polarization **ε** is written as

$$\mathbf{E}(\mathbf{r},t) = iE\boldsymbol{\varepsilon}[\, a \exp(-i\omega_p t + i\,\mathbf{k}\cdot\mathbf{r}) - a^\dagger \exp(i\omega_p t - i\,\mathbf{k}\cdot\mathbf{r})] \tag{2.7}$$

where E is electromagnetic field of single photon, as

$$E = \sqrt{\frac{\hbar\omega_p}{2\varepsilon_0 V_n}} \tag{2.8}$$

In Eq. (2.8), ε_0 is the permittivity of free space and V_n is the quantization volume. The electromagnetic field is treated classically and so E is considered as a vector of complex numbers.

By replacing **E**(**r**) in Eq. (2.4) with the quantized electric field operator and making the rotating-wave approximation to remove the explicit time dependence, the interaction Halmitonian H_{int} is read as

$$H_{\text{int}} = -i\hbar g(\sigma_+ + \sigma_-)(a - a^\dagger) \tag{2.9}$$

where

$$g = \mathbf{d} \cdot \boldsymbol{\varepsilon}\, E / \hbar \tag{2.10}$$

is the electric dipole coupling strength, known as the "single-photon Rabi frequency". It corresponds to the frequency at which an atom will spontaneously emit and reabsorb a single resonant photon of frequency [2.11]. The single photon Rabi frequency then has spatial dependence $f(x)$, the standing wave modes of a cavity, hence the constant depends on the position of the atom in the cavity.

Insert Eq. (2.2), (2.3) and (2.9) into Eq. (2.1), the total Hamiltonian H is

$$H = \frac{\hat{p}^2}{2m} + \hbar\omega_A\, \sigma_+\sigma_- + \hbar\omega_p(a^\dagger a + 1/2) - i\hbar g(\sigma_+ + \sigma_-)(a - a^\dagger) \tag{2.11}$$

By choosing the energy zero of the atom to be half way between the excited and ground levels, removing the zero point energy $\hbar\omega_p/2$ of the field and applying the unitary transformations and rotating wave approximation, the total Hamiltonian H is given by the Jaynes-Cummings Hamiltonian as

$$H = \frac{\hat{p}^2}{2m} + \hbar\omega_A \sigma_z + \hbar\omega_p a^\dagger a - i\hbar g(a\sigma_+ - \sigma_- a^\dagger) \tag{2.12}$$

In Eq. (2.12), the Pauli operator σ_z is the atomic inversion [2.12-2.14]. The two interaction terms $a\sigma_+$ and $\sigma_- a^\dagger$ correspond to a upward transition in the atom by absorption of photon and a downward transition with a photon emission. The other two terms $a^\dagger\sigma_+$ and $\sigma_- a$ are omitted due to the two corresponding processes rarely happen.

2.2.2 A two-level atom in a single mode optical cavity

In the general cavity cooling model, the two-level atoms are inside the cavity and interact with the standing wave. The single mode electric field along the cavity axis *x*can be written as

$$\mathbf{E}(x,t) = iE\boldsymbol{\varepsilon}(a - a^\dagger)\cos(kx) \tag{2.23}$$

The electric dipole coupling strength *g* in Eq. (2.9) to Eq. (2.12) is position-dependent and can be corrected as

$$g(x) = (\mathbf{d}\cdot\boldsymbol{\varepsilon}E/\hbar)\cos(kx) \tag{2.24}$$

The state of the two-level atom can be describe by the density matrix, which has a representation as the Hermitian square matrix

$$\rho = \begin{pmatrix} \rho_{ee} & \rho_{eg} \\ \rho_{ge} & \rho_{gg} \end{pmatrix} \tag{2.13}$$

where ρ_{ee} and ρ_{gg} are real,

$$\rho_{ee} + \rho_{gg} = 1 \tag{2.14}$$

and

$$\rho_{eg} = \rho_{ge}^* \tag{2.15}$$

The equation of motion for the density matrix is given as

$$\frac{d\rho}{dt} = -\frac{i}{\hbar}[H,\rho] + \left(\frac{\partial\rho}{\partial t}\right)_{damp} \tag{2.16}$$

where the $\left(\frac{\partial\rho}{\partial t}\right)_{damp}$ is the damping or relaxation term. In our model, the cavity decay and the atomic spontaneous emission are taken into account, i.e.

$$\left(\frac{\partial\rho}{\partial t}\right)_{damp} = \left(\frac{\partial\rho}{\partial t}\right)_{cav} + \left(\frac{\partial\rho}{\partial t}\right)_{spon} \tag{2.17}$$

Based on the quantum theory of damping, the term of the cavity loss can be written as

$$(\frac{\partial \rho}{\partial t})_{cav} = \kappa(2a\rho a^{\dagger} - a^{\dagger}a\rho - \rho a^{\dagger}a) \tag{2.18}$$

where the oscillator is the single mode field interacting with a reservoir, at zero temperature. κ is the half linewidth of the cavity [2.7].

The excited atom with momentum **p** decays into its ground state with a shifted momentum $\mathbf{p} - \hbar\,\mathbf{k}$[2.11]. We can use the momentum translation operator $S_{\mathrm{p}}(\mathbf{k})$=exp(-i**k**·**r**), with

$$e^{-i\mathbf{k}\cdot\mathbf{r}} \mid \mathbf{p}\rangle = \mid \mathbf{p} - \hbar\,\mathbf{k}\rangle \tag{2.19}$$

Writing $\mathbf{k} = k_A\mathbf{n}$, where **n** is a unit direction vector of the spontaneously emitted photon. The increase in population in the electronic ground state is given by $d\Gamma_{\mathrm{n}}\exp[-ik_A\mathbf{n}\cdot\mathbf{r}]\rho_{ee}\exp[ik_A\mathbf{n}\cdot\mathbf{r}]$, where

$$d\Gamma_{\mathrm{n}} = \gamma N(\mathbf{n})d^2\mathbf{n} \tag{2.20}$$

is the differential rate of spontaneous emission in the **n**-direction. $N(\mathbf{n})$ is a directional distribution function characteristic of the given atomic transition. The term of $N(\mathbf{n})d^2\mathbf{n}$ is the probability of emission in an solid angle $d^2\mathbf{n}$ along **n.**

Integrating over all directions yields

$$\dot{\rho}_{gg} = \int d\Gamma_{\mathrm{n}}\exp(-ik_A\mathbf{n}\cdot\mathbf{r})\rho_{ee}\exp(ik_A\mathbf{n}\cdot\mathbf{r}) \tag{2.21}$$

Combining Eq. (2.20) with the quantum theory of dampling, the term of spontaneous emission by a freely traveling atom is

$$(\frac{\partial \rho}{\partial t})_{spon} = \gamma(2\int d\Gamma_{\mathrm{n}}\exp(-ik_A\mathbf{n}\cdot\mathbf{r})\sigma_{-}\rho\exp(ik_A\mathbf{n}\cdot\mathbf{r})\sigma_{+} - \sigma_{+}\sigma_{-}\rho - \rho\sigma_{+}\sigma_{-}) \tag{2.22}$$

2.2.3 Quantum master equation of the general model

According to the result of the Hamiltonian to each two-level atom and single mode field, the quantum mechanical model of thegeneral model system can be cast in the form of a quantum master equation

$$\dot{\rho} = -\frac{i}{\hbar}[H, \rho] + L\rho \tag{2.22}$$

The total Hamiltonianwhich includes pump η and η_t is written as

$$H=\sum_{a=1}^{N}[\frac{\hat{p}_a^2}{2m}-\hbar\Delta_A\sigma_a^z]-\hbar\Delta_c a_n^\dagger a_n-i\hbar\sum_{n=1}^{M}\sum_{a=1}^{N}[g_n(\hat{x}_a)\sigma_a^\dagger a_n-g_n^*(\hat{x}_a)a_n^\dagger\sigma_a)]+H_\eta+H_{\eta_t} \quad (2.23a)$$

$$H_\eta=\sum_{n=1}^{M}[-i\hbar\eta_n(a_n-a_n^\dagger)] \quad (2.23b)$$

$$H_{\eta_t}=-i\hbar\eta_t[h(\hat{y}_a)\sigma_a^\dagger-h^*(\hat{y}_a)\sigma_a] \quad (2.23c)$$

The Liouville terms read as

$$L\rho=\sum_{m=1}^{M}\kappa_n(2a_n\rho a_n^\dagger-a_n^\dagger a_n\rho-\rho a_n^\dagger a_n)$$

$$+\gamma\sum_{a=1}^{N}(2\int N(\mathbf{n})\mathrm{d}^2\mathbf{n}\exp(-i\hbar k_A\,\mathbf{n}\,\hat{x}_a)\sigma_a\rho\exp(i\hbar k_A\,\mathbf{n}\,u\hat{x}_a)\sigma_a^\dagger-\sigma_a^\dagger\sigma_a\rho-\rho\sigma_a^\dagger\sigma_a) \quad (2.23d)$$

In the Hamiltonian, $a_n^\dagger$ and a_n are the field creation and annihilation operators for the *n*th mode field. $\hat{x}_a$ ($\hat{y}_a$) and $\hat{p}_a$ are the position and momentum operators of the CM motion of the *a*th atom. *M* is the mode number of the optical cavity, and *N* is the atom number. The third term of Eq. (2.23a) represents the interaction between the *a*th atom and the *n*th mode field. The position-dependent coupling constant is given by $g_n(x)=d\sqrt{\hbar\omega_c/(2\varepsilon_0 V_n)}f_n(x)$, where *d* is the atomic dipole moment, V_n is the effective mode volume, and $f_n(x)$ is the normalized mode function which has a maximum value 1 [2.10-2.18].

The cavity-field detuning is defined as $\Delta_c=\omega_p-\omega_c$. The external pumps are treated as classical fields with pumping strengths η and η_t. $h(\hat{y}_a)$ denotes the Rabi frequency of the transverse pump field and can be written as $h(\hat{y}_a)=h\cos(ky)$.

The field polarization issue is neglected, and the mode polarization can be incorporated into the definition of the dipole moment *d* and mode volumes. In the model, only single-atom terms appear while the direct atom-atom interactions (dipole-dipole or contact interaction) are neglected.

2.3 Dynamical Model of Particle in a Single Cavity Mode

In section 2.2, the full quantum master equation has been derived to describe the general model. However, it is complex to investigate the dynamic process of the model. The classical theory is often adopted to study the interaction as the induced polarization between the classical media and the classical electromagnetic fields. In a simple way,

we consider the status of a single particle in a single cavity mode first in this section. In this case, the charged particles are subjected to the Lorentz force, and also that the electromagnetic field is governed by Maxwell equations [2.11]. The dynamics of this model can be numerically simulated based on these results.

2.3.1 Classical model

We consider a particle in a cavity with a weak pump from one side of its mirrors. For simplicity, the particle is assumed to be a two-level at primary model which is coupled to a single mode of frequency ω_c. The frequency of the pump field is ω_p and the effective amplitude η [2.19-2.20].The spontaneous emission (γ) of the particle and the cavity decay (κ) are considered as the two losses in this model. The particle moves along the standing wave and a dipole moment isinducedby the interaction. The coupling strength function is $g(x)=g\cdot f(x)$, where $f(x)$ is the normalized mode function.

Inside a macroscopic medium, Maxwell equations are given by:

$$\nabla \cdot D = \rho \tag{2.24a}$$

$$\nabla \cdot B = 0 \tag{2.24b}$$

$$\nabla \times E = -\frac{\partial}{\partial t} B \tag{2.24c}$$

$$\nabla \times H = J + \frac{\partial}{\partial t} D \tag{2.24d}$$

where $\boldsymbol{D}$ is the effective electric field in a dielectric, ρ is the charge density, $\boldsymbol{B}$ is the imposed magnetic field, $\boldsymbol{E}$ is the electric field, $\boldsymbol{H}$ is the effective magnetic field in a dielectric, and $\boldsymbol{J}$ is the current density.

In linear materials, the polarization density $\boldsymbol{P}$ and magnetization density $\boldsymbol{M}$ are related to $\boldsymbol{E}$ and $\boldsymbol{H}$ by:

$$D = \varepsilon_0 E + P \tag{2.24e}$$

$$B = \mu_0 H + M \tag{2.24f}$$

$$J = \sigma(E - E^{ext}), \tag{2.24g}$$

where ε_0 is the permittivity of free space, μ_0 is the permeability of free space and σ is the electrical conductivity of the material. In our model, σ is treated as the conductivity of the cavity mirrors, the current density includes the external pump field E^{ext}. μ_0 and

ε_0 are related by $c = 1/\sqrt{\mu_0 \varepsilon_0}$, where c is the speed of light in vacuum. In non-dispersive, isotropic laser media $M = 0$.

Taking the curl of Eq. (2.24c) and combining Eq. (2.24d) to Eq. (2.24g), we obtain

$$\nabla \times (\nabla \times E) = -\mu_0 \sigma \frac{\partial}{\partial t}(E - E^{ext}) - \frac{1}{c^2}\frac{\partial^2}{\partial t^2} E - \mu_0 \frac{\partial^2}{\partial t^2} P \,. \tag{2.25}$$

For the left side of the above equation, $\nabla \times (\nabla \times E) = \nabla(\nabla \cdot E) - \nabla^2 E$ .Since the plane wave field vector is constant along the direction it points, $\nabla \cdot E = 0$. Eq. (2.25) can be written as

$$(-\nabla^2 + \frac{1}{c^2}\frac{\partial^2}{\partial t^2})\vec{E}(\vec{x},t) + \mu_0 \sigma \frac{\partial}{\partial t}\vec{E}(\vec{x},t) = -\mu_0 \frac{\partial^2}{\partial t^2}\vec{P}(\vec{x},t) + \mu_0 \sigma \frac{\partial}{\partial t}\vec{E}^{ext}(\vec{x},t) \tag{2.26}$$

where $\mu_0 \sigma \frac{\partial}{\partial t}\vec{E}(\vec{x},t)$ is the damping term of the field mode. For simplicity we consider a quasi-1D situation, where the field is a plane wave propagating in the x direction, which leads to

$$\frac{\partial^2}{\partial t^2}E(x,t) + \frac{\sigma}{\varepsilon_0}\frac{\partial}{\partial t}E(x,t) - c^2 \frac{\partial^2}{\partial x^2}E(x,t) = -\frac{1}{\varepsilon_0}\frac{\partial^2}{\partial t^2}P(x,t) + \frac{\sigma}{\varepsilon_0}\frac{\partial}{\partial t}E^{ext}(x,t) \tag{2.27}$$

The electromagnetic fields in the cavity can be represented by the scalar electric field

$$E(x,t) = \sum_{n=0}^{\infty} \widetilde{E}_n(t)\cos(k_n x) \tag{2.28}$$

with eigenfrequencies $\omega_n = ck_n = n\pi c / L$ for the two-mirror laser, where $\cos(k_n x)$ is the mode function of the standing waves, and L denotes the cavity length.

Inserting Eq. (2.28) into Eq. (2.27), we get the following equation for the dynamics of the model after some straightforward manipulations

$$\ddot{\widetilde{E}} + \frac{\sigma}{\varepsilon_0}\dot{\widetilde{E}} + {\omega_c}^2 \widetilde{E} = -\frac{1}{\varepsilon_0}\ddot{\widetilde{P}} + \frac{\sigma}{\varepsilon_0}\dot{\widetilde{E}}^{ext} \,. \tag{2.29}$$

where

$$\widetilde{P}(t) = \frac{2}{L}\int_{-L/2}^{L/2} dx P(x,t)\cos(kx) \tag{2.30}$$

and analogously for $\widetilde{E}^{ext}$, which means the total polarization and the pump are treated as the sum of all the positions in the whole cavity.

The ansatz for the electric fields and the polarization are given as

$$\widetilde{E}(t)=\varepsilon(t)e^{-i\omega_p t}+c.c.,\ \widetilde{E}^{ext}(t)=\varepsilon^{ext}(t)e^{-i\omega_p t}+c.c.,\ \widetilde{P}(t)=P(t)e^{-i\omega_p t}+c.c. \quad (2.31)$$

where the amplitude terms $\varepsilon(t)$, $\varepsilon^{ext}(t)$ and $P(t)$ vary slowly compared to the rapidly oscillating exponential functions, i.e., $|\dot{\varepsilon}| << \omega_p|\varepsilon|$ and analogously for P and ε^{ext}. Using the slowly-varying envelope approximations we can neglect the corresponding terms and rewrite Eq. (2.29) as

$$\dot{\varepsilon}+(\frac{\sigma}{2\varepsilon_0}-\frac{(\omega_c{}^2-\omega_p{}^2)}{2i\omega_p})\varepsilon=-\frac{\omega_p}{2i\varepsilon_0}P+\frac{\sigma}{2\varepsilon_0}\varepsilon^{ext} \quad (2.32)$$

Comparing the damping term with the cavity decay rate, we let $\kappa=\frac{\sigma}{2\varepsilon_0}$. In the near resonant case, $\omega_p\approx\omega_c, |\Delta_c| << (\omega_p+\omega_c)$, in which $\Delta_c=\omega_p-\omega_c$ is the cavity-pump detuning. By making the classical analog of the rotating-wave approximation, i.e., $(\omega_c{}^2-\omega_p{}^2)=-2\omega_p\Delta_c$, the Eq. (2.49) can be written as

$$\dot{\varepsilon}+(\kappa-i\Delta_c)\varepsilon=\frac{i\omega_p}{2\varepsilon_0}P+\kappa\varepsilon^{ext}. \quad (2.33)$$

2.3.2 Linear dipole oscillator model of an atom

The dynamics of the two-level atomic dipole can be simply depicted by the classical damped linear dipole oscillator. In this model, an electron cloud is elastically bound to a heavy positive nucleus and oscillates about its equilibrium position with the center of the nucleus. For small deviation from the equilibrium position, the motion of the electron cloud can be described as that of a damped simple harmonic oscillator driven by a standing-wave electric field $E(x,t)$ at the atomic position x_a. The motion obeys the Abraham-Lorentz equation

$$\ddot{y}(t)+2\gamma\dot{y}(t)+\omega_A^2 y(t)=\frac{e}{m}E(x_a,t) \quad (2.34)$$

where $E(x_a,t)=\left(\varepsilon(t)e^{-i\omega_p t}+cc\right)\cdot\cos(kx_a)$ according to Eq. (2.29) and Eq. (2.31). The displacement in Eq. (2.34) generally can be assumed as

$$y(t)=Y(t)e^{-i\omega_p t}+cc \quad (2.35)$$

where $Y(t)$ is the slowly varying complex amplitude [2.11].

Inserting the solution to Eq. (2.34), neglecting the small quantities and solving for the steady state $\dot{Y}=0$, we obtain

$$Y(t) = \frac{e\varepsilon(t)/m}{2\omega_p(-i\gamma + (\omega_A^2 - \omega_p^2)/(2\omega_p))}\cos(kx_a) \tag{2.36}$$

The polarization density of a particle at position x_a can be defined as

$$P(x,t) = ey(t)\delta(x - x_a)/A \tag{2.37}$$

where A is the cavity cross section.

Taking relevant equations from Eq. (2.30) to Eq. (2.37) into Eq. (2.33), we find

$$P(t) = i\frac{e^2\cos^2(kx_a)}{m\omega_p V(\gamma - i\Delta_A)}\varepsilon(t) \tag{2.38}$$

where $V=A\cdot L$ is the cavity volume, $\Delta_A = \omega_p - \omega_A$ is the pump-atom detuning and the rotating-wave approximation

$$(\omega_A^2 - \omega_p^2)/(2\omega_p) = (\omega_A - \omega_p)(\omega_A + \omega_p)/(2\omega_p) \approx -\Delta_A \tag{2.39}$$

is made.

2.3.3 Dynamical equations

Inserting Eq. (2.38) into Eq. (2.33), and splitting the polarization into a real and an imaginary part, we obtain the following equation

$$\dot{\varepsilon}(t) = (-\kappa - \Gamma(x_a) + i\Delta_c - iU(x_a))\varepsilon(t) + \kappa\varepsilon^{ext} \tag{2.40}$$

where

$$U(x_a) = \frac{\Delta_a}{\gamma^2 + \Delta_a^2}g_0^2\cos^2(kx_a) \equiv U_0\cos^2(kx_a) \tag{2.41a}$$

$$\Gamma(x_a) = \frac{\gamma}{\gamma^2 + \Delta_a^2}g_0^2\cos^2(kx_a) \equiv \Gamma_0\cos^2(kx_a) \tag{2.41b}$$

Here $\Gamma_0 = \frac{\gamma}{\gamma^2 + \Delta_a^2}g_0^2$, $U_0 = \frac{\Delta_a}{\gamma^2 + \Delta_a^2}g_0^2$, and $g_0{}^2 = e^2/(2V\varepsilon_0 m)$ is a measure of the cavity-atom coupling strength. By considering the atomic dipole transitions, the coupling strength term $g_0{}^2$ is often replaced by the corresponding term of the semiclassical model.

The force on the particle is then given by

$$f(x_a) = \nabla[e\sum_k y_{\omega_{Ak}}(x_a,t)E(x_a,t)] = -\nabla[\frac{e^2}{2\omega_p m}U_0\varepsilon(t)^2\cos^2(kx_a)] \tag{2.42}$$

The electric field amplitude ε is not easy to compare with some conclusion of

semiclassical model which is shown as photon number. This time we use the energy density $\frac{1}{2}\varepsilon_0|\varepsilon_s|^2$, i.e. the Poynting vector, to do the rescaling. For a single-mode field, the standing-wave electric field per photon is related to the running-wave electric field per photon by

$$\varepsilon_s = \sqrt{2}\varepsilon_r \tag{2.43}$$

In the above analysis, for simplicityonly a part of the mode field is considered as the ansatz $E = \varepsilon e^{-i\omega_p t} + c.c.$, therefore the energy density of the total standing wave field is $\varepsilon_0|\varepsilon|^2$. The average photon density in the cavity is $\frac{|\alpha|^2}{V_m} = \frac{\varepsilon_0|\varepsilon|^2}{\hbar\omega_p}$, where $|\alpha|^2$ is the average photon number in the cavity, V_m is the cavity mode volume.

Eq. (2.40) and Eq. (2.42) can be rewritten in terms of the parameter α, and the following set of equations for the atom-cavity dynamics is obtained

$$\dot{\alpha} = [-\kappa - \Gamma_0 \cos^2(kx) + i\Delta_c - iU_0 \cos^2(kx)]\alpha + \kappa\eta \tag{2.44a}$$

$$\dot{p} = f(x) = \hbar k U_0 |\alpha|^2 \sin(2kx) \tag{2.44b}$$

$$\dot{x} = p/m, \tag{2.44c}$$

where η characterizes the pump laser strength, $|\eta|^2$ is related to the average photon number in pump beam with $\frac{|\eta|^2}{V} = \frac{\varepsilon_0|\varepsilon^{\exp}|^2}{\hbar\omega_p}$. The index a for the atomic position has been omitted for convenience. Eq. (2.44 b) can also be written as

$$\dot{p} = f = -\nabla U = -\hbar U_0 |\alpha|^2 \frac{\partial}{\partial x}\cos^2(kx) \tag{2.44d}$$

which can depict a periodical potential along the propagating direction of the field.

The Eq. (2.44) can benormalized as following equations by $x_n(t) = kx(t)$, $p_n(t) = p(t)/\hbar k$ and $t_n = \kappa t$

$$\dot{\alpha} = [-1 - \frac{\Gamma_0}{\kappa}\cos^2(x_n) + i\frac{\Delta_c}{\kappa} - i\frac{U_0}{\kappa}\cos^2(x_n)]\alpha + \eta \tag{2.45a}$$

$$\dot{p}_n = \frac{U_0}{\kappa}|\alpha|^2 \sin(2x_n) \tag{2.45b}$$

$$\dot{x}_n = hk^2/(m\kappa)\cdot p_n \tag{2.45c}$$

where $\omega_{rec} = hk^2/(2m)$ is the recoil frequency of the atom or particle. These equations can be generalized to three dimensions.

2.3.4 Dynamics of a particle in the optical cavity

Eq. (2.45) is a set of ordinary differential equations. It can be numerical simulated with high accuracy to study the dynamic of the system. Fig. 2.3 shows the physical time evolution of the particle with initial normalized momentum p_n=2 being cooled down when it moves along a laser standing wave and is trapped in the periodic potential, which is described in Eq. (2.44d). The parameters are chosen for an optimized cavity cooling force. In this process, any kind of diffusion is not taken into account, and the effect of Doppler cooling is very small for the chosen parameters. When the initial momentum is set higher, the time needed to trap the particle is longer. However, a real cavity with a length limits the maximum initial momentum.

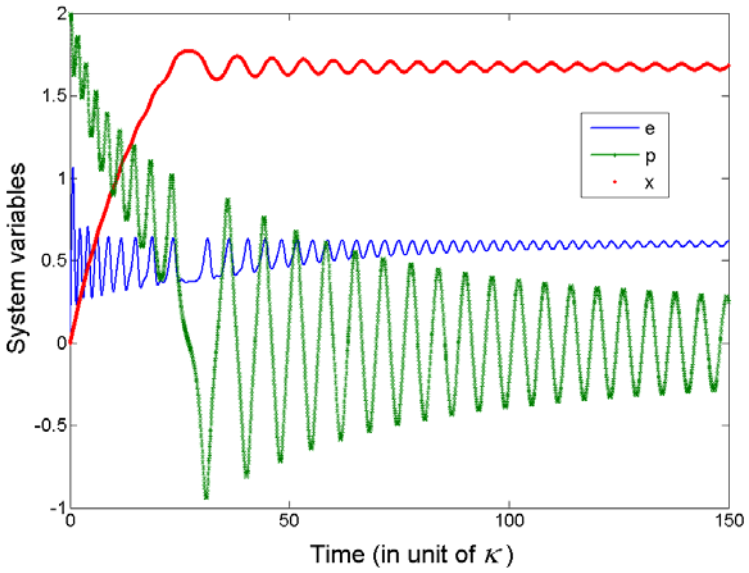

Fig. 2.3 Time evolution of the intracavity field intensity (e), momentum (p_n) and atomic position (x_n) for a single particle. The parameters are Δ_c=−4κ, U_0=−1κ, Γ_0=0.1κ, and η=2.5. The position is divided by 15 in order to show it with the other two in the same scale.

The figure shows two stages in this process, the particle first is slowed down and then is keeping to be cooled while it has been trapped. The cooling mechanics can be explained from a purely classical viewpoint. The dipole force of the particle within the

cavity standing wave, as shown in Eq. (2.44) is strongly dependent on the position of the intracavity intensity mode. For certain parameters, the intensity reaches a maximum for a particle at a node whereas the potential $U(x)$ is a minimum there. However, when the particle is slowly moving along the potential $U(x)$, the maximum field intensity will be reached after it has passed the potential minimum due to the finite cavity response time, i.e. the atom-field interaction lag time. According to the varying dynamics of the field and the position, the particle always experiences a higher field intensity which produces a stronger interactive damping force when it goes up in the potential $U(x)$, while an anti-damping force when it goes down. On average this leads to a damping force, i.e. cooling [2.19]. It could be understood as the friction [2.10].

However, this cooling effect may convert to a heating effect according to the the pump-cavity detuning Δ_c and the atom-pump detuning Δ_a [2.10]. P. Domokos and H. Ritsch studied the relationship of these two detunings under different conditions, as shown in Fig. 2.4.

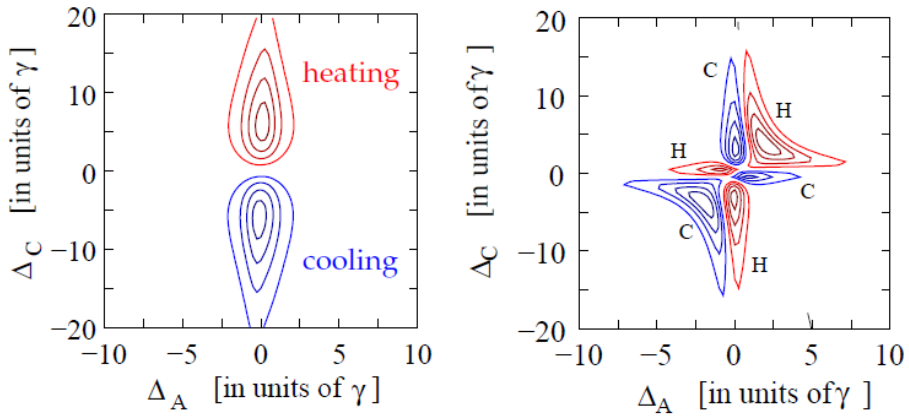

Fig. 2.4 Cooling and heating regions as a function of atom and cavity detunings. Shown are contour plots of the friction coefficient β (averaged over an optical wavelength) acting along the cavity axis on a laser-driven atom. Left: Bad-cavity regime, $g=\gamma/2$, $\kappa=10\gamma$; Right: Good cavity regime, $g=3\gamma$, $\kappa=\gamma$. Blue contour lines indicate cooling (C, $\beta<0$), red ones heating (H, $\beta>0$) regions.

2.3.5 Enhanced cooling and trapping methods

Based on the previous discussion of the atom-field dynamics, methods to quickly and effectively cool and trap the moving atom can be theoretically considered.

As shown in Fig. 2.5, there are two types of far-off resonant (FOR) waves are assumed to be added into the cavity.

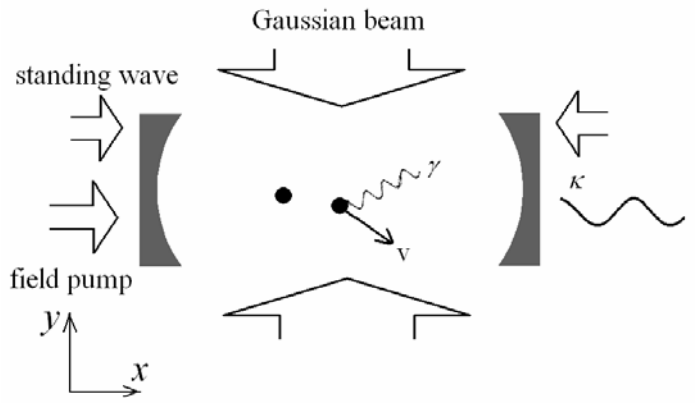

Fig. 2.5 Schematic representation of adding a standing wave or Gaussian beam

The effects of the FOR Gaussian beam in the transverse direction and the standing wave in Fig. 2.5 are different from the two coherent pump fields in Fig. 2.1. The interaction between the FOR laser and the particles can be treated conservatively and produces an extra dipole potential, which ultimately enhances the location and cooling process of the particles [2.21].

Now we consider the case of adding a transverse Gaussian beam with an intensity distribution given by

$$I(x) = I_0 g(t) \exp[-(\frac{x}{w_x})^{2n}] \tag{2.46}$$

where I_0 is the maximum intensity, w_x is the 1-D waist size, n is the order of the Gaussian beam and $g(t)$ is the normalized time-dependent function [2.48].

The dipole potential produced by the interaction is written as

$$U_G(x) = -\frac{1}{4}\alpha_p Z_0 I_0 g(t) \exp(-(\frac{x}{w_x})^{2n}) \tag{2.47}$$

where α_p is the polarizability of the atom or particle and Z_0 the impedance of the vacuum. For simplicity we consider the Gaussian field is constant by which $g(t)$=1.

We assume the maximum depth of the potential is a times the kinetic energy of the particle with momentum p_0, i.e.,

$$\Delta U_G = \frac{1}{4}\alpha Z_0 I_0 = -aKE = -a\frac{p_0^2}{2m}. \tag{2.48}$$

If we take the parameter $hk^2/(m\kappa)=1$, the force of this potential on the particle is

$$F_G = -U_G' = a\frac{p_0^2\kappa}{2\hbar k^2}(-2n\frac{x^{2n-1}}{w_x^{2n}}\exp(-(\frac{x}{w_x})^{2n})). \tag{2.49}$$

So the second equation in Eq. (2.44) can be modified to

$$\dot{p} = \hbar\kappa k U_0|\alpha|^2\sin(2kx) - an\frac{x^{2n-1}}{w_x^{2n}}\frac{p_0^2\kappa}{\hbar k^2}\exp(-(\frac{x}{w_x})^{2n}), \tag{2.50}$$

which corresponds to the potential

$$U = \hbar\kappa U_0|\alpha|^2\cos^2(kx) - a\frac{p_0^2\kappa}{\hbar k^2}\exp(-(\frac{x}{w_x})^{2n}). \tag{2.51}$$

Similarly, in the case of adding a standing wave, the potential term read as

$$U_S(x) = -\frac{1}{4}\alpha Z_0 I_0\cos^2(k_s x+\frac{\varphi}{2}), \tag{2.52}$$

where k_s is the wave number of the standing wave, $\frac{\varphi}{2}$ is the added phase.

In this case, the second equation in Eq. (2.44) is modified to

$$\dot{p} = \hbar\kappa k U_0|\alpha|^2\sin(2kx) - ak_s\frac{p_0^2\kappa}{2\hbar k^2}\sin(2k_s x+\varphi) \tag{2.53}$$

and the potential is

$$U = \hbar\kappa U_0|\alpha|^2\cos^2(kx) - a\frac{p_0^2\kappa}{\hbar k^2}(\cos^2(k_s x+\frac{\varphi}{2})). \tag{2.54}$$

The dipole potential produced by the transverse Gaussian beam can keep the particles with higher KE within a finite region of the cavity. This enables the particles to be continuously cooled down by the interaction between them and the intracavity field.

In the case where a standing wave is added, the effect of the added dipole potential can be shown in Fig. 2.6. The figure depicts the potential distributions along the cavity axis when the standing wave is added with a=1, $k_s = k/2$ and φ_n=π/3. U is the dipole potential between the particle and the introcavity field, U_S is between the particle and the added standing wave. For simplicity the potentials are both normalized.

U_S gives an extra force which localizes the particle to the high gradient part of the dynamic potential produced by the intracavity field. The cooling effect of the varying intracavity field is enhanced due to the longer time the particle spends in these regions.

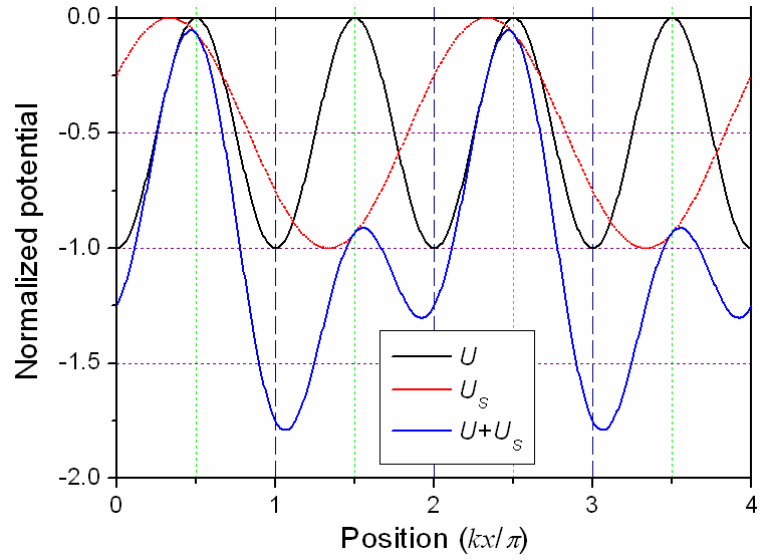

Fig. 2.6 The normalized distribution of potential

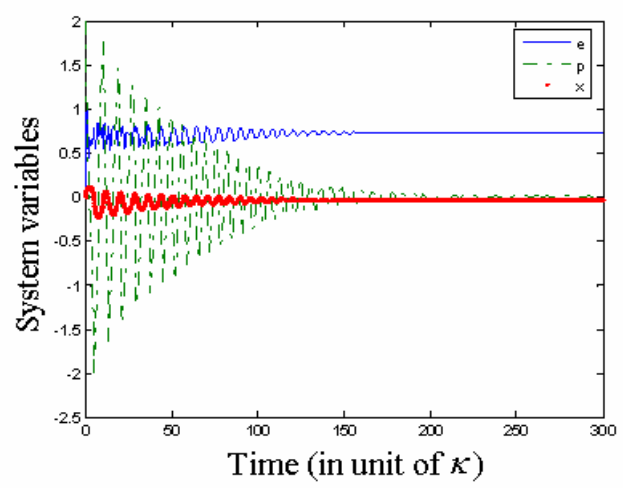

Fig. 2.7 Time evolution of the adding standing wave case

Fig. 2.7 shows the simulation results with the above setting. All the parameters are same as those in Fig. 2.3. It indicates that this method enhanced the cooling effect by comparing the final momentums of the particle of the two cases.

2.3.6 Cavity trapping and cooling many atoms

The dynamics of an atom in an optical cavity can be simulated based on the theoretical studies. The cooling effect caused by the atom-field interaction has been demonstrated experimentally. However, the normal cavity cooling scheme meets some limit when many-body atoms are applied. When an ensemble is placed in a cavity, it is

quite obvious that the dynamics of different atoms are coupled by interaction with the same field modes. The field intensity and phase modification induced by one atom is immediately felt by other remote atoms. The dipole-dipole and atom-atom interaction will strongly modify the cooling process in cavities yielding nontrivial scaling properties [2.6-2.9].

The classic model of single atom in this section can be expanded to the case of many-body atoms by treating the polarization term $P(x,t)$ in Eq. (2.37) as the sum of all the particles in the cavity

$$P(x,t)=\sum_{j=1}^{N}P_{\omega_A}(x,t)=ey_{\omega_A}(t)\delta(x-x_a)/A \tag{2.55}$$

The dynamic of each particle can be treated as one classical damped linear dipole oscillator. With the simple and similar induction, the equations for the field amplitude the forces, neglecting noise, are normalized as

$$\dot{\alpha}=[\frac{i\Delta_c}{\kappa}-1]\alpha-[\frac{\Gamma_0}{\kappa}+\frac{iU_0}{\kappa}]\sum_{j=1}^{N}\cos^2(x_{nj})\alpha+\eta$$

$$\dot{p}_{nj}=\frac{U_0}{\kappa}|\alpha|^2\sin(2x_{nj})$$

$$\dot{x}_{nj}=p_{nj}\cdot(\hbar k^2/(m\kappa)) \qquad (j=1\ldots N) \tag{2.56}$$

From the equations, we can find that each of the atoms leads to a frequency shift of the cavity mode according to its actual position. For each individual atom, the total shift induced by all the atoms hence defines an effective mode frequency. As this effective frequency determines the dynamic of the field intensity, one gets an effective atom-atom interaction mediated by the cavity mode. It can be concluded that the force on an atom depends on the positions of all atoms.

2.3.7 Dynamics of two particles case

For simplify, we only discuss the case of two atoms in a field mode.

Fig. 2.8 shows the time evolution of the field intensity and the momenta of two particles. The parameters are same as those in Fig. 2.3. The figure illustrates that the atoms are slowed down and trapped in an optical potential well after a short time. Subsequently the oscillations are cooled, but only until their motion becomes correlated in such a way that they oscillate almost undamped with a phase lag of 90°. We could

take the phase correlation of the two moving atoms into Eq. (2.56) and get the equation of a linear field equation, which has the effect to keep cooling the atoms.

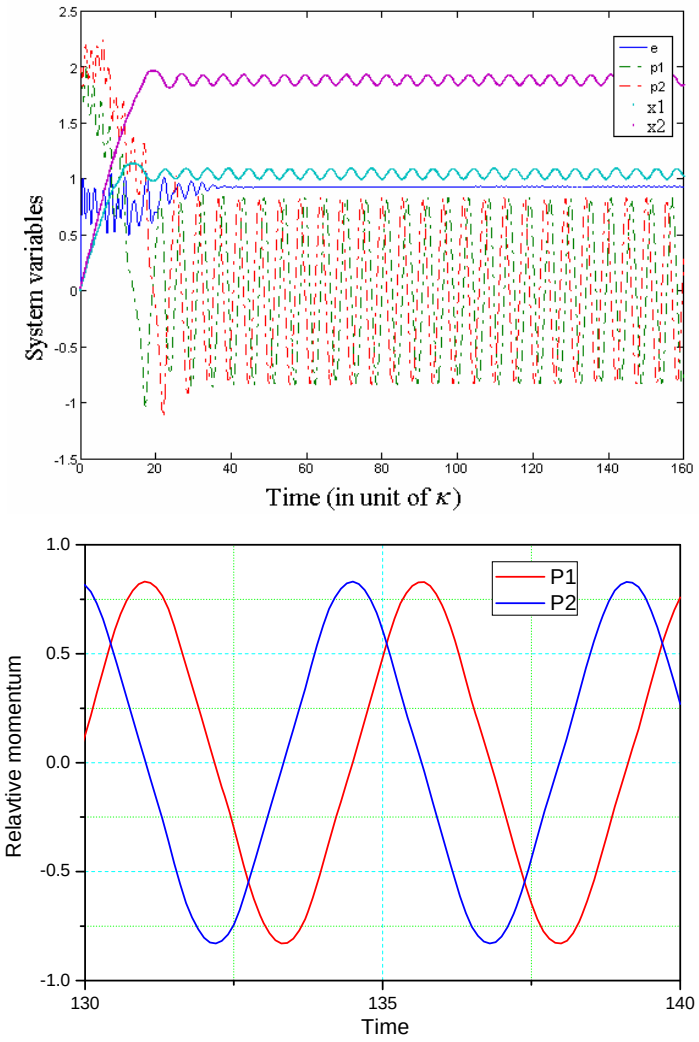

Fig. 2.8 Time evolution of two particles case

The dynamical simulation result for 10 particles is depicted in Fig. 2.9 and shows the stronger correlation. The particles can not be slow down and localized. The kinetic energy of the system which seems unstable can not be cooled down.

This type of correlation demonstratedby these examples of evolution is a kind of cavity-induced atom-atom interaction. As all particles are coupled to the same cavity mode, the modification of the field is related to the position of every particle inside the whole ensemble. The cavity cooling mechanism may become inefficient since the delicate dynamical correlation between one particle and the field mode could be perturbed by the motion of another particle.

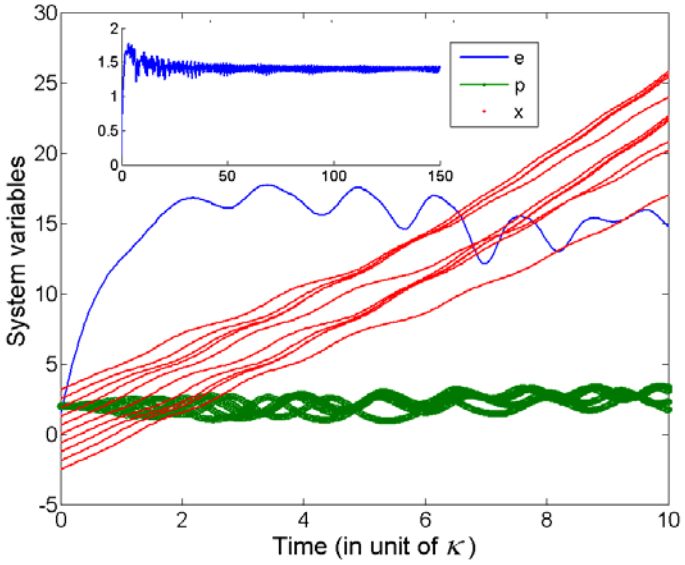

Fig. 2.9 Time evolution of the intracavity field intensity (e), momenta (p_n) and atomic positions (x_n) for the case of 10 particles with same initial momentums p_{ni}=2 and uniform position distribution in the space of [-π π]. The parameters are Δc=−4κ, U_0=−1κ, Γ_0=0.1κ, and η=2.5. The field intensity is multiplied by 10 in order to show it with the other two in the same scale. A long time evolution of the field intensity is shown on the upside.

Furthermore, it also shows that the buildup of correlations can decouple the particle and field motion and render the cooling process inefficient even if the Gaussian beam or the standing wave is added [2.6]. The dynamics of cooling particles in an optical cavity get to be unapproachable with this many-body problem even at a small density of the ensemble.

2.4 Multi Particles Case: Atomic Self-organization

J. K. Asboth *et al*. exploit the cavity-mediated atom-atom coupling [2.4, 2.7, 2.8], and present an extra phenomenon that leads to a dramatically different scaling behavior when the standing wave pump with a red atom-pump detuned field is sent into the cavity field from the sides instead of directly. For a single atom, this scattering pump only yields quantitative changes in driving efficiency, cooling rate and temperature, without drastic modifications of the system properties. However, when more atoms are put into the mode, a strong cooperative action between atom and atom

occurs, which leads to fast and efficient trapping and cooling of the whole ensemble. This effect is called “atomic self-organization”.

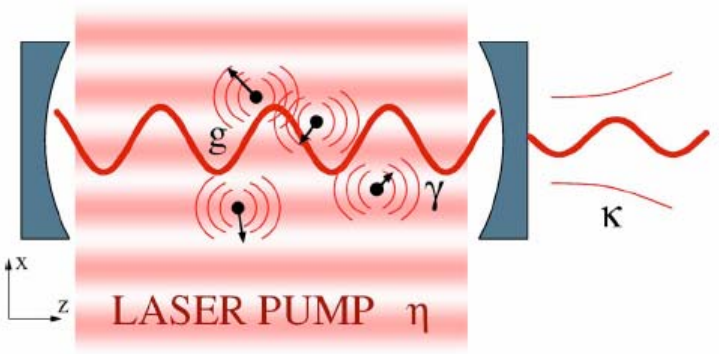

Fig. 2.10 Model of perpendicular pump case

In this case, photons of the pump light which is perpendicular to the cavity axis are coherently scattered by the atoms into the cavity field. The scattering strength of certain atoms is generally relative to its position in the cavity and pump fields. For example, in a standing-wave field with mode function cos(*kx*), a maximum scattering occurs from atoms close to antinodes while atoms in the nodes do not contribute. The phase of the coherent part of the scattered field is position dependent. For an ensemble of atoms with aninitially uniform distribution along the cavity axis, atoms are separated by half wavelength fields with opposite phase, which have been observed in an experiment by Black, Chan, and Vuletić [2.5]. This is also a kind of correlation between atoms in a cavity which cause their scattering contributions to cancel. Hence a coherent field can not build up for this destructive interference [2.4].

Owning to density fluctuations of the atoms, a small scattered field builds up with random phase. For a red detuned pump, thefield can create an attractive dipole potential for the atoms toward the antinodes of the cavity field. The effect can redistribute the atoms and lead to a periodic localization. More atoms usually with smaller kinetic energies can be located into this potential and thus enhance the scattering field. Therefore the periodic potential is in turn further self deepened.

With suitable operating conditions, the cavity cooling effect can be available to these atoms by the cavity loss dissipating the kinetic energy, which ultimately leads to stable trapping. For the counteracted heating processes, such as spontaneous emission and cavity intensity fluctuations, the system will reach a stable state at some finite atomic position spread.

As an attractive development in cavity cooling many-body schemes, atomic self-organization has been tested and applied experimentally. For the advantage of the cavity cooling method, a similar effect may be applied to many-body molecules. However, duo to the weak coupling strength and other properties, the possibility of self-organization of molecules still needs to be investigated under laboratory conditions. On the other side, most of the discussions are based on the steady state. The study of such cooling and trapping process simulations will be interesting. The extension from current near-off resonant to far-off resonant cavity cooling based on this effect is also attractive. In the following chapters, we will discuss these contents in detail.

2.5 References

[2.1] P. Horak, G. Hechenblaikner, K. M. Gheri, H. Stecher, and H. Ritsch, *Cavity-Induced Atom Cooling in the Strong Coupling Regime*, Physical Review Letters, 79, 4974-4977 (1997).

[2.2] V. Vuletic and S. Chu, *Laser Cooling of Atoms, Ions, or Molecules by Coherent Scattering*, Physical Review Letters, 84, 3787-3790 (2000).

[2.3] P. Maunz, T. Puppe, I. Schuster, N. Syassen, P. W. H. Pinkse, and G. Rempe, *Cavity cooling of a single atom*, Nature, 428, 50-52 (2004).

[2.4] P. Domokos and H. Ritsch, *Collective Cooling and Self-Organization of Atoms in a Cavity*, Physical Review Letters, 89, 253003-1-4 (2002).

[2.5] H. W. Chan, A. T. Black, and V. Vuletic, *Observation of Collective-Emission-Induced Cooling of Atoms in an Optical Cavity*, Physical Review Letters, 90, 063003-1-4 (2003).

[2.6] J. K. Asboth, P. Domokos, and H. Ritsch, *Correlated Motion of Two Atoms Trapped in a Single-mode Cavity Field*, Physical Review A, 70, 013414-1-11 (2004).

[2.7] W. Vogel and D. G. Welsch, *Quantum Optics, Third, revised and extended edition*, WILEY-VCH Verlag GmbH & Co. KGaA, Weinheim (2006).

[2.8] J. K. Asboth, P. Domokos, H. Ritsch, and A. Vukics, *Self-organization of atoms in a cavity field: Threshold, bistability, and scaling laws*, Physical Review A, 72, 053417-1-12 (2005).

[2.9] J. K. Asboth, *Interaction between optically trapped particles due to optomechanical coupling*, PhD Thesis (2008)

[2.10] P. Domokos and H. Ritsch, *Mechanical effects of light in optical resonators*, Journal of the Optical Society of America B-Optical Physics, 20, 1098-1130 (2003).

[2.11] P. Meystre and M. Sargent III, *Elements of Quantum Optics*, Springer Berlin Heidelberg, New York (2007).

[2.12] G. Johansson and T. Bauch, *Quantized electromagnetic field and the Jaynes-Cummings Hamiltonian*, Lectures in Quantum Informatics.

[2.13] Y. T. Chough, J. B. Kim, and K. W. An, *Single Dressed-Atom Laser: Lasing Out of a Driven Jaynes-Cummings System*, CLEO, 876-877 (1999).

[2.14] R. Tanas, *Two-Level atom in a squeezed vacuum*, Turkish Journal of Physics, 23, 861-868 (1999).

[2.15] M. Trupke, J. Goldwin, B. Darquie, G. Dutier, S. Eriksson, J. Ashmore, and E. A. Hinds, *Atom Detection and Photon Production in a Scalable, Open, Optical Microcavity*, Physical Review Letters, 99, 063601-1-4 (2007).

[2.16] P. Domokos, P. Horak, and H. Ritsch, *Semiclassical theory of cavity-assisted atom cooling*, Journal of Physics B: Atomic, Molecular and Optical Physics, 34, 187-198 (2001).

[2.17] C. Maschler, H. Ritsch, *Quantum motion of laser-driven atoms in a cavity field*, Optics Communications, 243, 145-155 (2004).

[2.18] J. Dalibard and C. Cohen-Tannoudji, *Atomic motion in laser light: connection between semiclassical and quantum descriptions*, Journal of Physics B: Atomic, Molecular and Optical Physics, 18, 1661-1683 (1985).

[2.19] G. Hechenblaikner, M. Gangl, P. Horak, and H. Ritsch, *Cooling an atom in a weakly driven high-Q cavity*, Physical Review A, 58, 3030-3042 (1998).

[2.20] S. Zippilli, J. Asboth, G. Morigi, and H. Ritsch, *Forces and spatial ordering of driven atoms in a resonator in the regime of fluorescence suppression*, Applied Physics B: Lasers and Optics, 79, 969-978 (2004).

[2.21] G. Dong, S. Edvadsson, W. Lu, and P. F. Barker, *Super-Gaussian mirror for high-field-seeking molecules*, Physical Review A, 72, 031605-1-4 (2005).

Chapter 3

Trapping and cooling many molecules

3.1 Introduction

The spatial self-organization of atoms in a cavity occurs when a detuned pump is sent into the cavity from the direction perpendicular to the cavity axis. This scheme can reduce or eliminate the undesirable atom-atom correlations. It has demonstrated significant enhancement of the cooling process through the collective dynamics of many body species.

Compared with two-level atoms that are pumped typically at visible to infrared wavelengths, with 100 MHz-10 GHz detuning from the resonance transition, the pump frequency required for a rotational-vibrational transition of molecules is in the UV and VUV regions for most molecules and we have to take into account the limited availability of laser sources and high finesse cavity optics in these frequency regions. Also the dipole momentum strengths of molecules corresponding to these transitions are generally much weaker than those of well-studied atoms such as Rubidium, which will lead to significant differences in the operating conditions between the two. The work may provide several new and important findings beyond the scope of previous investigations on cooling atoms in optical cavities.

In this chapter we explore how this transverse cavity cooling scheme can be extended to diatomic molecules. In section 3.2, we discuss how to extend the cavity cooling casefrom atoms to molecules. A semiclassical model for this scheme is introduced, which give us a powerful conclusion for the numerically dynamic simulation in section 3.3. After that, we discuss the theoretical and experimental limitations of conditions in this model in section 3.4. As an example, we study cooling of a CN molecular gas in a millimeter-long optical cavity.

3.2 From Atoms to Molecules

When we study cavity cooling scheme for molecules, we should first discuss some characteristics specific to molecules.

3.2.1 Electric dipole moment of molecules

The electric dipole moment of a molecule in a light field usually includes two parts: a permanent dipole moment and an induced dipole moment [3.1-3.2]. The molecule whose permanent dipole moment is equal to zero ($\boldsymbol{\mu}= 0$) is of non-polar type. The other is a polar molecule. In an electric $\boldsymbol{E}$, both types of molecules have an induced dipole moment given by $\alpha\cdot\boldsymbol{E}$, where α is a polarizability tensor. For a molecule in an optical field, the dipole moment **d** is equal to $\boldsymbol{\mu}+\alpha\cdot\boldsymbol{E}$. The interaction Hamiltonian between the optical field and molecules can be written as

$$H_{\text{int}} = -\,\mathbf{d}\cdot\boldsymbol{E} = \boldsymbol{\mu}\cdot\boldsymbol{E} + \frac{1}{2}\alpha\cdot\boldsymbol{E}\boldsymbol{E} \tag{3.1}$$

Usually the order of magnitude of the transition dipole moment μ is about 10^{-30} C·m in SI units, while the polarizability is about 10^{-40} $C^2m^2J^{-1}$. As to be discussed in the following chapters, almost all current discussions of the cavity cooling have two limitations, low saturation with a relatively low intracavity field and on effective pump in the near off-resonant region rather than a far off-resonant region. The interaction magnitude of the induced dipole moment is usually far less than that of the permanent dipole moment in this case. However, the far-off resonant cavity cooling will be proposed in Chapter 5 to achieve trapping of a huge ensemble of molecules. Therefore, we mainly discuss the molecular transition dipole moment first.

Due to the complex energy structure of molecule, the interaction between the molecule and the light field generally involves multiple molecular energy levels. A two-level model may not be enough to describe all the possible transitions.

For a spontaneous emission transition of a particle, the Einstein A coefficient, i.e. the Einstein transition probability, between specified ro-vibrational states, an upper level (ν', J') and a lower level (ν'', J'') , is given by the expression

$$A_{\nu''J''}^{\nu'J'} = \frac{64\pi^4}{3h} p_{\nu''J''}^{\nu'J'} (\upsilon_{\nu''J''}^{\nu'J'})^3 \tag{3.2}$$

where $\upsilon_{\nu''J''}^{\nu'J'}$ is the transition frequency and $p_{\nu''J''}^{\nu'J'}$ is the transition probability which are the integrals of the ro-vibrational wave functions of the upper and lower states together

with the electronic transition moment:

$$p_{v''J''}^{v'J'} = \left| \int \Psi_{v'J'}(r)\,\mathrm{Re}(r)\Psi_{v''J''}(r)dr \right|^2 \tag{3.3}$$

In this equation, the Born-Oppenheimer approximation is assumed and Re(r) is the electronic transition moment [3.3-3.5]. According to the work of Schadee and others, the rotational wave functionswhich can be separated from the above convolution and Eq. (3.3) can be written as

$$p_{v''J''}^{v'J'} = \left(\frac{g_e'}{g_e''} \left| \int \Psi_{v'}(r)\,\mathrm{Re}(r)\Psi_{v''}(r)dr \right|^2 \beta_{J''}^{J'} \right) \tag{3.4}$$

In the expression, the electronic degeneracy is $g_e = (2-\delta_{\mathrm{O},\Lambda})(2S+1)$, where $2S$+1 is the state spin multiplicity, and $\delta_{\mathrm{O},\Lambda}$=1 for Σ state and 0 for all the others. $\left| \int \Psi_{v'}(r)\,\mathrm{Re}(r)\Psi_{v''}(r)dr \right|^2$ is only related to the vibration states and equal to the square of the transition dipole moment

$$\mu_{v'v''}^2 = \left| \langle v' | er | v'' \rangle \right|^2 \equiv e^2 r_{v'v''}^2 \tag{3.5}$$

Another term $\beta_{J''}^{J'}$ is the rotational line strength usually expressed as

$$\beta_{J''}^{J'} = \frac{S_{J''}^{J'}}{2J'+1} \tag{3.6}$$

and $S_{J''}^{J'}$ is the Honl-London rotational intensity factor, i.e. the line strength.

3.2.2 Line strength

The intensity of all possible transitions of a molecule in thermal equilibrium usually may be expressed, apart from a constant and from the frequency factor, as a product of the lines strength S_J and the Boltzmann distribution factor [3.6].

The precise formula for the line strengths of the symmetric top, which are independent of whether or not thermal equilibrium applies, were first given by Honl and London based on the old quantum theory. They were later derived on the basis of wave mechanics by Dennison, Reiche and Rademacher, and other researchers.

The formula, which is called the Honl-London formulae, can be written in different forms according to the status of different transitions. For a transition with $\Delta\Lambda = \Lambda' - \Lambda'' = 0$, where Λ is the quantum number of the angular momentum of the molecule, the formulae are

$$S_J^R = \frac{(J''+1+\Lambda'')(J''+1-\Lambda'')}{J''+1} = \frac{(J'+\Lambda')(J'-\Lambda')}{J'}$$

$$S_J^Q = \frac{(2J''+1)\Lambda''^2}{J''(J''+1)} = \frac{(2J'+1)\Lambda'^2}{J'(J'+1)}$$

$$S_J^P = \frac{(J''+\Lambda'')(J''-\Lambda'')}{J''} = \frac{(J'+1+\Lambda')(J'+1-\Lambda')}{J'+1} \tag{3.7}$$

For $\Delta\Lambda = +1$

$$S_J^R = \frac{(J''+2+\Lambda'')(J''+1+\Lambda'')}{4(J''+1)} = \frac{(J'+\Lambda')(J'-1+\Lambda')}{4J'}$$

$$S_J^Q = \frac{(J''+1+\Lambda'')(J''-\Lambda'')(2J''+1)}{4J''(J''+1)} = \frac{(J'+\Lambda')(J'+1-\Lambda')(2J'+1)}{4J'(J'+1)}$$

$$S_J^P = \frac{(J''-1-\Lambda'')(J''-\Lambda'')}{4J''} = \frac{(J'+1-\Lambda')(J'+2-\Lambda')}{4(J'+1)} \tag{3.8}$$

and for $\Delta\Lambda = -1$

$$S_J^R = \frac{(J''+2-\Lambda'')(J''+1-\Lambda'')}{4(J''+1)} = \frac{(J'-\Lambda')(J'-1-\Lambda')}{4J'}$$

$$S_J^Q = \frac{(J''+1-\Lambda'')(J''+\Lambda'')(2J''+1)}{4J''(J''+1)} = \frac{(J'-\Lambda')(J'+1+\Lambda')(2J'+1)}{4J'(J'+1)}$$

$$S_J^P = \frac{(J''-1+\Lambda'')(J''+\Lambda'')}{4J''} = \frac{(J'+1+\Lambda')(J'+2+\Lambda')}{4(J'+1)} \tag{3.9}$$

Here the superscript R, Q, or P indicates the branch for which the particular expression holds ($\Delta J = +1,0,-1$, respectively). Of the two alternative forms given the first is more useful for absorption, the second for emission, since the Boltzmann factor contains J'' and J', respectively.

For the emission transition, the normalization of Honl-London factor is as suggested by Whiting [3.7]:

$$\sum_{J''} S_{J''}^{J'} = (2-\delta_{O,\Lambda})(2S'+1)(2J'+1) \tag{3.10}$$

For an absorption transition, the Einstein absorption coefficient is given by Schadee [3.5] as

$$B_{v'J'}^{v''J''} = \frac{c^2}{8\pi h((\upsilon_{v''J''}^{v'J'})^3)} \frac{2J'+1}{2J''+1} A_{v''J''}^{v'J'} = \frac{8\pi^3 c^2}{3h^2} \frac{g_e'}{g_e''} \frac{S_{J''}^{J'}}{2J''+1} \mu_{v'v''}^2 \tag{3.11}$$

and the normalization is as

$$\sum_{J'} S_{J'}^{J''} = (2-\delta_{O,\Lambda})(2S''+1)(2J''+1) \tag{3.12}$$

According to the above discussion, we can deal the case of the transition of molecules. For simplicity, we only consider all possible rotational transitions of an absorption transition from a certain lower level (ν'', J''). The transition probability, i.e. the square of dipole moments can be expressed as a sum of

$$\sum \mu_{abs}^2 = \sum_{J'} u_{v'J',v''J''}^2 = \frac{\sum_{J'} g_e' S_{J'}^{J''} \mu_{v'v''}^2}{g_e''(2J''+1)} \tag{3.13}$$

Similarly, the formula of a spontaneous emission transition is written as

$$\sum \mu_{spo}^2 = \mu_{v'v''}^2 \frac{\sum_{J''} g_e'' S_{J''}^{J'}}{g_e'(2J'+1)} \tag{3.14}$$

Eq. (3.13) and (3.14) indicate that the transitions model of molecules can be treated as a sum of several two-level models with different weighted factors, as shown in Fig. 3.1.

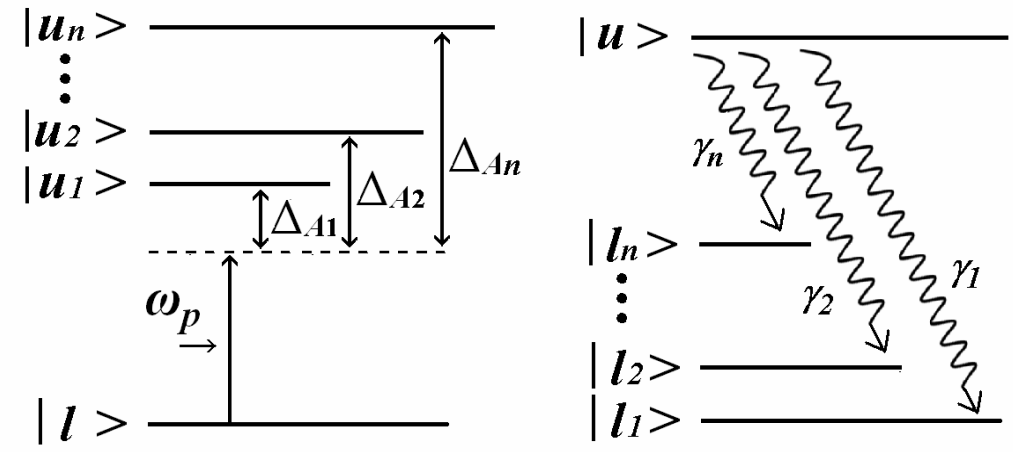

(a) **(b)**

Fig. 3.1 (a) An absorption transition model of a molecule on lower level l in an optical field with frequency ω_p. The detuning between pump and the lowest upper level u_1 is Δ_{A1}. (b) A spontaneous emission transition model of a molecule on upper level u.

However, if the molecule is located on a state which possesses either up or down transition, the model becomes much more complex and intractable. Therefore some consideration about our general cooling model should be discussed.

3.2.3 Conditions and limitations

As discussed in section 3.2.2, the distribution of an ensemble of molecules in thermal equilibrium obeys the Boltzmann distribution law as

$$N_{v,J} = N_0 \cdot f(v,J) = N_0 \cdot \frac{e^{-\frac{E_v(v)}{kT_{vib}}} \cdot (2J+1) \cdot e^{-\frac{E(J)}{kT_{rot}}}}{Q_{vib} \cdot Q_{rot} \cdot Q_{elec}} \tag{3.15}$$

where N_0 is the total number densityof molecules in the system, and $f_B(v, J)$ is the Boltzmann function, $E_v(v) = (v + \frac{1}{2})\hbar\omega_e$ is the vibrational state energy, $E_v(v) = BJ(J+1)$ is the rotational state energy, Q_{elec} is theelectronic partition function (Q_{elec}= g_e). Q_{vib} and Q_{rot} are the sums of the rotational and vibrational partitions calculated numerically.

In our QED cooling model, we consider stationary cold molecules, which could be created by using some schemes, such as optical Stark deceleration and buffer gas cooling. For this gas ensemble which could be at a few K or even the hundred mK range, only the lowest ro-vibrational energy level is populated according to the Boltzmann distribution.

For example, we assume an ensemble of CN molecules. The vibrational frequency ω_e of the CN molecule is about 2069 cm^{-1} ($X\ ^2\Sigma^+$) and 2164 cm^{-1} ($A^2\Sigma^+$), and the rotational constant B_e is about 1.9 cm^{-1} and 1.97 cm^{-1} accordingly. When the ro-vibrational temperature of the system is assumed to be equal to the kinetic temperature around 10K, 100% of molecules are on the lowest vibration state, in which more than 99% are on the lowest 4 rotation states $X\ ^2\Sigma^+$ ($N'' = 0$ to 3). If the rotational temperature is below 1K, more than 98.7% are on the lowest rotation state $X\ ^2\Sigma^+$ ($N'' = 0, J'' = 1/2$). Under the initial temperature conditions, only the possible absorption transitions need to be considered.

On the other side, the pump frequency ω_p is set to be off-resonant from the lowest possible transition frequency ω_{A1}. Due to the off-resonant nature of the interactions, molecular population transitions are suppressed, or even neglected when the detuning is large. And the upper levels are consequently almost unpopulated. More details will be introduced in the next section.

3.2.4 General model for cavity cooling of molecules

Based on the above discussion and limitations, the cavity cooling of molecules can be dealt with physical model and mathematical analysis according to a similar way to that of the atom already derived in Chapter 2. In this section, first we need to obtain the quantum master equation of the general model of cavity cooling of molecules.

Follow the same step in section 2.2, section 3.2.2 and Eq. (2.9), the interaction Hamiltonian H_{int} between a molecule and one single cavity field can be written as

$$H_{\text{int}} = -i\hbar\sum_{s} g_s(x)(\sigma_s^{+} + \sigma_s^{-})(a - a^{\dagger}) \tag{3.16}$$

where $g_s(x)$ is the coupling strength of each possible rotational transition:

$$g_s(x) = (\boldsymbol{u_s}\cdot \boldsymbol{\varepsilon} E/\hbar)\cos(kx) \tag{3.17}$$

where $\boldsymbol{u_s}$ is each transition dipole moment.

For the general model of cavity cooling molecules, the total Hamiltonian is written as

$$H = \sum_{a=1}^{N}[\frac{\hat{p}_a^2}{2m} - \hbar\sum_{s}(\Delta_s\sigma_{a,s}^{z})] - \hbar\Delta_c a_n^{\dagger}a_n - i\hbar\sum_{n=1}^{M}\sum_{a=1}^{N}[\sum_{s}\left(g_{n,s}(\hat{x}_a)(\sigma_{a,s}^{\dagger}a_n - a_n^{\dagger}\sigma_{a,s})\right)]$$

$$-\sum_{n=1}^{M}[i\hbar\eta_n(a_n - a_n^{\dagger})] - i\hbar\eta_t[\sum_{s}h_s(\hat{y}_a)\sigma_{a,s}^{\dagger} - h_s^{*}(\hat{y}_a)\sigma_{a,s}] \tag{3.18}$$

The Liouville terms can be written as

$$L\rho = \sum_{m=1}^{M}\kappa_n(2a_n\rho a_n^{\dagger} - a_n^{\dagger}a_n\rho - \rho a_n^{\dagger}a_n)$$

$$+\sum_{a=1}^{N}\sum_{s}\left(\gamma_s(2\int N(\mathbf{n})\mathrm{d}^2\mathbf{n}\exp(-i\hbar k_s\,\mathbf{n}\,\hat{x}_a)\sigma_{a,s}\rho\exp(i\hbar k_s\,\mathbf{n}\,\hat{x}_a)\sigma_{n,s}^{\dagger} - \sigma_{a,s}^{\dagger}\sigma_{a,s}\rho - \rho\sigma_{a,s}^{\dagger}\sigma_{a,s})\right) \tag{3.19}$$

For simplicity, the photon operator of all the possible transitions with off-resonant pump is generated in our model. There is no general solution for this master equation (3.18), and even a numerical approach seems feasible only for very simple examples. In the following we resort to further approximations to render the problem into a tractable form for analytic treatment or numerical simulation.

3.2.5 Dynamical equations for cavity cooling of molecules

From the discussion in section 3.2.3, the dipole moment of a molecule can be treated as a cumulative effect of all the possible electronic transitions which correspond

to the electrons harmonically bound to the nuclear with eigen frequencies ω_{Ak}. Similar to Eq. (2.37), the polarization density of a molecule at position x_a can be written as

$$P(x,t) = \sum_k P_{\omega_{Ak}}(x,t) = \sum_k e y_{\omega_{Ak}}(t)\delta(x - x_a)/A \tag{3.19}$$

The oscillator model of a molecule therefore consists of a set of equations of the form

$$\ddot{y}_{\omega_{Ak}}(t) + 2\gamma_k \dot{y}(t) + \omega_{Ak}^2 y(t) = \frac{e}{m} E(x_a, t) \tag{3.20}$$

Following the same operation, the total polarization of a molecule reads is written as

$$P(t) = i\frac{e^2}{m\omega_p V}\varepsilon(t)\cos^2(kx_a)\sum_k \frac{1}{(\gamma_k - i\Delta_{Ak})} \tag{3.21}$$

The weight factors $\beta_{\omega_{Ak}}$ should be added into each term when the effect of the line strength is considered.

After a series of similar operations, we can get the same equations as Eq. (2.45), while the combined molecular polarization can be written as

$$U_0 = \sum_k \frac{\Delta_{Ak}}{\gamma_k^{\,2} + \Delta_{Ak}^2} g_{\omega k}^2 \tag{3.22a}$$

$$\Gamma_0 = \sum_k \frac{\gamma_k}{\gamma_k^{\,2} + \Delta_{Ak}^2} g_{\omega k}^2 \tag{3.22b}$$

Eq. (3.22) shows that the interaction between the light field and the molecule can be treated as the case of a quasi-atom.

3.3 The Semiclassical Model of Molecular Self-organization

An ensemble of atoms in optical cavity can self organiz with a transverse driving optical field, which can lead to cavity trapping and cooling. Generally the scattered photon numbers involved in this scheme are very high. Therefore, the intracavity field modes can be represented as coherent and time-dependent complex amplitudes with some fluctuations [3.8]. A semiclassical model for cavity cooling of atoms in this case was presented by P. Domokos and H. Ritsch [3.9]. This semicalssical model can be extended to the case of molecules.

3.3.1 The model of transverse pump

Based on the discussion in section 2.5, a dipole potential is built up due to the interaction between the scattered field and self-organized particles. The motion of one particle can be generally approximated by stochastic Brownian motion in a potential, which varies following time-dependent conservative forces, dissipation and noise. In statistical physics, this motion can be described by a set of Langevin equations as

$$\dot{x} = p / m \tag{3.23a}$$

$$\dot{p} = f - \beta \frac{p}{m} + \xi \tag{3.23b}$$

In the above equations, f is the conservative force, β is the linear friction tensor, and ξ is the noise term which describes the fluctuation. With the Markoff approximation, which assumes that this correlation time is extremely short compared to evolution time of the system, this white-noise term has zero mean and second order correlation function

$$\left\langle \xi(t) \otimes \xi(t') \right\rangle = D\delta(t - t')$$

where D is the diffusion coefficient. Eq. (3.23) can be extended to multi-particle case.

The master equation of the general cavity cooling model for molecules is obtained as Eq. (2.22), Eq. (3.18) and Eq. (3. 91). Now we only consider the case of a single intracavity mode. In the Heisenberg picture, the internal variables of this system obey the following quantum Langevin equations [3.10]:

$$\dot{a} = (i\Delta_c - \kappa)a + \sum_{j=1}^{N} \sum_{s} g_s f^*(\hat{x}_j)\sigma_{j,s} + \eta + \xi_a , \tag{3.24a}$$

$$\dot{\sigma}_{j,s} = (i\Delta_s - \gamma_s)\sigma_{j,s} + 2\sigma_{j,s}^z g_s f(\hat{x}_j)a + 2\sigma_{j,s}^z \eta_t h(\hat{y}_j) + \xi_j , \tag{3.24b}$$

where ξ_a and ξ_j are the Langevin white-noise operators, suffix j is the molecule number, and s indicates one of the possible transitions of the molecules.

When the pump detuning Δ_s or the damping rate γ_s is large, the population in the excited atomic state can be adiabatically eliminated, for example, $\left\langle \sigma_{j,s}^z \right\rangle \approx \frac{1}{2}$. In the case of this low saturation regime, the induced polarization of the particles in steady state of Eq. (3.24b) can be approximately written as

$$\sigma_{j,s} \approx \frac{g_s}{i\Delta_s - \gamma_s}\left(f(\hat{x})a + \frac{\eta_t h(y)}{g_s} \right) = \frac{g_s}{i\Delta_s - \gamma_s}\hat{E}_s(\hat{x}) \tag{3.25}$$

where $\hat{E}_s(\hat{x})$ can be treated as the total dimensionless field operator, and only the effect on the cavity axis x is considered. In numerical analysis, the fluctuation of the inversion population can be set with $\left\langle \sigma_j^z + \frac{1}{2} \right\rangle \le 0.1$ for atoms. However, for molecules, a more strictly limitation $\left\langle \sum_s \sigma_{j,s}^z + \frac{1}{2} \right\rangle \le 0.01 \sim 0.05$ should be adopted due to their multi decay transitions, as discussed in section 2.3 [3.8, 3.26].

The effective Hamiltonian and Liouville operators after adiabatic elimination as

$$H_{eff} = \sum_{j=1}^{N} \frac{\hat{p}_j^2}{2m} - \hbar\Delta_c a^\dagger a - i\hbar\eta(a - a^\dagger) - i\hbar \sum_{j=1}^{N} \sum_s g_s [E_s(\hat{x}_j)\sigma_{j,s}^\dagger - E_s^\dagger(\hat{x}_j)\sigma_{j,s}],$$

$$= \sum_{j=1}^{N} \frac{\hat{p}_j^2}{2m} - \hbar\Delta_c a^\dagger a - i\hbar\eta(a - a^\dagger) + \hbar \sum_{j=1}^{N} \sum_s [U_{0s} E_s^\dagger(\hat{x}_j) E_s(\hat{x}_j)] \tag{3.26}$$

The Liouville terms are

$$L\rho = \kappa(2a\rho a^\dagger - \{a^\dagger a, \rho\})$$

$$+ \sum_{j=1}^{N} \sum_s \Gamma_{0s} (2 \int N(\mathbf{n}) \mathrm{d}^2\mathbf{n} \exp(-i\hbar k_s \mathbf{n}\, \hat{x}_s) E_s(\hat{x}_j) \rho \exp(i\hbar k_s \mathbf{n}\, \hat{x}_s) E_s^\dagger(\hat{x}_s)$$

$$- \{E_s^\dagger(\hat{x}_a) E_s(\hat{x}_a), \rho\}) \tag{3.27}$$

where $U_{0s} = \frac{\Delta_s}{\gamma_s^2 + \Delta_s^2} g_s^2$, $\Gamma_{0s} = \frac{\gamma_s}{\gamma_s^2 + \Delta_s^2} g_s^2$.

To represent the particle's motion and the state of the cavity light field in the total phase space, the joint Wigner function $W(\alpha, \alpha^*, x, p)$ is very well adapted to derive semiclassical equations from the quantum model [3.8, 3.11]. The Wigner transform of the quantum master equation leads to a partial differential equation, which is truncated at second-order derivatives to yield a Fokker–Planck-type equation, which can effectively be numerical simulated [3.14].

In this representation, The Wigner function can be defined as

$$W(\alpha, \alpha^*, x, p) =$$

$$\frac{1}{\pi^2} \int d\zeta \exp[i(\alpha\zeta + \alpha^*\zeta^*)] Tr \left[\frac{\exp[-i(a\zeta + a^\dagger\zeta^*)]}{\frac{1}{2\pi\hbar} \int d\xi \exp(-\frac{i}{\hbar} p\xi) \left\langle x + \frac{1}{2}\xi \middle| \hat{\rho} \middle| x + \frac{1}{2}\xi \right\rangle} \right]$$

$$= \frac{1}{2\pi\hbar} \int d\xi \exp(-\frac{i}{\hbar} p\xi) \left\langle x + \frac{1}{2}\xi \middle| f(\alpha, \alpha^*) \middle| x + \frac{1}{2}\xi \right\rangle \tag{3.28}$$

where

$$f(\alpha,\alpha^*)=\frac{1}{\pi^2}\int d\zeta\exp[i(\alpha\zeta+\alpha^*\zeta^*)]Tr\{\exp[-i(a\zeta+a^\dagger\zeta^*)]\hat{\rho}\} \tag{3.29}$$

For the operator $G(\hat{x})$ on the density matrix, we have the relationship as [3.12]

$$\frac{1}{\pi^2}\int d\zeta\exp[i(\alpha\zeta+\alpha^*\zeta^*)]Tr\left[\frac{\exp[-i(a\zeta+a^\dagger\zeta^*)]}{\frac{1}{2\pi\hbar}\int d\xi\exp(-\frac{i}{\hbar}p\xi)\left\langle x+\frac{1}{2}\xi\middle|G(\hat{x})a\hat{\rho}\middle|x+\frac{1}{2}\xi\right\rangle}\right]$$

$$\approx\frac{1}{\pi^2}\int d\zeta\exp[i(\alpha\zeta+\alpha^*\zeta^*)]Tr\left[\frac{\exp[-i(a\zeta+a^\dagger\zeta^*)]}{\frac{1}{2\pi\hbar}\int d\xi\exp(-\frac{i}{\hbar}p\xi)\left\langle x+\frac{1}{2}\xi\middle|G(x)a\hat{\rho}\middle|x+\frac{1}{2}\xi\right\rangle}\right]$$

$$+i\hbar\frac{1}{\pi^2}\int d\zeta\exp[i(\alpha\zeta+\alpha^*\zeta^*)]\frac{\partial}{\partial p}Tr\left[\frac{\exp[-i(a\zeta+a^\dagger\zeta^*)]}{\frac{1}{2\pi\hbar}\int d\xi\exp(-\frac{i}{\hbar}p\xi)\left\langle x+\frac{1}{2}\xi\middle|\partial_x G(x)a\hat{\rho}\middle|x+\frac{1}{2}\xi\right\rangle}\right]$$

$$=(\alpha+\frac{1}{2}\frac{\partial}{\partial\alpha^*})W(\alpha,\alpha^*,x,p)+\hbar\alpha\left[\frac{1}{2}\partial_x G(x)\right]\partial_p W(\alpha,\alpha^*,x,p)$$

$$+i\hbar\frac{1}{\pi^2}\int d\zeta\exp[i(\alpha\zeta+\alpha^*\zeta^*)]\frac{\partial}{\partial p}Tr\left[\frac{\exp[-i(a\zeta+a^\dagger\zeta^*)]}{\frac{1}{2\pi\hbar}\int d\xi\exp(-\frac{i}{\hbar}p\xi)\left\langle x+\frac{1}{2}\xi\middle|\partial_x G(x)a\hat{\rho}\middle|x+\frac{1}{2}\xi\right\rangle}\right] \tag{3.30}$$

The first two terms in Eq. (3.30) show the method to deal with the operator which includes the function of position $G(x)$.

According to the Wigner transform relationships obtained from Eq. (3.28) and Eq. (3.30), the quantum master equation can be written as partial differential equations of evolution for $W(\alpha,\alpha^*,x,p)$, and truncated at second-order derivatives to yield a Fokker–Planck-type equation with the form

$$\frac{\partial f}{\partial t}=-\sum_{c_1}\frac{\partial}{\partial c_1}[D^1_{c1}(\alpha,\alpha^*,x,p)f]+\sum_{c_1}\sum_{c_2}\frac{\partial^2}{\partial c_1\partial c_2}[D^2_{c1c2}(\alpha,\alpha^*,x,p)f] \tag{3.31}$$

where D^1 is the linear friction term, D^2 is the diffusion term, c_1 and c_2 represent the set of macro variables. This equation describes the time evolution of the probability density function of the position of a particle, and can be generalized to other observables as well.

The Fokker-Planck Equation for the combined molecule-field Wigner function reads

$$\frac{d}{dt}W = \{i\Delta_c(-\frac{\partial}{\partial\alpha}\alpha + \frac{\partial}{\partial\alpha^*}\alpha^*) - \eta(\frac{\partial}{\partial\alpha} + \frac{\partial}{\partial\alpha^*})$$
$$- i\sum_{j=1}^{N}\sum_s U_{0s}[f^*(x_j)f(x_j)(-\frac{\partial}{\partial\alpha}\alpha + \frac{\partial}{\partial\alpha^*}\alpha^*) + \frac{\eta_t h(y_j)}{g}f^*(x_j)\frac{\partial}{\partial\alpha} - (\frac{\eta_t h(y_j)}{g})^* f(x_j)\frac{\partial}{\partial\alpha^*}]\}W$$
$$+ \{\kappa(\frac{\partial}{\partial\alpha}\alpha + \frac{\partial}{\partial\alpha^*}\alpha^* + \frac{\partial^2}{\partial\alpha\partial\alpha^*}) + \sum_{j=1}^{N}\sum_s \Gamma_{0s}[f^*(x_j)f(x_j)(\frac{\partial}{\partial\alpha}\alpha + \frac{\partial}{\partial\alpha^*}\alpha^* + \frac{\partial^2}{\partial\alpha\partial\alpha^*})$$
$$+ \frac{\eta_t h(y_j)}{g_s}f^*(x_j)(\frac{\partial}{\partial\alpha}) + (\frac{\eta_t h(y_j)}{g})^* f(x_j)(\frac{\partial}{\partial\alpha^*})]\}W$$
$$+ \{-\sum_{j=1}^{N}\frac{p_j}{m}\frac{\partial}{\partial x}$$
$$+ \hbar\sum_{j=1}^{N}\sum_s U_{0s}[\nabla_{x_j}(\varepsilon_s^*(x)\varepsilon_s(x))]\frac{\partial}{\partial p} + i\hbar\sum_{j=1}^{N}\sum_s \Gamma_{0s}[\nabla_{x_j}(\varepsilon_s^*(x)\varepsilon_s(x)]\frac{\partial}{\partial p}\}W$$
$$+ \sum_{j=1}^{N}\sum_s \Gamma_{0s}[(\hbar\nabla_{x_j}(\varepsilon_s^*(x)\varepsilon_s(x))^2 + \hbar^2k^2\overline{u^2}\varepsilon_s^*(x_j)\varepsilon_s(x_j)]\frac{\partial^2}{\partial p^2}W$$
$$+ i\hbar\sum_{j=1}^{N}\sum_s \Gamma_{0s}\{\nabla_{x_j}[f^*(x)f(x)]\left(-\frac{\partial}{\partial\alpha}\alpha + \frac{\partial}{\partial\alpha^*}\alpha^*\right)$$
$$+ \frac{\eta_t h(y_j)}{g_s}\nabla_{x_a}f^*(x)(\frac{\partial}{\partial\alpha}) + (\frac{\eta_t h(y_a)}{g_s})^*\nabla_{x_j}f(x)(\frac{\partial}{\partial\alpha^*})\}\frac{\partial}{\partial p}W \tag{3.32}$$

where

$$\varepsilon_s(x_j) = f(x_j)\alpha + \eta_t h(y_j)/g_s \tag{3.33}$$

In this equation, the first term is the coherent evolution of the cavity field; the second term is the decay and diffusion of the cavity field due to cavity decay and scattering of photons out of the cavity by the molecules; the third term is the conservative molecular motion; and the forth term is the momentum diffusion due to scattering of photons by the molecules. Note that this latter term can become negative, which reflects the breakdown of the semiclassical model at very weak intracavity field intensities. Additionally, the fifth term gives rise to correlated momentum and cavity field noise.

The approach has several important validity conditions.

Firstly, the momentum width Δp of the Wigner distribution is large compared with the photon momentum $\hbar k$, i.e. $\hbar k/\Delta p = \vartheta << 1$. This means that a single-photon absorption or emission process does not change the momentum distribution considerably. At the starting point of a Fokker-Planck treatment of this process, the smallness of the elementary steps should be concerned with this assumption [3.13]. The powers of the small parameter ϑ can justify the truncation procedure.

Secondly, only slow molecules are considered in this model. Compared with the optical wavelength λ, these particles move a small distance during the transition time γ^{-1}, i.e. $kv/\gamma << 1$. Therefore, the position change of the molecules during this process is very small, while the system can be treated quasi-adiabatically and internal variables are almost in steady state at any time.

The other condition concerns the quantized field state. In order to neglect a term containing third-order derivatives in momentum and field variables, the second-order derivative $\partial^2/\partial\alpha\partial\alpha^*$ is neglected compared with $|\alpha|^2$.

For an intracavity field on coherent states, a sufficient condition is that the mean photon numbers is higher than one, which makes the model "semiclassical" in the description of the cavity field as well [3.11]. This condition can be used to justify whether the dipole potential is steadily built up. Therefore, the fluctuations of the system due to the cavity decay loss can be taken into account and dealt consistently.

The resulting Fokker–Planck-type equation Eq. (3.32) for the Wigner function can effectively be simulated by stochastic differential equations of the Ito type [3.14], given by

$$\dot{\alpha} = (i\Delta_c - \kappa)\alpha - \sum_{j=1}^{N}\sum_{s}[(iU_{0s} + \Gamma_{0s})f^*(x_j)\varepsilon_s(x_j)] + \eta + \xi_\alpha \tag{3.33a}$$

$$\dot{p}_j = -\hbar\sum_{s} U_{0s}\nabla|\varepsilon_s(x_a)|^2 - i\hbar\Gamma_0[\varepsilon^*(x_a)\nabla\varepsilon(x_a) - \varepsilon(x_a)\nabla\varepsilon^*(x_a)] + \xi_p^{(j)} \tag{3.33b}$$

The diffusion is represented by the noise terms, which obey the second-order correlations

$$\langle \xi_\alpha^* \xi_\alpha \rangle = \sum_s \Gamma_{0s}\sum_{a=1}^{N} f(x)f^*(x) + \kappa \tag{3.33c}$$

$$\langle \xi_p^{(j)} \xi_\alpha \rangle = -i\hbar\sum_s \Gamma_{0s}\partial_j\varepsilon(x_j)f^*(x_j) \tag{3.33d}$$

$$\langle \xi_p^{(i)} \xi_p^{(j)} \rangle = 2\hbar^2 k_A^2\Gamma_0|\varepsilon(x_a)|^2\overline{u_i^2}\delta_{ij} + \hbar^2\Gamma_0[\partial_i^*\varepsilon(x_a)\partial_j\varepsilon(x_a) + \partial_i\varepsilon(x_a)\partial_j^*\varepsilon(x_a)] \tag{3.33e}$$

3.3.2 Dynamical equations

By means of the above systematic semiclassical approximation and similar normalization as section 3.3.1, the 1-D equations for the field amplitude, the forces, and the noise, are written as

$$\dot{\alpha} = [\frac{i\Delta_c}{\kappa} - 1]\alpha - [\frac{\Gamma_0}{\kappa} + \frac{iU_{0s}}{\kappa}]\sum_j \cos^2(x_{nm})\alpha - \eta_{eff}\sum_j \cos^2(x_{nm}) + \xi_\alpha \tag{3.34}$$

$$\dot{p}_{nj} = \frac{U_{0s}}{\kappa}(|\alpha|^2 - \frac{1}{2})\frac{\partial}{\partial x_{nj}}\cos^2(2x_{nj}) - i\frac{(\eta_{eff} * g - \eta_{eff} g^*)}{\kappa}\frac{\partial}{\partial x_{nj}}\cos(x_{nj}) + \xi_{pj} \tag{3.35}$$

which can be change to

$$\dot{p}_{nj} = \frac{U_0}{\kappa}(|\alpha|^2 - \frac{1}{2})\sin(2x_{nj}) - i\frac{(\eta_{eff} * g - \eta_{eff} g^*)}{\kappa}\sin(x_{nj}) + \xi_{pj} \tag{3.36}$$

$$\dot{x}_{nj} = p_{nj} \cdot (\hbar k^2/(m\kappa)) \qquad (j=1\ldots N) \tag{3.37}$$

where the effective position dependent pumping term proportional to

$$\eta_{eff} = \sum_k \frac{\eta g_{\omega k}}{-i\Delta_{Ak} + \gamma_k} = \sum_k \frac{\eta g(\gamma_k + i\Delta_{Ak})}{\Delta_{Ak}^2 + \gamma_k^2} \tag{3.38}$$

is responsible for the photon creation in the mode.

The self-organization can be still partly interpreted on the basis of the conservative forces. These are quite directly exposed in Eq. (3.35). The first term corresponds to the dipole force in the $\cos^2(kx)$ optical lattice potential, having potential wells at $kx=n\pi$ with a periodicity of $\lambda/2$. The additional force term proportional to $\cos(kx)$ has opposite sign for positions around $kx=2n\pi$ and $kx=(2n+1)\pi$.

The Brownian Noise wasn't taken into account in the semiclassical model before for simplicity and convenient conclusion. The damping processes, i.e. the trapping and cooling processes are always accompanied by fluctuations, which imply Langevin-type noise terms for the momentum, ξ_{pm}, and the complex field amplitude, ξ_α [3.9].

These are defined by the second-order correlation coefficients, which include nontrivial cross correlations between the momentum noise terms ξ_{pm} and the phase component of the field noise. In J. K. Asboth's simulation the proper random increment by decomposing the noise terms is generated from semiclassical model into uncorrelated and correlated components, $\xi_\alpha = \xi_\alpha^{(0)} + \xi_\alpha^{(1)}$ and $\xi_{pm} = \xi_{pm}^{(0)} + \xi_{pm}^{(1)}$ [3.15], where

$$\xi_\alpha^{(0)} = (-\frac{\sqrt{\Gamma_0}}{2}\sum_j \cos(x_{nj})\zeta_1^{(a)} + \sqrt{\kappa/2}\zeta_r^{(a)}) + i(\frac{\sqrt{\Gamma_0}}{2}\sum_j \cos(x_{nj})\zeta_2^{(a)} + \sqrt{\kappa/2}\zeta_i^{(a)}) \tag{3.39a}$$

$$\xi_{pj}^{(0)} = \sqrt{2\overline{u^2}\Gamma_0}((\alpha_1\cos(x_{nj}) + \frac{\eta}{g})\zeta_{pj}^1 + \sqrt{|\alpha_2^2 - \frac{1}{2}|}\cos(x_{nj})\zeta_{pj}^2) \tag{3.39b}$$

$$\xi_{\alpha}^{(1)} = \frac{i\alpha_1 - \alpha_2}{|\alpha|}\sqrt{\frac{\Gamma_0}{2}}\sum_j \cos(x_{nj})\zeta_m \tag{3.39c}$$

$$\xi_{pj}^{(1)} = -\sqrt{2\Gamma_0}|\alpha|\sin(x_{nj})\zeta_m \tag{3.39d}$$

where ζ_j, $\zeta_r^{(a)}$, $\zeta_i^{(a)}$, ζ_{pj}^{1}, ζ_{pj}^{2} are random numbers with mean 0 and variance 1.

The noise terms obey

$$\left\langle \left|\xi_{\alpha}^{(0)}\right|^2 \right\rangle = \frac{\Gamma_0}{2}\sum_j \cos^2(x_{nj}) + \kappa \tag{3.40a}$$

$$\left\langle \xi_{pj}^{(0)}\xi_{pj}^{(0)} \right\rangle = 2(\hbar k)^2\overline{u^2}\left(|\alpha|^2 - \frac{1}{2}\right)\cos^2(x_{nj}) - \frac{\eta}{g}(\alpha + \alpha^*)\cos(x_{nj}) \tag{3.40b}$$

Note the equations above are not normalized. Here $k\sqrt{\overline{u^2}}$ is the mean projection of the momentum recoil along the cavity axis due to spontaneous emission [3.15].

3.4 The Dynamics of Atomic Self-organization

In section 2.3.4, we studied the dynamics of single atom in the optical cavity pumped along the cavity axis. In section 2.3.7, we discussed the correlation between two atoms in the cavity. The noise and diffusion are neglected in those simulations.

In this chapter, we have discussed the model of the self-organization of molecules, which is also available for the two-level atoms with a replacement of η_{eff}. In section 3.3, the effect of noise has been taken into account. However, the model needs to be validated first. We simulate the dynamic process for atoms first according to the work of J. K. Asboth *et al*. with this model.

3.4.1 Dynamic process

In the strong-coupling regime ($g>\kappa, \gamma$) and for suitable detunings Δ_A and Δ_C, the cavity field exerts an efficient friction force and the atoms are driven into a near stationary distribution. The temperature limit still depends primarily on κ.

As introduced in section 2.3.4, for a single atom case, a large atomic detuning Δ_a is assumed to ensure small saturation, then cavity detuning Δ_c need to match an efficient cooling region in accordance with Fig. 2.4, and finally, a small light-shift effect U_0. For the many-particle case, which all couple to the same field mode, we can investigate the dynamics by numerically integrating Eq. (3.34). When the frequency

shift induced by the particles is of the order of the cavity detuning Δ_c =-κ, which reduces the cooling efficiency and consequently increases the steady-state temperature. For even larger particle numbers the cavity is shifted into positive detuning, where the friction force changes sign and the particles are accelerated [3.8, 3.28]. Therefore the cavity detuning $\Delta_c - U_0 \sum_j \cos^2(x_{nj}) < 0$ is assumed.

According to J. K. Asboth's method, we have done some simulations using the ^{85}Rubidium atom [3.15]. The atomic mass$m$ of ^{85}Rb is 85u, transition light wavelength is 780nm, recoilfrequency $\omega_{rec} = \hbar k^2/(2m) \approx 2\pi$x3.8 kHz. The half linewidth of the cavity is assumed as $\kappa \approx 10^7$Hz. The dipole moment of the ^{85}Rubidium atom is 2.5377$\times$ 10^{-29} C·m [3.25]. We consider a near-resonant pump, therefore the couple constant of ^{85}Rb g=5κ and the spontaneous linewidth γ=2κ, the parameter in Eq. (3.37) $\hbar k^2/(m\kappa) = c_1 \approx 207.5$.

For each value of N the detuning Δ_c is rescaled such that the effective mode detuning, including the index effect of the atoms, is kept constant provided the atoms are exactly in antinodes, for example, $\Delta_c - NU_0 = -\kappa$.

A type of self-organization process and the effect of the remaining momentum fluctuations are illustrated in a typical example of trajectories in Fig.3.2.

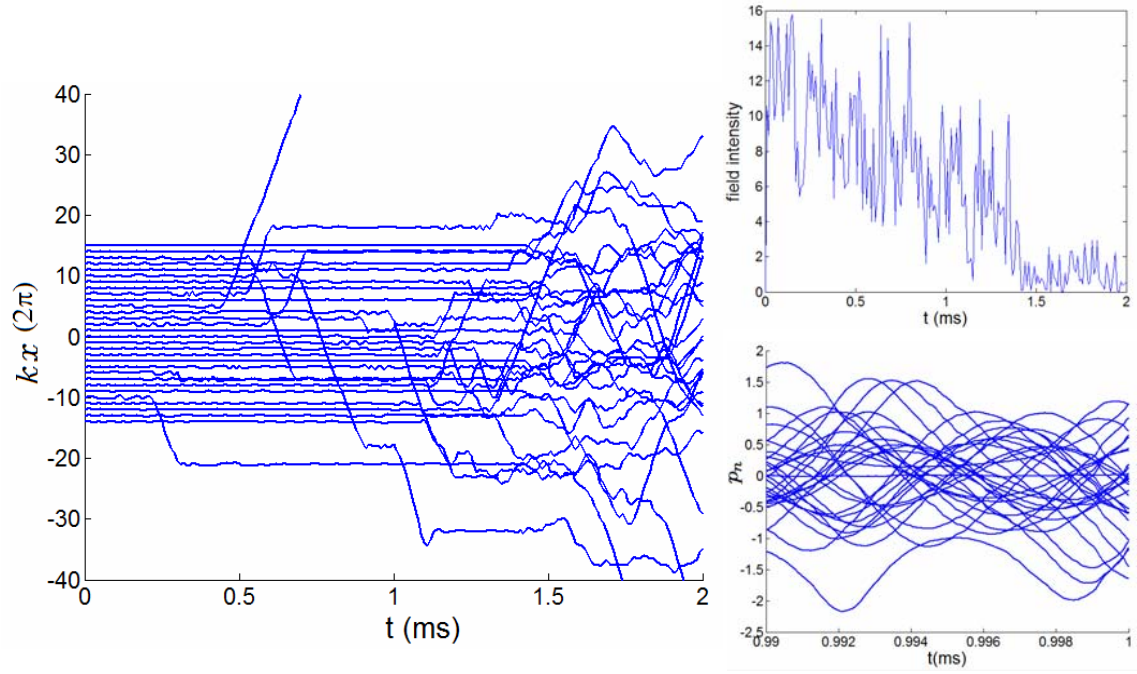

Fig. 3.2 A type of self-organization process of 30 ^{85}Rb atoms under the threshold. Left: Time evolution of the positions of the atoms. The initial normalized

momentum of each atom is p_n=1; right up: Time evolution of the intracavity field intensity; right down: the snapshot of the momentum of the atoms from 0.99ms to 1ms. The position *kx* is divided by 2π.

To contrast with the result of J. K. Asboth, in our simulation, the initial position of 30 ^{85}Rb atoms were on the $kx=2n\pi$ and the initial normalized momentum of each atom is p_n=1. The pump strength $\eta=400\mu s^{-1}$, which was just near the threshold, and the red-detuning $\Delta_A=-1000\kappa$. The figure shows these atoms are only weakly bound and show a lot of hopping between different trapping positions at beginning. However, the system is getting to unstable with the decreasing of the intracavity field intensity.

Figure 3.3 shows the result in the case of these atoms with same higher initial momentums p_n=3. All the others conditions are same as those in Fig. 3.2. After cooling and a short self-organization process, the field can not be built up and maintained steadily, which causes instabilities.

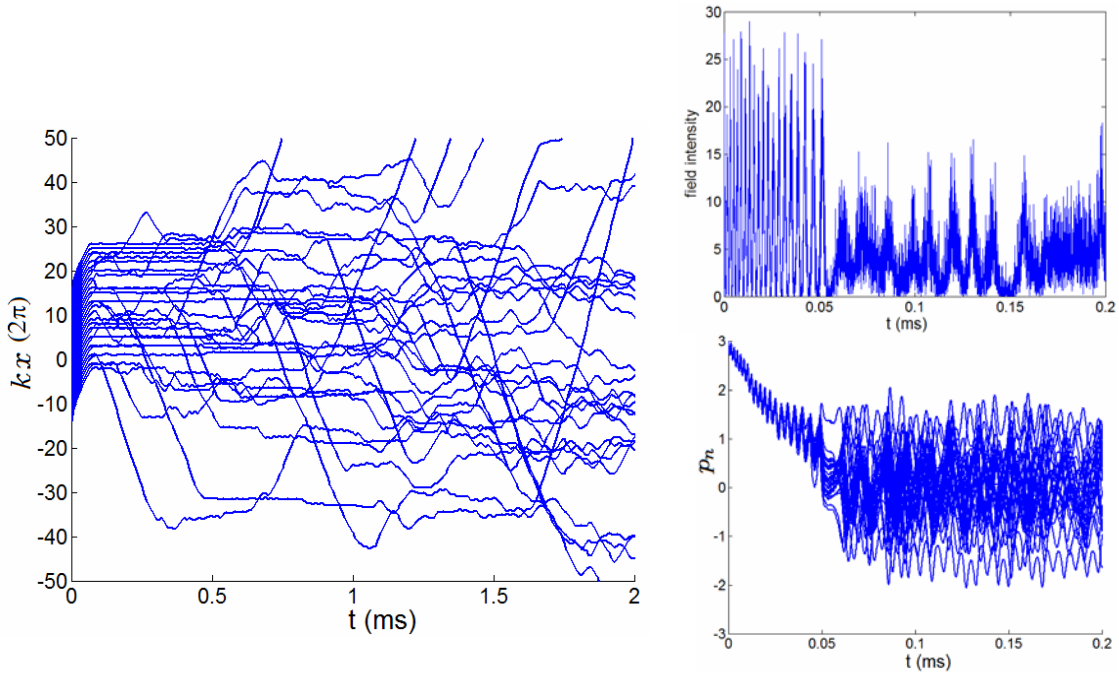

Fig. 3.3 A type of self-organization process of 30 ^{85}Rb atoms under the threshold with higher initial momentums. Left: Time evolution of the positions of the atoms. The initial normalized momentum of each atom is p_n=3; right up: Time evolution of the intracavity field intensity; right down: the snapshot of the momentum of the atoms. The position *kx* is divided by 2π.

If the pump power is increased, the stable case appears, as shown in Fig. 3.4 and 3.5. These results are coincident with those of J. K. Asboth [3.15].

As shown in the numerical simulations, 30 atoms starting from a uniform distribution breaks the translational invariance and finds a very particular state by self-organization: the atoms accumulate either all in the even or all in the odd wells, i.e., in positions x_j (j=1 ... N) such that cos(kx_j) is close to 1 or close to -1 for all.

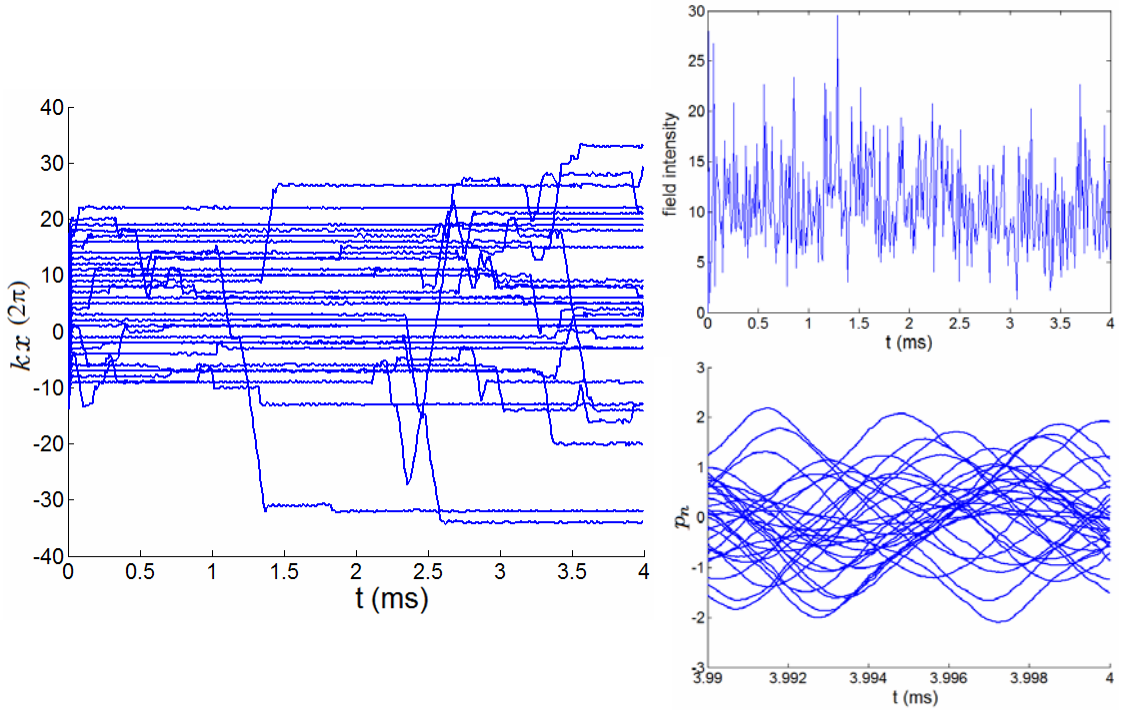

Fig. 3.4 A type of self-organization process of 30 ^{85}Rb atoms above the threshold. The pump strength is η=500μs^{-1}, and other conditions are same as those in Fig. 3.3. Left: Time evolution of the positions of the atoms; right up: Time evolution of the intracavity field intensity; right down: the snapshot of the momentum of the atoms of the atoms from 0.99ms to 1ms. The position *kx* is divided by 2π.

The self-organization process is relatively fast, on the microsecond time scale. Because the field is created by the atoms traps and simultaneously cools in the system, the organized pattern can stably remains on a long time scale of 10 ms [3.9, 3.15].

There are two parameters, the threshold of the pump light and the minimum number of atoms to produce self-organization. J. K. Asboth *et al.* [3.15] make many important conclusions. The simulation shows that for a small number of atoms self-organization is unlikely to occur, because the maximum number of photons generated in an optimally ordered state occupying exactly every second well is too low to trap the atoms for long times. On the other hand, for the chosen parameters of ^{85}Rb, no cavity

field builds up below η=400μs^{-1}, which can be regarded as the threshold of pump strength under these simulation conditions for self-organization. So the deep enough potential wells can be created to trap the atoms at the steady-state temperature of the atomic ensemble.

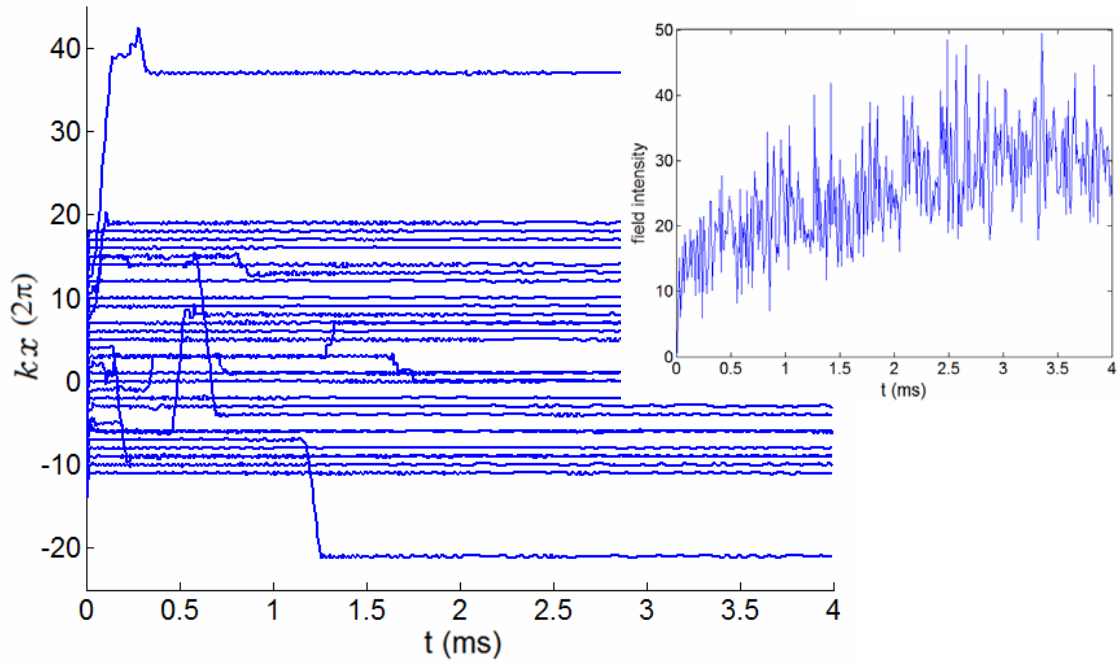

Fig. 3.5 A stable case after self-organization process of 30 ^{85}Rb atoms. The pump strength is η=600μs^{-1}, and other conditions are same as those in Fig. 3.3. The position *kx* is divided by 2π.

3.4.2 Scaling law

From Eq. (3.34), the atoms oscillate around the antinodes with an average light shift proportional to the mean of $\cos^2(kx)$ less than 1. Hence the more atoms there are in the cavity; the further the pumping field is detuned from the actual atom-shifted mode resonance. In fact, at high pump laser intensities (above a threshold), constructive interference of the scattered light in this final state then gives rise to a quadratic dependence of the stationary mode intensity, i.e., the number of cavity photons on the atom number *N*, which can serve as the signature of reaching the self-organized state and as unambiguous evidence for the atomic cooperative dynamics.

According to Eq. (3.34), a type of steady state can be considered, for example,

$$\dot{\bar{\alpha}} = \overline{[\frac{i\Delta_c}{\kappa} - 1]\alpha} - \overline{[\frac{\Gamma_0}{\kappa} + \frac{iU_0}{\kappa}]\sum_j \cos^2(kx)\alpha} - \overline{\eta_{eff}\sum_j \cos^2(kx)} + \overline{\xi_\alpha} = 0 \qquad (3.41)$$

The mean value of the noise term is 0. With the limit of a large atomic detuning, $\Delta_A >> \gamma$ ($|U_0| << |\Delta_c|, \Gamma_0 << \kappa$) is obtained, and for atoms closely localized at antinodes, $k^2\overline{x^2}$ <<1. Then the results of the numerical simulation are well described by the simple expression

$$|\alpha|^2 = N^2 \frac{|\eta_{eff}|^2}{\kappa^2} \frac{(1-k^2\overline{x^2})}{1+[1-(U_0N/\kappa)k^2\overline{x^2}]^2} \tag{3.42}$$

which is obtained as the steady state of Eq. (3.34).

The position uncertainty of a single atom $\overline{x^2}$ is a good parameter to evaluate the localization of these atoms. Fig. 3.6 shows the correlation between $a = k^2\overline{x^2}$ and $b = \frac{1-k^2\overline{x^2}}{1+[1-(U_0N/\kappa)k^2\overline{x^2}]^2}$ with our simulation parameters. When the range of atoms is increased, the field intensity decreases.

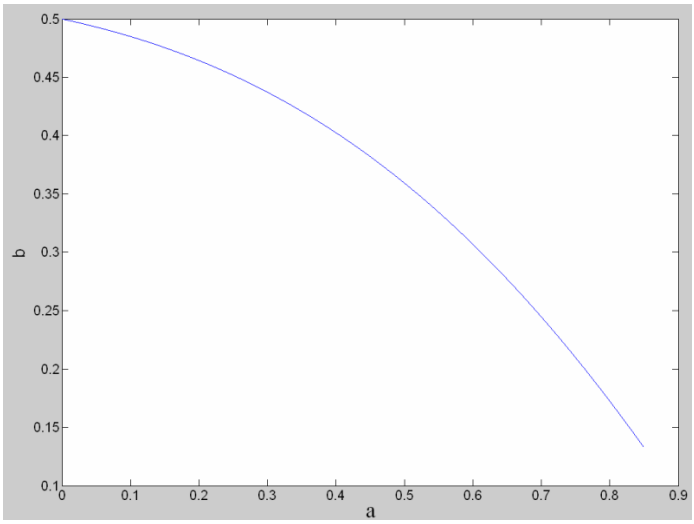

Fig. 3.6 The correlation between $a = k^2\overline{x^2}$ and $b = \frac{1-k^2\overline{x^2}}{1+[1-(U_0N/\kappa)k^2\overline{x^2}]^2}$ with our simulation parameters

According to Eq. (3.34), if more atoms happen to be momentarily in the even wells so that $\sum_j \cos(x_{nj}) > 0$, then the cosine potential has wells at $kx=2n\pi$ deepening the $\cos^2(kx)$ optical lattice, while it has hills at $kx=(2n+1)\pi$ that reduce or can even suppress the attractive wells in these points. If the populations in the different type of wells are unbalanced, the asymmetry between the two wells will be stimulated and increased. In

the end of the simulation in this case, all the atoms are in the same class of wells for the self-amplifies process.

In a closely related setup, Vuletic´ and coworkers observed fast and efficient sub-Doppler cooling of 10^6 cesium atoms in a multimode cavity field, accompanied by a relatively weak, near-resonant pump [3.16].

3.5 A Case Study of Molecular Self-organization

According to Eq. (3.33), the dynamics of molecules can be simulatedin a similar way as that of atoms with different numerical parameters. As introduced in chapter 2, deeper depth of a dipole potential that it builds up can trap more random particles with less kinetic energy, therefore the coupling strength between the particle and the field should be as strong as possible. However, two-level atoms are pumped typically at visible to infrared wavelengths, with 100 MHz - 10 GHz detuning from the resonance transition. For most molecules, the pump frequency required for a rotational-vibrational transition of molecules is in the UV and DUV regions. We have to take into account the limited availability of laser sources and high finesse cavity optics in these frequency regions. Also the permanent dipole moments of polar molecules of these corresponding transitions are generally much weaker than those of well-studied atoms such as Rubidium, which will lead to significant differences in the operating conditions between the two. The work may provide several new and important findings beyond the scope of previous investigations on cooling atoms in optical cavities.

In this section, we study cooling of a CN molecular gas in a millimeter-long optical cavity.

3.5.1 General model

We propose a study of the cooling of molecules in optical cavities. We investigate the centre-of-mass motion of N molecules in an optical cavity pumped by a laser source from the direction that is transverse to the cavity axis, as shown in Fig. 3.7(a).

For simplicity, we restrain the model to one-dimension in the cavity axis direction. We consider CN molecules in this study because the pump source that is required for the transition is in the UV region for which cavity optics are readily

available, and stationary cold molecules could be created using optical Stark deceleration [3.17]. For this gas at the hundred mK range only the lowest ro-vibrational energy level is populated.

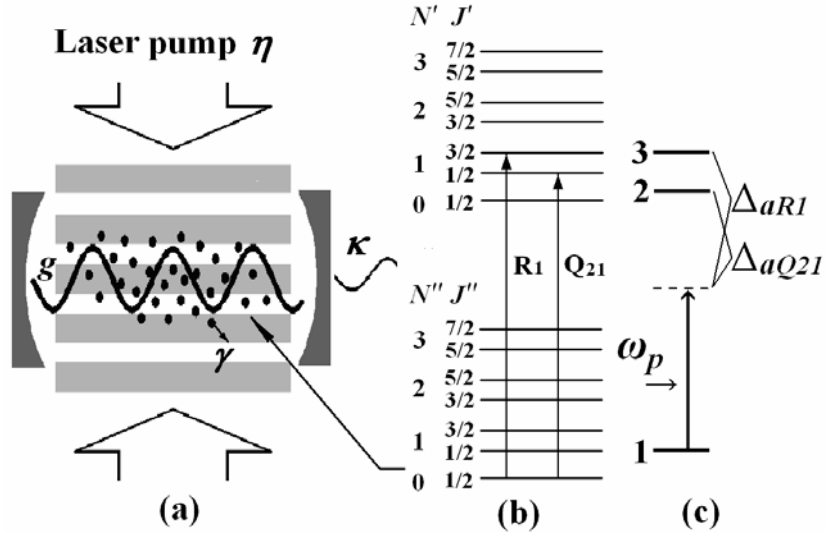

Fig. 3.7 Schematic of cooling of molecules in an optical cavity. The insert shows the transitions for near and far off resonant interactions

3.5.2 CN molecule

The molecular mass of CN is 26u, the transition B $^2\Sigma^+ \rightarrow$ X $^2\Sigma^+$ with dipole decay rate γ=15.4 MHz, dipole moment d^2=2.954$\times 10^{-60}$(C^2m^2) [3.22-3.24].

We consider a pump laser source at around 387.6nm, for which there are only two allowed transition lines as shown in Fig. 3.7(b).These are the R_1 line: $B^2\Sigma^+(v'=0,N'=1,J'=3/2) \leftrightarrow X^2\Sigma^+(v''=0,N''=0,J''=1/2)$ and the Q_{21} line: $B^2\Sigma^+(v'=0,N'=1,J'=1/2) \leftrightarrow X^2\Sigma^+(v''=0,N''=0,J''=1/2)$.

The transition light wavelengths are both around 387.5nm, and the frequency separation of the two is around 5 GHz. A three-level model is therefore sufficient to describe the system, as depicted in Fig. 3.7(c).

Levels |1> and |3> corresponds to the R_1 line and levels|1> and |2> to the Q_{21} line. To reduce diffusive heating, we consider a large pump frequency detuning of 15 GHz from the Q_{21} line and 20 GHz from the R_1 line, for which populations in levels |2> and |3> can be neglected. The three-level system can thus be simplified as two two-level interactions.

The parameters

$$U_0 \equiv U_{R1} + U_{Q21} = \frac{\Delta_{aR1} g_{R1}^2}{\gamma^2 + \Delta_{aR1}^2} + \frac{\Delta_{aQ21} g_{Q21}^2}{\gamma^2 + \Delta_{aQ21}^2},$$

$$\Gamma_0 \equiv \Gamma_{R1} + \Gamma_{Q21} = \frac{\gamma g_{R1}^2}{\gamma^2 + \Delta_{aR1}^2} + \frac{\gamma g_{Q21}^2}{\gamma^2 + \Delta_{aQ21}^2} \tag{3.43}$$

describe the dispersion and absorption of the molecules when both transition lines are taken into account, where γ is the spontaneous emission linewidth, g_{R1} and g_{Q1} are the coupling strengths of the two lines and $\Delta_{aR1} = \omega - \omega_{aR1}$ and $\Delta_{aQ21} = \omega - \omega_{aQ21}$ are the pump-molecule detuning for the two lines. The photon number scattered into the cavity by the pump η is $|\eta_{eff}|^2$, where

$$\eta_{eff} = \frac{\eta g_{R1}(\gamma + i\Delta_{aR1})}{\Delta_{aR1}^2 + \gamma^2} + \frac{\eta g_{Q21}(\gamma + i\Delta_{aQ21})}{\Delta_{aQ21}^2 + \gamma^2}, \tag{3.44}$$

which also has two terms for each transition.

The pump frequency is detuned to be $\Delta_{aQ21} = -15\,\text{GHz}$ and $\Delta_{aR1} = -20\,\text{GHz}$, which are much larger than γ.

Using the well-documented parameters for (B-X), (0, 0) transitions of CN molecule, we obtain the coupling strengths, $g_{R1} = 14.1\,\text{MHz}$, $g_{Q21} = 10.0\,\text{MHz}$ and total coupling strength that combines the two lines $g = \sqrt{g_{R1}^2 + g_{Q21}^2} = 17.3\text{MHz}$ [3.18].

3.5.3 Cavity parameters

According to Eq. (2.8) and (2.10), for a certain dipole moment, small mode volume and high photon energy can improve this parameter *g*, but are limited by the experimental conditions such as cavity parameters and pump source.

To obtain a strong coupling constant*g*, the cavity is assumedto have: length *l*=1.5mm, reflectivity r_1=r_2=0.9999, and beam waist $w_0 \approx 5\mu m$ .The linewidth of the cavity is $\kappa \approx 20\times10^6$ Hz, the finesse is 3.1×10^4. Consequently the coupling constant of CN molecule is g=0.866κ and the recoilfrequency $\omega_{rec} = \hbar k^2/(2m) \approx 2\pi$x51kHz.

The normalization coefficient of momentum is $\hbar k^2/(m\kappa) = c_1 \approx 1/32$. To get a potential U_0 as deep as possible, we set $\Delta_a = -30\kappa = -600MHz$. The effective mode detuning Δ_c is set as similar to the case of atoms, for example, $\Delta_c - NU_0 = -\kappa$.

Due to the weak dipole moment strength of molecules, a variable order Adams-Bashforth-Moulton PECE solver is adopted to numerically simulate the dynamic procession. It may be more efficient than other methods at stringent tolerances [3.27]. The simulation in Fig. 2.8 in a long time (>1s) shows a highly steady performance and accuracy of this method. To check the validity of our model, we firstly study the case of Rb atoms and compare the results with those published or verified [3.9, 3.15].

3.5.4 Comparison with Rb atom

We have done some work on the scaling character of CN molecules, which is in contrast with that of Rb atoms, as dicussed in section 3.4.2. These simulation results are shown in Fig. 3.6, where the X axis is the pump strength η, the Y axis is the variable value, and index $b = \dfrac{1-k^2\overline{x^2}}{1+[1-(U_0N/\kappa)k^2\overline{x^2}]^2}$.

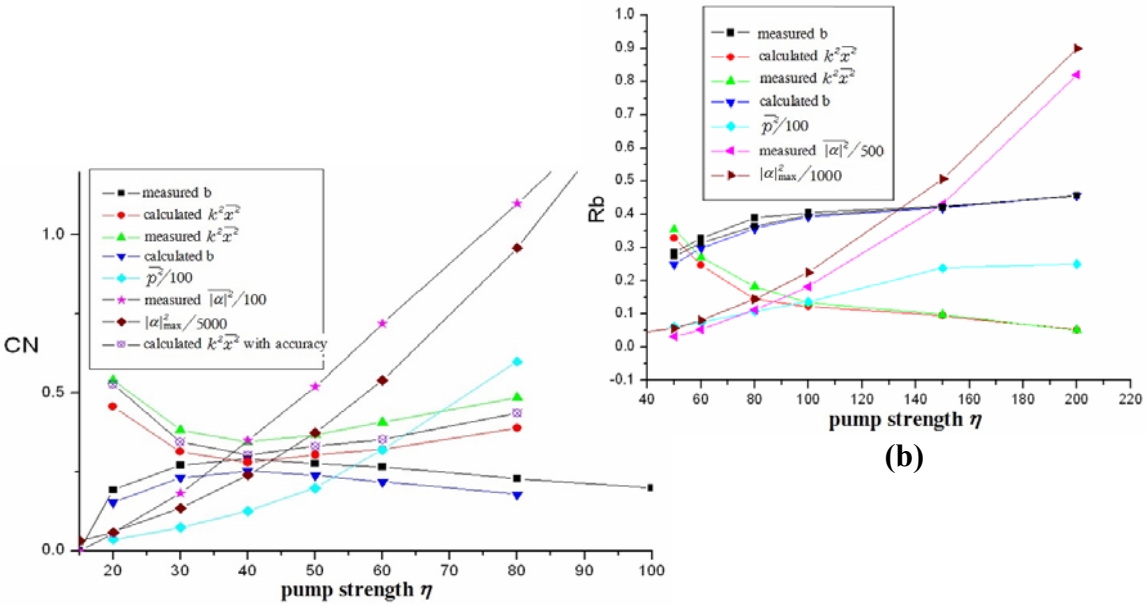

(a) **(b)**

Fig. 3.6 The contrast simulation results between CN molecule and Rb atom

As shown in Fig. 3.6, some characters of CN molecule are similar with those of Rb atom when the pump strength is appropriate. The collective cooling dynamics and scaling of molecules in the two-level interaction model has taken place through spatial self-organisation in realistic conditions. However, when the pump increases, the k^2x^2 of CN is getting higher, which can cause instability of the optical field.

3.5.5 Dynamics study

We first study the dynamics of the CN gas in the cavity that has an initial temperature of 100 mK, which is significantly higher than the cavity cooling temperature limit of $\hbar\kappa = 150\,\mu K$ for our system [3.19].

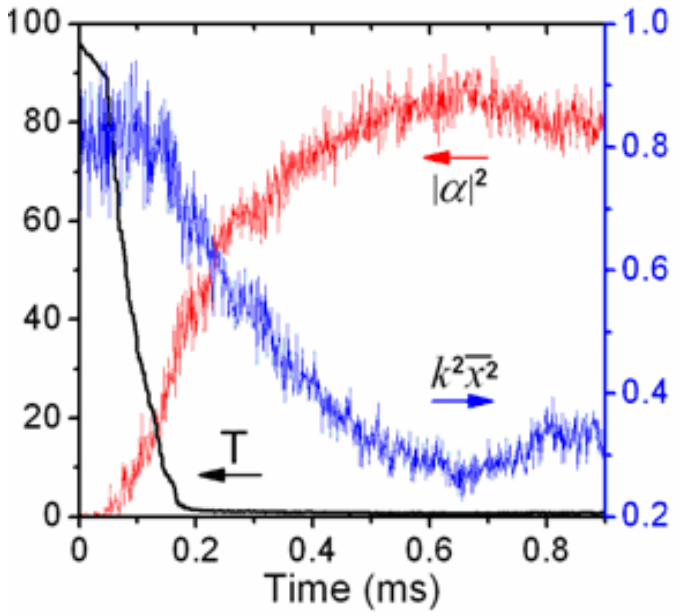

(a)

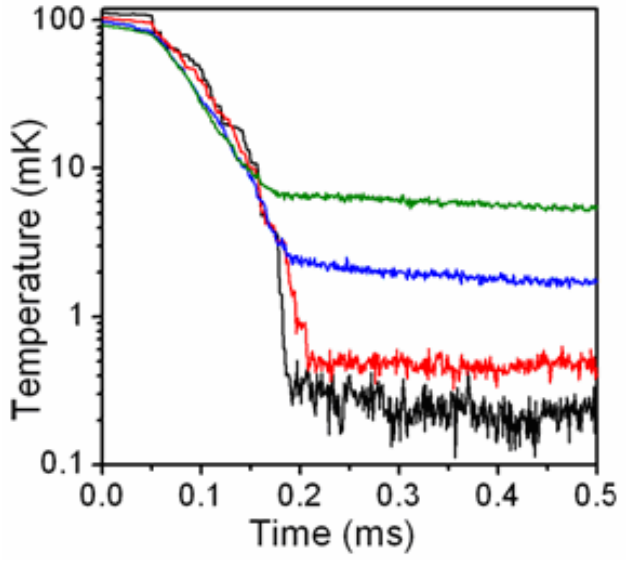

(b)

Fig.3.7 (color online) (a) Time evolution of the photon number $|\alpha|^2$ in the cavity (divided by 10 to fit the figure), the temperature of molecules (in unit of mK) and the molecular spreading parameter, $k^2\overline{x^2}$. (b) The temperature of the CN gas vs. time for different initial molecular numbers in the cavity (from bottom to top: *N*= 50, 100, 400, 1000)

Fig.3.7 shows the evolution of temperature, intracavity photon number and the spatial spreading parameter for 200 CN molecules that are initially placed uniformly in the central region of the cavity. The spreading parameter, $k^2\overline{x^2}$, measures the averaged distance of molecules to their nearest antinodes of the intracavity field. When a pump intensity of 54 kW/cm^2 (η=300κ) is applied to the cavity, the intracavity field rapidly builds up through the molecule-mediated scattering.

Accompanying this process is the dissipation of the kinetic energy of the molecules owing to the cavity cooling mechanism. This results in molecules becoming trapped in the dipole potential wells produced by the intracavity field. The spatial self-organization of molecules in the cavity is evident with the decrease of the spreading parameter. In this simulation, 120 of the 200 molecules are trapped and rapidly cooled to 850 μ K in around 0.2ms. The remaining molecules are accelerated and eventually escape from the cavity. The latter happens because these molecules are out of phase with the majority and do not benefit from the cavity induced cooling process. We note that the pump intensity is high because a limited number of molecules are simulated for computational efficiency.

According to the 1/N law discussed later in this chapter, the pump intensity is reduced to about 1 kW/cm^2 to observe similar dynamics for 10^4 molecules. We have carried out many simulation runs with different initial temperatures and molecular numbers and show that using the same pump intensity the molecules with initial temperature of 300 mK can be cooled to the similar final temperature on the same time scale.

In general, for a given pump intensity the number of trapped molecules is reduced on increasing their initial temperatures, while the increase of the pump intensity traps and cools more molecules. The number of trapped molecules also increases with the increase of the cavity length. We have further found that once the pump intensity is set above its threshold for cooling, the cooling time for the trapped molecules remains essentially unchanged for different molecular numbers and initial temperatures.

Fig. 3.7(b) shows the cooling process in time for different initial numbers of molecules with same starting temperature. The jumps shown in the curves, which are more prominent in the cases of smaller molecular numbers, implies the loss of hot molecules from the cavity and consequently the reduction of temperature for molecules remaining in the cavity.

The cooling time is around 0.2 ms for all cases we simulated. The final molecular temperature depends on the operating conditions of the system; a lower temperature is obtained when the system operates just above the pump threshold.

3.5.6 Defect and stable defect particles

The averaged photon number in the cavity can be well approximated by the steady state solution of Eq. (3.34) without the noise terms, which in the limit of large molecular detuning $\Delta_{aR1}, \Delta_{aQ21} >> \gamma$, small molecular spreading $k^2 x^2 << 1$ and the cavity detuning condition $\Delta_c = -\kappa + N_{tr} U_0$, is given as

$$\overline{|\alpha|^2} = N_{tr}^2 \frac{|\eta_{eff}|^2}{\kappa^2} \frac{(1 - k^2 \overline{x^2})}{1 + [1 - (U_0 N_{tr} / \kappa) k^2 x^2]^2} \quad . \tag{3.42}$$

Here the number of trapped molecules N_{tr} in the cavity has replaced the initial molecular number N [3.9, 3.15].

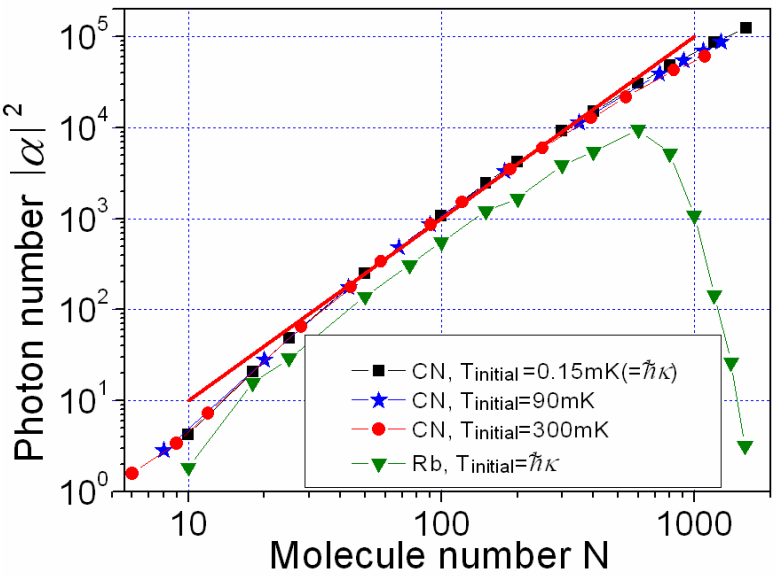

Fig. 3.8 (color online) The relationship between photon number and molecular number for different initial temperatures for the CN molecular gas. The results for Rb atoms are also shown for comparison.

This modification allows us to describe the cases with different initial temperatures. As depicted in Fig. 3.8, the curves for initial temperatures of 0.15 mK ($=\hbar\kappa$), 90 mK and 300 mK are very close together and all obey the quadratic relation

$\overline{|\alpha|^2} \propto N_{tr}^2$ in the parameter window around $N_{tr} = 100$, where $k^2\overline{x^2}$ is small and the motion of the trapped molecules are well correlated. We also plot the curve for Rb atoms for comparisons. Rb atoms behave in a similar way to those of CN for $N_{tr} < 600$, beyond which, however, the photon numbers is rapidly reduced on increasing N_{tr}.

The latter effect is due to the appearance of significant number of stable defect molecules [3.15]. The "defect" is defined as the ratio of atoms closer to minority sites than majority sites. A uniform distribution of particles gives a defect ratio close to 50%.

We can use the potential curve to describe this defect parameter. According to Eq. (3.36) and discussion in section 2.3.5, the dipole potential can be described as

$$U_{dip} = \frac{U_0}{\kappa}(|\alpha|^2 - \frac{1}{2})\cos^2(x_{nj}) - i\frac{(\eta_{eff} * g - \eta_{eff} g^*)}{\kappa}\cos(x_{nj}) \tag{3.45}$$

as shown in Fig. 3.9.

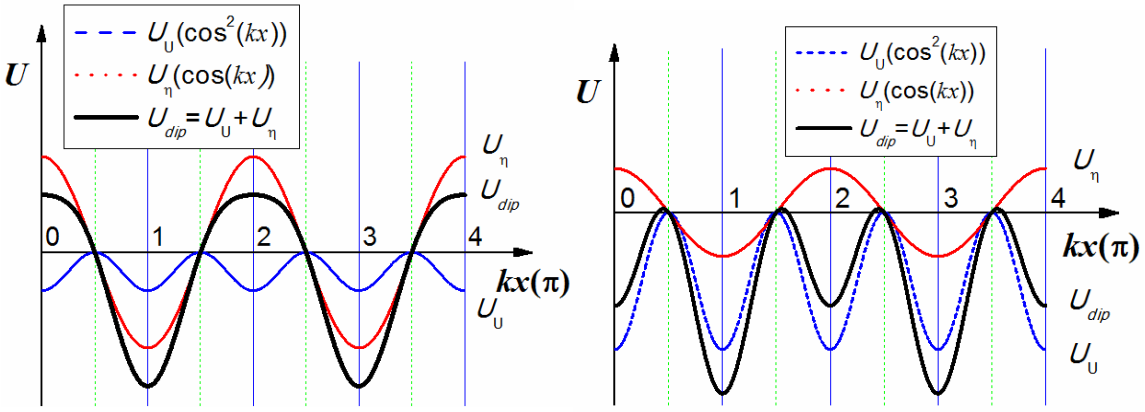

Fig. 3.9 (color online) The dipole potential distribution of self-organization. There are two type potentials. Left: when the intracavity field is small, the period of the potential U_{dip} is 2π; Right: when the intracavity field is increased above a limit, even wells appear.

According to the introduction in Fig. 3.9, two type defects exist in the self-organization process due to the two cases of potential distribution. Fig. 3.10 shows the defect value in the cases of different conditions. When the pump is not strong enough, the particle with higher momentum has a large localization distribution in the dipole potential, which caused the defect. However, if the particle number exceeds a limit, a type of stable defect appears.

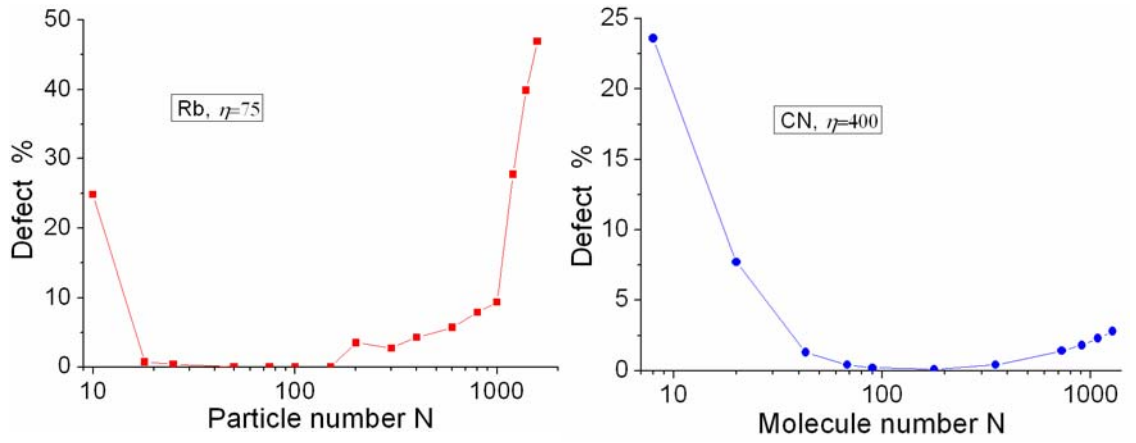

Fig. 3.10 Defect of Rb atom (left) and CN molecule (right) in the stable state of self-organization. The parameters of Rb are g=5κ, Δ_A=-1000κ, γ=2κ; CN are g=5κ, Δ_A=-1000κ, γ=0.75κ.

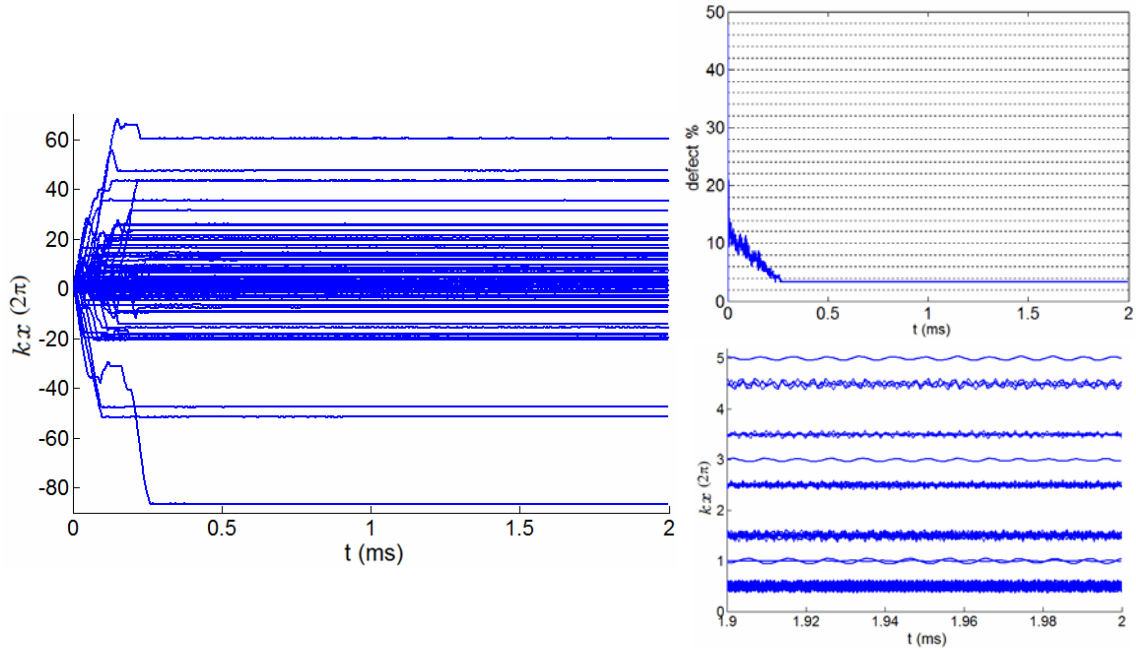

Fig. 3.11 Stable defect in the self-organization of 300 ^{85}Rb atoms. The parameters are g=5κ, Δ_A=-1000κ, γ=2κ, η=75κ. Left: Time evolution of the positions of the atoms; right up: Time evolution of the defect; right down: the snapshot of the position of the atoms of the atoms from 1.99ms to 2ms. The position kx is divided by 2π.

The stable defect molecules are those trapped in different type of wells from the majority and they destroy the intracavity field through destructive interference with the rest molecules. A simple theoretical estimation of the threshold for the occurrence of the defects is given as $N_{thr} = \kappa / |U_0| \approx 40$ for Rb atoms [3.15].

Our simulations show that noticeable number of defects appears at much higher molecular number, around N=200, and their percentage increases on further increasing the molecular number in the cavity, at N=600 the defects reach >5% and start to reduce the intracavity field. CN molecules have a much larger threshold, at $N_{thr} \approx 1200$, according to the estimation.

Based on the results of Rb atoms, the same effect for CN molecules due to stable defects should appear at around N=10^4, which is beyond our simulation range. This finding shows that cavity cooling occurs only for a molecular gas whose number does not significantly exceed the threshold N_{thr} for the emergence of stable defects. This restriction will be further discussed later in this chapter.

3.5.7 Scaling law

The observation that the quadratic relation $\overline{|\alpha|^2} \propto N_{tr}^2$ holds only in a limited parameter window is due to the fact that collective dynamics of molecules occurs only in a certain parameter region of the system. This is evident by examining the relation of molecular spreading $k^2\overline{x^2}$ with other parameters of the system.

For example, while an increase of the molecular number deepens the potential trap which compresses the molecular spatial size around the antinodes, it also increases the noise effects due to the increased intracavity field intensity, which tend to spread the molecular clouds and also raise the final molecular temperatures.

To investigate its functional dependence on the parameters, we consider the dipole potential energy produced by the intracavity field intensity. When a molecule is cooled in the cavity, the averaged potential energy experienced by the molecule is, from the right hand side of Eq. (3.35),

$$\overline{U} = -\hbar\{U_0(\overline{|\alpha|^2} - \frac{1}{2})\cos^2(\overline{kx}) + 2(\mathrm{Im}(\eta_{eff})\overline{\alpha_1} - \mathrm{Re}(\eta_{eff})\overline{\alpha_2})\cos(\overline{kx})\} \qquad (3.46)$$

where α_1 and α_2 are the real and imagery parts of α. The averaged potential energy variation due to molecular spatial spreading from the antinodes of the field is therefore

$$\left|\Delta\overline{U}\right| = \hbar\{\left|U_0\right|\overline{|\alpha|^2}(1-\cos^2(\overline{kx})) + 2\left|(\mathrm{Im}(\eta_{eff})\overline{\alpha_1} - \mathrm{Re}(\eta_{eff})\overline{\alpha_2})\right|(1-\left|\cos(\overline{kx})\right|)\} \qquad (3.47)$$

Here we have assumed $\overline{|\alpha|^2} >> 1$. In the case of $\Delta_{aR1}, \Delta_{aQ21} >> \gamma$, $|\overline{\alpha_1}| \approx |\overline{\alpha_2}| \approx |\alpha|/\sqrt{2}$, and $|\mathrm{Re}(\eta_{eff})| << |\mathrm{Im}(\eta_{eff})| \approx |\eta_{eff}|$. Eq. (3.47) can be simplified in the limit of $k^2\overline{x^2} << 1$ to

$$|\Delta\overline{U}| \approx \hbar\{|U_0||\alpha|^2 + |\eta_{eff}|\frac{|\alpha|}{\sqrt{2}}\}k^2\overline{x^2} \tag{3.48}$$

When the molecules reach the steady state, the potential energy difference given by Eq.(3.48) equals the kinetic energy. Since all degrees of freedom have the same energy $k_BT/2$, the relation $|\Delta\overline{U}| = k_BT/2$ gives

$$k^2\overline{x^2} \approx \frac{k_BT}{2\hbar}\{|U_0||\alpha|^2 + |\eta_{eff}|\frac{|\alpha|}{\sqrt{2}}\}^{-1} \tag{3.49}$$

By substituting Eq. (3.46) to Eq. (3.49), we obtain the relation of the molecular spatial spreading with the number,

$$k^2\overline{x^2} \approx \frac{k_BT}{\hbar\kappa}\{\frac{|\eta_{eff}|^2}{\kappa^2}N_{tr}\}^{-1} \tag{3.50}$$

where we have imposed the restriction $\frac{|U_0|}{\kappa}N_{tr} << 1$. For comparison, we have plotted 3 curves in the ($k^2\overline{x^2}$, N) space in Fig. 3.9, which are obtained by using Eq. (3.49), Eq. (3.50) and directly from numerical results of Eq. (3.34).

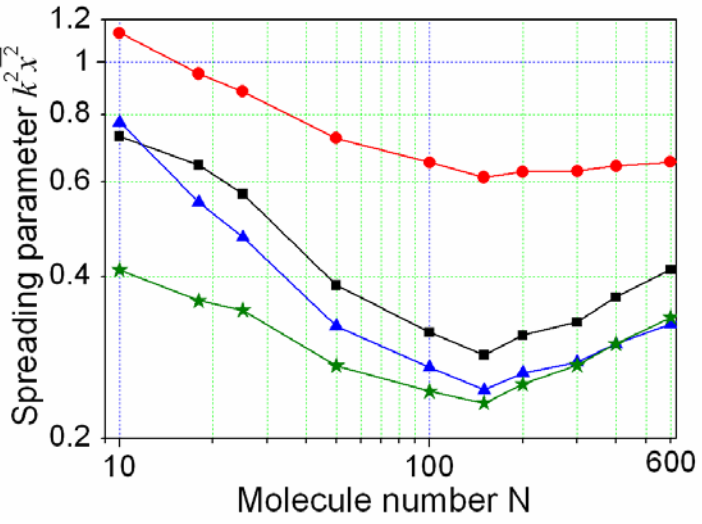

Fig. 3.9 The spreading parameter vs. molecular number. The square curve is generated directly from numerical integration of Eq. (3.34). The triangle curve is plotted using Eq. (3.49) with photon numbers and temperatures from numerical

simulation. The star curve is from Eq. (3.50). The dot curve is produced using the expression from ref. 3.15 for CN parameters for the purpose of comparison.

The curve generated by Eq. (3.49) fits well with the numerical results for different molecular numbers except in the small window just above the threshold, where collective dynamics has not been fully established and noise effects are relatively strong.

The deviation of Eq. (3.50) from the numerical results is also mainly in the region of small *N*. This is because of the existence of finite number of defect molecules in this region and consequently Eq. (3.45) should be corrected by removing these molecules from N_{tr}. We note that Eq. (3.50) does not imply a simple $1/N_{tr}$ law because the temperature also varies with the molecular numbers and its expression is not yet available. Our extensive numerical simulations show that the temperature increases monotonically with the molecular number once collective dynamics occurs (*N*>10 in Fig. 3.9) and can be approximated by $T \propto a_0 + a_1 N_{tr} + a_2 N_{tr}^2$, where $a_0 >> a_1 >> a_2$. By substituting this relation to Eq. (3.50), we obtain $k^2\overline{x^2} \propto a_1 + a_0 / N_{tr}$ for the region of small molecular numbers and $k^2\overline{x^2} \propto a_1 + a_2 N_{tr}$ for large molecular numbers. These functional dependences fit qualitatively with the curves in the figure.

The above analysis and simulation show that in cavity cooling, the pump intensity should be set in the region close to the threshold, in which the collective dynamics of molecules is strong and the final molecular temperature is low. We note that a different expression from Eq. (3.49) was obtained in ref. [3.15] using a harmonic oscillation model and the 1/*N* law were suggested for a small window of molecular numbers where the changes of cooling temperature with molecular number are neglected.

For comparison we have plotted this expression (Eq. (31) of Ref. [3.15]) using our simulation results of CN molecules. The curve captures the main features for small number of molecules but is shifted significantly upward.

We have further investigated the relation of the pump intensity threshold with the molecular numbers. This relation is obtained based on our extensive numerical results on CN molecules. We start with a finite number of molecules, *N*, in uniform distribution in space and low initial temperature ($=\hbar\kappa$). On increasing the pump

intensity, the molecules tend to accumulate in either odd or even numbered potential wells through the self-organization processing. The pump threshold is defined at the point where the statistical difference, δN, of the molecules around the odd and even wells equals the root square of the molecular number, for example, $\delta N = \sqrt{N}$. Since the intracavity field fluctuates significantly in the region of the threshold, the pump intensity is determined using extensive numerical runs and statistical analysis. Fig. 3.10 shows that the effective pump threshold is inversely proportional to the molecular number, for example, $|\eta_{eff,thr}|^2 \propto 1/N$.

Using Eq. (3.38) and Eq. (3.44), we have

$$|\eta_{thr}|^2 \propto \frac{(\Delta_{aR1}\Delta_{aQ21})^2}{(g_{R1}\Delta_{Q21} + g_{Q21}\Delta_{R1})^2}\frac{\kappa^2}{N} \tag{3.51}$$

where we have assumed $\Delta_{aR1}, \Delta_{aQ21} >> \gamma$. Eq. (3.51) can be further simplified in the case that the pump frequency detuning is much larger than the frequency difference between the two transition lines, for example, $\Delta_{aR1} \approx \Delta_{aQ21} \equiv \Delta_a$. We have from Eq.(3.51) under this condition

$$|\eta_{thr}|^2 \propto \frac{\Delta_a^2\kappa^2}{g^2 N} \tag{3.52}$$

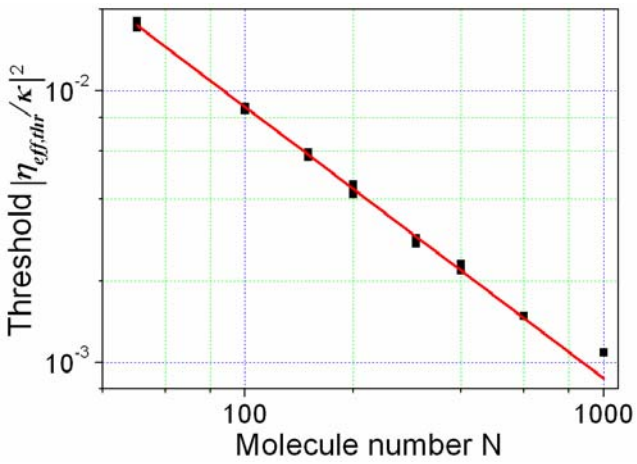

Fig. 3.10 (color online) Numerical simulations show the 1/*N* law for the pump intensity threshold for CN molecules.

This relation implies that a smaller value of the coupling strength g for a certain molecular gas can be compensated by larger molecular number in the cavity to have the

same pump intensity threshold for cooling. For example, the transition strength of the relevant lines in CN molecules is some two orders of magnitude smaller than that in Rb atoms, and consequently a relatively small cavity mode volume was used in our CN simulations to boost the coupling strength. In fact, given by the relation Eq. (3.52), we can reduce the coupling strength and increase molecular number at the same time to achieve effective cooling. We have verified this in simulations.

This relation therefore gives the flexibility in cavity configurations for cooling molecules. We note that two different scaling laws have been suggested based on the mean-field continuous and statistical models in the study of atoms in a cavity field and they gave respectively $1/N$ and $1/\sqrt{N}$ law to the threshold for the pump intensity [3.15].

While our definition for the pump intensity threshold follows the statistical model, and numerical simulations involve a limited number of molecules, we observe the $1/N$ law, as given by Eq. (3.52), which is consistent with the mean-field continuous analysis. We further note that there is a noticeable constant shift between the threshold values given in Fig. 3.10 and those derived from the mean-field analysis.

Finally we discuss how the scaling relations given by Eq. (3.45), Eq. (3.50) and Eq. (3.52) can be used to extend our results obtained based on the simulations of hundreds of molecules to a very large molecular ensemble.

First, these relations are valid only when the number of molecules to be cooled in the cavity does not significantly exceed the threshold value N_{thr} for the appearance of stable defects. Since $N_{thr} = \kappa / |U_0|$, the dispersion parameter $|U_0|$ must be reduced and/or the cavity relaxation rate κ increased to increase N_{thr}.

For example, for the value of κ given earlier, if the pump frequency detuning Δ_a ($|U_0|$) is increased (decreased) by 5 orders of magnitude, a gas of 10^9 CN molecules can be cooled in the cavity without the occurrence of significant stable defects. Thus, in order to cool an ensemble of 10^9 CN molecules, the pump field must be detuned further from the molecular resonance from the near resonant regime (GHz to tens of GHz detuning) to far off-resonance (detuning in the order of half of the resonant transition frequency). The pump intensity threshold for molecular self-organization and cooling, as given by Eq. (3.52), is increased by 4 orders to 6×10^6 W/cm^2.

This estimate shows that cavity cooling of a large molecular sample is possible by use of a far off-resonant, high intensity pump. In this new parameter set for cooling of a 10^9 CN molecular gas, the scaling relations of Eq. (3.45) and Eq. (3.50) should still be observed when molecules are self-organized above the pump threshold.

The intracavity photon number in this case is increased by 6 orders because of the scaling $\overline{|\alpha|^2} \propto N_{tr}^2 |\eta_{eff}|^2$ given by Eq. (3.45), whereas the spatial spreading parameter remains unchanged due to the fact that $\overline{x_{nm}^{\ 2}} \propto (|\eta_{eff}|^2 N_{tr})^{-1}$ given by Eq. (3.50). We note that varying κ gives more flexibility to the choice of the pump intensity and other parameters.

3.6 Summary

In summary, we have studied a cavity scheme for molecules and predicted, by example, that CN molecules can be cooled from the hundred milliKelvin range to sub milliKelvin temperatures in less than one millisecond. While CN molecules have a complex energy level structure, the near-resonant interaction model can be simplified to comprise only three levels. This approach can be extended to other molecular species of current interest in cold molecule research for which the scaling laws discussed in this paper can be generalized. These results may therefore benefit researchers working on other species such as NH [3.20] and OH [3.21]. We note that the 1D cavity model is a good approximation which captures the main results of a more complete description that includes transverse effects [3.15]. Moreover, through the analysis of the scaling laws, it was shown that cavity cooling of a very large molecular sample is possible by use of a far off-resonant, high intensity pump. Interestingly, since far off-resonant interactions do not rely on specific internal energy levels of particles, cavity cooling can in principle be realized for any polarisable species. We note that the molecule-field coupling in far off-resonance is described by the polarizability of molecules that accounts for all transition lines. Further investigation is required to extend the current model to the far off-resonance regime.

3.7 References

[3.1] A. Hinchliffe, B. Nikolaidi, and H. J. S. Machado, *Density Functional Studies of the Dipole Polarizabilities of Substituted Stilbene,* Azoarene and Related Push-Pull Molecules, International Journal of Molecular Sciences, 5, 224-238 (2004).

[3.2] M. A. Castro and S. Canuto, *Dipole moment, polarizability, and their derivatives for the SiC molecule*, Physical Review A, 48, 826-828 (1993).

[3.3] J. W. Daily, C. Dreyer, A. Abbud-Madrid, and M. C. Branch, *Transition Probabilities in the $B^1\Sigma$-$X^1\Sigma^+$ and the $B^1\Sigma^+$-$A^1\Pi$ electronic systems of MgO*, 2nd Joint Meeting of the U.S. Sections of the Combustion Institute (2001).

[3.4] J. Luque and D. R. Crosley, *Lifebase: Database and Spectral Simulation*, SRI International (1999).

[3.5] A. Schadee, *Unique definitions for the band strength and the electronic vibrational dipole moment of diatomic molecular radiative transitions*, Journal of Quantitative Spectroscopy and Radiative Transfer, 19, 451-453 (1978).

[3.6] G. Herzberg and J. W. T. Spinks, *Molecular Spectra and Molecular Structure: I Spectra of Diatomic Molecules*, D. Van Nostrand Company, Inc (1951).

[3.7] E. E. Whiting, J. A. Paterson, I. Kovacs, and R. W. Nicholls, *Computer checking of rotational line intensity factors for diatomic molecules*, Journal of Molecular Spectroscopy, 47, 84-98 (1973).

[3.8] P. Domokos and H. Ritsch, *Mechanical effects of light in optical resonators,* Journal of Optical Society of America, 20, 1098-1130 (2003).

[3.9] P. Domokos and H. Ritsch, *Collective cooling and self-organization of atoms in a cavity,* Physical Review Letters, **89,** 253003-1-4 (2002).

[3.10] O.Marlan, Scully and M. Suhail Zubairy. *Quantum Optics,* Cambridge University Press, Cambridge, UK (1997).

[3.11] P. Domokos, P. Horak and H. Ritsch, *Semiclassical theory of cavity-assisted atom cooling,* Journal of Physics B: Atomic, Molecular and Optical Physics. 34, 187-198 (2001).

[3.12] Stephen M. Barnett and Paul M. Radmore, *Methods in theoretical quantum optics,* Claredon press, Oxford, UK (2005).

[3.13] N. G. Van Kampen, *Stochastic processes in Physics and chemistry,* North Holland, Amsterdam (1992).

[3.14] Crispin Gardiner, *Stochastic Methods-A Handbook for the Natural and Social Sciences,* Springer, Berlin (1985).

[3.15] J. K. Asboth, P. Domokos, H. Ritsch and A. Vukics, *Self-organization of atom in a cavity field: Threshold, bistability, and scaling laws,* Physical Review A, 72, 053417-1-12 (2005).

[3.16] V. Vuletic´ and S. Chu, *Laser cooling of atoms, ions or molecules by coherent scattering,* Physical Review Letters, 84, 3787-3790 (2000).

[3.17] R. Fulton, A. I. Bishop, M. N. Shneider and P. F. Barker, *Controlling the motion of cold molecules with deep periodic optical potentials,* Naural Physics, 2, 465-468 (2006).

[3.18] www.sri.com/psd/lifbase/.

[3.19] P. Horak, G. Hechenblaikner, K. M. Gheri, H. Stecher and H. Ritsch, *Cavity – induced atom cooling in the strong coupling regime,* Physical Review Letters, 79, 4974- 4977 (1997).

[3.20] D. Egorov, W. C. Campbell, B. Fredrich, S. E. Maxwell, E. Tsikata, L. D. Van Buuren and J. M. Doyle, *Buffer-gas cooling of NH via the beam loaded buffer-gas method,* The European Physical Journal D, 31, 307- 311 (2004).

[3.21] S. Y. T. Van de Meerakker, P. H. M. Smeets, N. Vanhaecke, R. Y. Jongma and G. Meijer, *Deceleration and electrostatic trapping of OH radicals,* Physical Review Letters, 94, 023004-1-4 (2005).

[3.22] K. D. Bayes, *A Study of the CN Emission from Active Nitrogen Flames*, Canadian Journal of Chemistry, 39, 1074-1085 (1961).

[3.23] R. F. Gutterres, J. Verges, and C. Amiot, *The BaI $X^2\Sigma^+$ and $B^2\Sigma^+$ Electronic States Through $B^2\Sigma^+$-$X^2\Sigma^+$ and $C^2\Sigma^+$- $X^2\Sigma^+$ Band Systems Analysis*, Journal of Molecular Spectroscopy, 196, 29-44 (1999).

[3.24] H. Ito, K. Suzuki, T. Kondow, and K. Kuchitsu, *Electronic transition moment for the emission of CN. Analysis of dependence on the internuclear distance*, Journal of Chemical Physics, 94, 5353-5359 (1991).

[3.25] D. A. Steck, *Rubidium 85 D Line Data*, available online at http://steck.us/alkalidata (revision 0.1.1, 2 May 2008)

[3.26] I. Protsenko, P. Domokos, V. Lefe´vre, J. Hare, J. M. Raimond, and L. Davidovich, *Quantum theory of a thresholdless laser*, Physical Review A, 59, 1667-1681 (1999).

[3.27] L. F. Shampine and M. K. Gordon, *Computer Solution of Ordinary Differential Equations: the Initial Value Problem*, W. H. Freeman, SanFrancisco, 1975.

[3.28] P. Horak and H. Ritsch, *Scaling properties of cavity-enhanced atom cooling*, Physical Review A, 64, 033422-1-7 (2001).

Chapter 4

Statistical model

4.1 Introduction

It has been observed that the damped atomic motion in an optical cavity due to the coupled atom-field dynamics which leads to a friction force [4.1-4.2]. This cavity cooling scheme avoids or reduces several problems of the laser-cooling scheme, such as photon re-absorption and recoil heating. Moreover, cavity cooling is an attractive approach for creating ultracold molecules as there is no requirement of a closed multilevel system. Now a range of techniques is able to produce and trap stable cold molecules at temperatures in the 10-100 mK range [4.3-4.6]. Cavity cooling appears to be a effective method towards further cooling a large range of species1 to the ultracold regime below 1 mK [4.7-4.11].

In cavity cooling, the commonly used mathematical model comprises a set of equations of motion for each particle that is coupled to the same intracavity field [4.9-4.10]. This many-particle model can be represented quantum mechanically or semi-classically. The latter has shown good agreement with the former in recent extensive studies for temperatures higher than the cavity cooling limit. While the model is effective, it becomes impractical when a large ensemble is involved according to realistic particle number [4.40, 4.41]. Our understanding so far of cooling of an ensemble of particles is based on scaling laws which are obtained using various approximations and have not yet been fully tested to reliably predict the instability thresholds or other conditions [4.9, 4.42, 4.43]. The quantities are very important to study system status in theory or to estimate the potential of future experimental applications as molecular cooling [4.39].

In this chapter, we have developed a new statistical model based on the Boltzmann equation. This model could be used to statistical analysis the probability and other properties characteristic of a number of particles. We show a good agreement between the theory and numerical simulations.

4.2 One-Dimensional Collisionless Boltzmann Equation

In this section, we present one-dimensional collisionless Boltzmann equation for modeling molecular motion in a one-dimensional optical cavity as shown in Fig. 4.1.

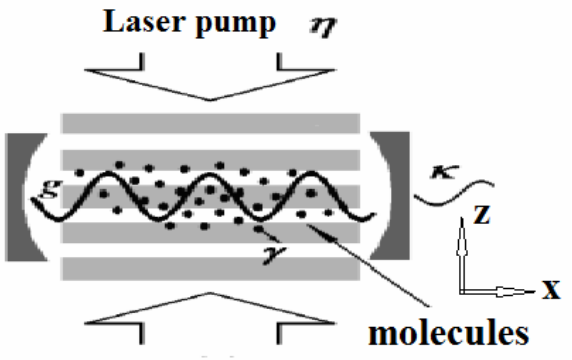

Fig. 4.1 The modeling of molecular motion with Boltzmann equation in a one-dimensional optical cavity

The one-dimensional collisionless Boltzmann Equation is initially used in recent experimental work in coherent Rayleigh scattering and its applications where the distribution function was measured using light scattering techniques [4.12-4.13].

Eq. (4.1) has also been used in theoretical treatments which describe a pulsed standing wave mirror, and the deceleration of cold molecules in a molecular beam using a one dimensional far-off resonant optical lattice [4.14-4.16]. This formalism could also be used to model recent experiments demonstrating the decelerating, trapping, and bunching of molecules by a Stark deceleration, and measurement of the polarizability of molecules with the optical dipole force [4.17-4.23].

The motion of molecules are considered in a high intensity optical cavity in which the momentum transferred to the molecules is several orders of magnitude larger than the recoil momentum, and then the molecules can be treated as classical particles under these conditions [4.14, 4.24]. Because the interaction time between the optical

fields and molecules is shorter than the collision time in many experimental schemes, thus most of collisionless conditions can be created within a pulsed supersonic beam [4.25-4.26]. For this situation, the collisionless Boltzmann equation, as shown in equation 4.1, can be used to describe the position and velocity distribution function of the molecules in the cavity [4.27-4.29].

$$\frac{\partial f(\vec{r},\vec{v},t)}{\partial t}+v\frac{\partial f(\vec{r},\vec{v},t)}{\partial \vec{r}}+\frac{F(\vec{r},t)}{m}\frac{\partial f(\vec{r},\vec{v},t)}{\partial \vec{v}}=0 \tag{4.1}$$

Where $f(\vec{r},\vec{v},t)$ is the distribution function of molecules, $F(\vec{r},t)$ is the dipole force, and m is me mass of a single molecule.

Typically the interaction time of the transverse motion of molecules is very short with nanosecond magnitude, and the effect of the transverse force *Fz* on the molecules is weak and not significant, thus this transverse force *Fz* can be treated as a perturbation and neglected in the zero-order approximation of the position and velocity distribution function. With this approximation, the transverse motion can be decoupled from the longitudinal motion as

$$f(\vec{r},\vec{v},t)=f_x(x,v_x,t)f_z(\vec{z},\vec{v}_z,t) \tag{4.2}$$

where the transverse molecular beam distribution function $f_z(\vec{z},\vec{v}_z,t)$ is independent of the longitudinal molecular beam distribution function $f_x(x,v_x,t)$. Inserting Eq. (4.2) into Eq. (4.1) in which the transverse force *Fz* is neglected, and using the variable separation technique, we obtain that the molecular beam distribution function $f_x(x,v_x,t)$ in direction x can be determined by the 1-D Boltzmann equation

$$\frac{\partial f(x,v,t)}{\partial t}+v\frac{\partial f(x,v,t)}{\partial x}+\frac{F(x,t)}{m}\frac{\partial f(x,v,t)}{\partial v}=0 \tag{4.3}$$

where *x* is the position in the cavity, *v* is the velocity, *F* is the force on the molecule, *m* is the mass of the molecule.

Eq. (4.3) can be readily solved without the force term [4.30-4.31], however, if the force is present, an analytical result can hardly be obtained. In section 4.3, we present a numerical algorithm. We also find that in a special case that the force is produced by the lattice with a constant travelling velocity, the equation could be solved. The details are presented in section 4.4.

4.3 Normalization of Collisionless Boltzmann Equation

4.3.1 Normalization of the force

In the discrete model, the force on a certain particle j in the cavity (N particles, j=1, 2, …, N) is

$$\dot{p}_j = U_0(|\alpha|^2 - \frac{1}{2})\sin(2x_j) - i(\eta_{eff}^*\alpha - \eta_{eff}\alpha^*)\sin(x_j) + \xi_{pj} = \frac{\partial p}{\hbar k}/\partial(\kappa t) = \frac{\partial p}{\partial t}/(\hbar k\kappa) = \frac{Force}{\hbar k\kappa} \tag{4.4}$$

This force includes two terms, the dipole force and the noise ξ_{pj} which occurs due to recoil caused by reason due to the spontaneous emission (linewidth γ) of the particles.

The intracavity field equation in the discrete model is (x_j is normalized by k_x)

$$\dot{\alpha} = [i\Delta_c - 1]\alpha - [\Gamma_0 + iU_0]\sum_{j=1}^{N}\cos^2(x_j)\alpha - \eta_{eff}\sum_{j=1}^{N}\cos(x_j) + \xi_a, \tag{4.5}$$

where the noise term ξ_α includes two parts, γ and the cavity linewidth κ.

When we choose a large detuning of Δ_a, the effect of spontaneous emission will be reduced, and the parameter $\Gamma_0 \approx \frac{\gamma g^2}{\Delta_a{}^2}$ in the noise term approaches to 0. The stable temperatures of the molecule ensembles are related with the noise.

This result proved we can only consider the noise caused by cavity linewidth κ. Then $\xi_\alpha = \sqrt{\kappa/2}\zeta_r^{(a)} + i\sqrt{\kappa/2}\zeta_i^{(a)}$, where $\zeta_r^{(a)}$ and $\zeta_i^{(a)}$ are the random numbers with mean 0 and variance 1, ξ_{pj} could be neglected.

4.3.2 Normalization from velocity v to momentum p

In our discrete model's equations, the parameters are normalized by

$x_n(t) = kx(t)$,

$p_n(t) = p(t)/(\hbar k)$,

$t_n = \kappa t$.

The wave number

$$k = \frac{2\pi}{\lambda} \approx \frac{2\pi}{\lambda_{R1}} \approx \frac{2\pi\times 10^9}{387.5704} \approx 1.6212\times 10^7\ (\mathrm{m}^{-1}).$$

The coefficient on equation of position is $\hbar k^2/(m\kappa) = c_1$, for CN, $c_1 = 1/32$. With these parameters, we should do some normalization in the statistical model.

According to the kinetic energy relation, we got

$$\frac{1}{2}mv^2 = \frac{p^2}{2m} = \frac{p^2 c_1 \kappa}{2(\hbar k^2)} = (\frac{p}{\hbar k})^2 \frac{c_1 \hbar \kappa}{2} = {p_n}^2 \frac{c_1 \hbar \kappa}{2}.$$

On the other hand, the kinetic energy relation can also be shown as

$$\frac{1}{2}mv^2 = \frac{v^2 \hbar k^2}{2(c_1 \kappa)} = {p_n}^2 \frac{c_1 \hbar \kappa}{2}.$$

Then

$$v^2 = {p_n}^2 \frac{(c_1 \kappa)^2}{k^2}.$$

So we get

$$v = p_n \frac{c_1 \kappa}{k},\ \frac{c_1 \kappa}{k} = c_2. \tag{4.5}$$

c_2 is a dimensionless parameter. For example, under the conditions of our discrete model,

$$c_2 \approx 1/26.$$

So if the location of p_n is [-50, 50], the velocity should be [-1.93, 1.93] (m/s).

4.3.3 Normalization of Boltzmann Equation

We put $p_n = p/\hbar k = mv/\hbar k$ and other conditions into Eq. (4.3), then get

$$\frac{\partial f(x,v,t)}{\frac{\kappa}{\kappa}\cdot\partial t} + \frac{\frac{m}{\hbar k}v}{\frac{m}{\hbar k}} \frac{\partial f(x,v,t)}{\frac{k}{k}\cdot\partial x} + \frac{F(x,t)}{\hbar k}\frac{\partial f(x,v,t)}{\frac{m}{\hbar k}\cdot\partial v} = 0,$$

which equals to

$$\frac{\partial f(x_n,p_n,t_n)}{\frac{\partial t_n}{\kappa}} + \frac{p_n}{\frac{m}{\hbar k}} \frac{\partial f(x_n,p_n,t_n)}{\frac{\partial x_n}{k}} + \frac{F(x_n,t_n)}{\hbar k}\frac{\partial f(x_n,p_n,t_n)}{\partial p_n} = 0.$$

Finally, we can obtain

$$\frac{\partial f(x_n,p_n,t_n)}{\partial t_n} + \frac{\hbar k^2}{m\kappa} p_n \frac{\partial f(x_n,p_n,t_n)}{\partial x_n} + \frac{F(x_n,t_n)}{\hbar k \kappa}\frac{\partial f(x_n,p_n,t_n)}{\partial p_n} = 0,$$

then

$$\frac{\partial f(x_n,p_n,t_n)}{\partial t_n}+c_1 p_n\frac{\partial f(x_n,p_n,t_n)}{\partial x_n}+\frac{F(x_n,t_n)}{\hbar k\kappa}\frac{\partial f(x_n,p_n,t_n)}{\partial p_n}=0\,. \tag{4.6}$$

According to the discussion in chapter 3, when the particle number in the cavity is large, their positions and velocities can be described by a continuous distribution function $f(x,v,t)$. The sum term $\sum_{j=1}^{N}\cos^2(x_j)$ in Eq. (4.5) of the statistical model should be $N\int P(x)\cos^2(x)dx$. $P(x)$ is the probability distribution, which corresponds to $f(x,p,t)$ in Boltzmann Equation. Thus the sum term is replaced as $N\iint f(x,p,t)dv\cos^2(x)dx$.

The dynamics of the intracavity field in this statistical model is given by

$$\begin{aligned}&\dot{\alpha}=[i\Delta_c-\kappa]\alpha-[\Gamma_0+iU_0]N\iint f(x,v,t)dv\cos^2(x)dx\alpha\\&-\eta_{eff}N\iint f(x,v,t)dv\cos(x)dx+\xi_\alpha\end{aligned} \tag{4.7}$$

which is a straightforward extension from the first equation of Eq. (3.34).

The dipole force $F(x,t)$ exerted on the particles can be written as

$$F(x,t)=\hbar k\left\{U_0(|\alpha|^2-\frac{1}{2})\sin(2x)-i(\eta_{eff}^*\alpha-\eta_{eff}\alpha^*)\sin(x)\right\}+\xi_p \tag{4.8}$$

which comprises 3 sources: the dipole force, the force resulting from pump-intracavity field interference and noise ξ_p due to the recoil.

In our study we are interested in the case of large detuning, for example, $\Delta_A>>\gamma,\kappa,g$, and in this case only the noise term in the field equation needs to be considered.

4.4 An algorithm for Solving the Collisionless Boltzmann Equation

In this section, a numerical algorithm is developed for solving the one dimensional Boltzmann Equation Eq. (4.3) with the initial condition of

$$f(x, v, t=0)=f_0(x, v) \tag{4.9}$$

and the periodic boundary condition in real space

$$f(-L, v, t)=f(L, x, t) \tag{4.10}$$

together with the natural boundary condition in velocity space

$$f(x, v, t)\rightarrow 0 \text{ as } |v|\rightarrow\infty \tag{4.11}$$

In this algorithm, Eq. (4.3) will be split into two partial differential equations: one governs the spatial evolution and is solved with fast Fourier transform [4.32], while, the other describes the propagation in velocity space and is solved with the Beam-Warming method [4.33].

Eq. (4.3) is solved in one period, $-L \leqslant x \leqslant L$， due to the periodic boundary condition in real space (Eq. (4.10)). Also, the natural boundary condition in velocity space (Eq. (4.11)) is approximated by choosing two large velocities $v_L<0$ and $v_R>0$ where $f(x, v_L, t)\approx 0$ and $f(x, v_R, t)\approx 0$.

For numerical calculations， we plot grids in the space(z, u) with uniform spacing in each coordinate direction as shown in Fig. 4.2.

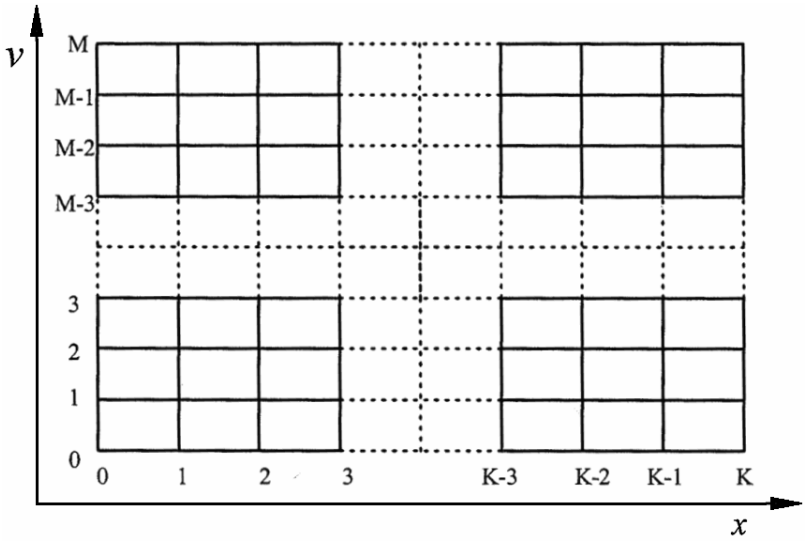

Fig. 4.2 Discrete grid points in phase space (x, v)

In the x and v directions, the spaces are denoted respectively as $\Delta x=2L/K$ and $\Delta v \equiv(v_R-v_L)/M$, so $x_k=-L+k\Delta x$ (k=0, 1, 2, …, K) and $v_m=v_L+m\Delta v$ (m=0, 1, 2, …, M). The time evolution for t=0 to $t=T$ is also discretized with the time step denoted as Δt. In the following $t=n\Delta t$ is denoted as t_n where n=0, 1, 2, …, N, Δt is determined by $\Delta t=T/N$. For convenience, the function value of $f(x, v, t)$ at $x=x_k$, $v=v_m$, $t=t_n$ is denoted as $f_{k,m,n}$. In the following we will present the details of the algorithm.

4.4.1 Split-step technique

From the Boltzmann equation Eq. (4.3), the position and velocity distribution function $f(x, v, t)$ at time $t_{n+1}=(n+1)\Delta t$ is given by [4.32]

$$\frac{\partial f(x,p,t)}{\partial t} = -c_1 p \frac{\partial}{\partial x} f(x,p,t) - \frac{F(x,t)}{\hbar k \kappa} \frac{\partial}{\partial p} f(x,p,t) \tag{4.12}$$

By the formal integration of both sides of Eq. (4.12) from t_n to t_{n+1},

$$f(x,p,t_{n+1}) = \exp\{-c_1 p \Delta t \frac{\partial}{\partial x} - \int_{t_n}^{t_{n+1}} \frac{F(x,t)}{\hbar k \kappa} \frac{\partial}{\partial p} dt\} f(x,p,t_n) \tag{4.13}$$

Generally, the right side of Eq. (4.13) cannot be solved analytically. When the time step size Δt is small, it can be approximated by

$$f(x,p,t_{n+1}) \approx \exp(-c_1 p \Delta t \frac{\partial}{\partial x}) \exp[-\int_{t_n}^{t_{n+1}} \frac{F(x,t)}{\hbar k \kappa} dt \frac{\partial}{\partial p}] f(x,p,t_n) \tag{4.14}$$

In obtaining Eq. (4.14), we have used the Baker-Hausdorff formula [4.34]

$$\exp(\hat{a}) \exp(\hat{b}) = \exp(\hat{a} + \hat{b} + \frac{1}{2}[\hat{a},\hat{b}] + \frac{1}{12}[\hat{a} - \hat{b},[\hat{a},\hat{b}]] + ...) \tag{4.15}$$

where $\hat{a}$ and $\hat{b}$ are operators, and $[\hat{a},\hat{b}] = [\hat{a}\hat{b} - \hat{b}\hat{a}]$. By using Eq. (4.15) with $\hat{a} = -c_1 p \Delta t \frac{\partial}{\partial x}$, and $\hat{b} = -\int_{t_n}^{t_{n+1}} \frac{F(x,t)}{\hbar k \kappa} dt \frac{\partial}{\partial p}$, the dominant error term in the approximation, Eq.(4.14), is found to result from the single commutator $[-c_1 p \Delta t \frac{\partial}{\partial x}, -\int_{t_n}^{t_{n+1}} \frac{F(x,t)}{\hbar k \kappa} dt \frac{\partial}{\partial p}] \sim (\Delta t)^2$. Thus, the calculation of $f(x,p,t_{n+1})$ by Eq. (4.15) is accurate to second order in the time step size Δt. The accuracy can be improved further by a symmetric split-step method [4.35], for example,

$$f(x,p,t_{n+1}) \approx \exp(-c_1 \frac{p\Delta t}{2} \frac{\partial}{\partial x}) \exp[-\int_{t_n}^{t_{n+1}} \frac{F(x,t)}{\hbar k \kappa} \frac{\partial}{\partial p} dt] \exp(-c_1 \frac{p\Delta t}{2} \frac{\partial}{\partial x}) f(x,p,t_n) \tag{4.16}$$

Then we can estimate the accuracy of Eq. (4.16) for calculating $f(x,p,t_{n+1})$. Let $\hat{a} = -c_1 \frac{p\Delta t}{2} \frac{\partial}{\partial x}$, and $\hat{b} = -\int_{t_n}^{t_{n+1}} \frac{F(x,t)}{\hbar k \kappa} dt \frac{\partial}{\partial p}$, and we also define an operator $\hat{c}$ by $\hat{c} = \exp(\hat{b}) \exp(\hat{a})$. Using Eq. (4.15), we have

$$\begin{aligned}
&\exp(\hat{a}) \exp(\hat{b}) \exp(\hat{a}) \\
&= \exp(\hat{a} + \hat{c} + \frac{1}{2}[\hat{a},\hat{c}] + \frac{1}{12}[\hat{a} - \hat{c},[\hat{a},\hat{c}]] + ...) \\
&= \exp(2\hat{a} + \hat{b} + \frac{1}{6}[\hat{b} + \hat{a},[\hat{b},\hat{a}]] + ...) \\
&= \exp\{-c_1 p \Delta t \frac{\partial}{\partial x} - \int_{t_n}^{t_{n+1}} \frac{F(x,t)}{\hbar k \kappa} dt \frac{\partial}{\partial p}\} + \frac{1}{6}[\hat{b} + \hat{a},[\hat{b},\hat{a}]] + ...\}
\end{aligned} \tag{4.17}$$

Comparing Eq. (4.16) with Eq. (4.17), we find that the leading error of Eq. (4.17) results from the double communator, $[\hat{b}+\hat{a},[\hat{b},\hat{a}]]\sim(\Delta t)^3$, and therefore the accuracy of Eq. (4.16) is third order in the time step size Δt. The disadvantage of Eq. (4.16) is that we have to calculate the factor of $\exp(-c_1\frac{p\Delta t}{2}\frac{\partial}{\partial x})$ twice. However, this disadvantage can be overcome by the following technique.

Using Eq. (4.13), the Boltzmann distribution function is calculated by

$$
\begin{aligned}
&f(x,p,t_{n+1})=\exp(-c_1p\frac{\Delta t}{2}\frac{\partial}{\partial x})\exp[\int_{t_n}^{t_{n+1}}\frac{F(x,t)}{\hbar k\kappa}\frac{\partial}{\partial p}dt]\exp(-c_1p\frac{\Delta t}{2}\frac{\partial}{\partial x})\\
&\cdot\exp(-c_1p\frac{\Delta t}{2}\frac{\partial}{\partial x})\exp[\int_{t_{n-1}}^{t_n}\frac{F(x,t)}{\hbar k\kappa}\frac{\partial}{\partial p}dt]\exp(-c_1p\frac{\Delta t}{2}\frac{\partial}{\partial x})\cdot\ldots\cdot\\
&\exp(-c_1p\frac{\Delta t}{2}\frac{\partial}{\partial x})\exp[\int_{t_0}^{t_1}\frac{F(x,t)}{\hbar k\kappa}\frac{\partial}{\partial p}dt]\exp(-c_1p\frac{\Delta t}{2}\frac{\partial}{\partial x})f(x,p,t_0)\\
&=\exp(-c_1p\frac{\Delta t}{2}\frac{\partial}{\partial x})\exp[\int_{t_n}^{t_{n+1}}\frac{F(x,t)}{\hbar k\kappa}\frac{\partial}{\partial p}dt]\exp(-c_1p\Delta t\frac{\partial}{\partial x})\cdot\ldots\cdot\\
&\exp(-c_1p\Delta t\frac{\partial}{\partial x})\exp[\int_{t_0}^{t_1}\frac{F(x,t)}{\hbar k\kappa}\frac{\partial}{\partial p}dt]\exp(-c_1p\frac{\Delta t}{2}\frac{\partial}{\partial x})f(x,p,t_0)
\end{aligned}
\tag{4.18}
$$

4.4.2 Numerical procedures for solving the Boltzmann equation

Eq. (4.18) gives a numerical calculation for the Boltzmann distribution function at the time T, $f(x, v, T)$. Before discussing this procedure, we first define a function $h(x, v, n)$ by

$$h(x,v,n)=[BA(n-1)][BA(n-2)]\ldots[BA(1)][BA(0)]\exp(-c_1p\frac{\Delta t}{2}\frac{\partial}{\partial x})f(x,p,0) \tag{4.19}$$

For $n>1$, where

$$A(n)=\exp[\int_{t_n}^{t_{n+1}}\frac{F(x,t)}{\hbar k\kappa}dt\frac{\partial}{\partial p}].$$

$$B=\exp(-c_1p\Delta t\frac{\partial}{\partial x}).$$

And for n=0

$$h(x,v,0)=\exp(-c_1p\frac{\Delta t}{2}\frac{\partial}{\partial x})f(x,p,0)$$

Using these definitions, we briefly present a procedure for calculating the Boltzmann distribution function $f(x,p,T)$ based on Eq. (4.18):

1. Get solution of $h(x,p,t_0)=\exp(-c_1 p\frac{\Delta t}{2}\frac{\partial}{\partial x})f(x,p,t_0)$.

2. Calculate $s(x,p,t_1)=\exp[\int_{t_0}^{t_1}\frac{F(x,t)}{\hbar k\kappa}\frac{\partial}{\partial p}dt]h(x,p,t_0)$.

3. Get solution of $h(x,p,t_1)=\exp(-c_1 p\Delta t\frac{\partial}{\partial x})s(x,p,t_1)$ as the first step output distribution function $f(x,p,t_1)=h(x,p,t_1)$. However, there is a half step error between $h(x,p,t_1)$ and real $f(x,p,t_1)$.

4. Repeat step 2 and 3, get solution of $s(x,p,t_2)$, $f(x,p,t_2)=h(x,p,t_2)$,…, until $s(x,p,t_n)$.

5. Get solution of final output distribution function of

$$f(x,p,t_n)=h(x,p,t_n)=\exp(-c_1 p\frac{\Delta t}{2}\frac{\partial}{\partial x})s(x,p,t_n).$$

4.4.3 Numerical calculation of operation functions

First, we need to get

$$h(x,p,t_n)=\exp(-c_1 p\Delta t\frac{\partial}{\partial x})g(x,p,t_n) \tag{4.20}$$

where

$$g(x,p,t_n)=\exp[\int_{t_{n-1}}^{t_n}\frac{F(x,t)}{\hbar k\kappa}\frac{\partial}{\partial p}dt]h(x,p,t_0).$$

If we consider each step at $(n\text{-}1)\Delta t$ with an initial condition $g(x,p,t_{n-1})=h(x,p,t_{n-1})$, Eq. (4.20) is equivalent to a partial differential equation,

$$\frac{\partial h(x,p,t)}{\partial t}=-\frac{\partial h(x,p,t)\frac{F(x,t)}{\hbar k\kappa}}{\partial p}\qquad (n-1)\Delta t\le t\le n\Delta t. \tag{4.21}$$

We can use the Beam-Warning method to solve Eq. (4.21) [4.33, 4.44], as

$$\begin{aligned}h(x,p,n)&=h(x,p,n-1)-\Delta t\frac{\partial h(x,p,t)\frac{F(x,t)}{\hbar k\kappa}}{\partial p}\\&=h(x,p,n-1)-\Delta t\frac{1}{2}(\frac{F(x,n)}{\hbar k\kappa}\frac{\partial h(x,p,n)}{\partial p}+\frac{F(x,n-1)}{\hbar k\kappa}\frac{\partial h(x,p,n-1)}{\partial p})\\&=g(x,p,n-1)-\Delta t\frac{1}{2}(\frac{F(x,n)}{\hbar k\kappa}\frac{\partial h(x,p,n)}{\partial p}+\frac{F(x,n-1)}{\hbar k\kappa}\frac{\partial g(x,p,n-1)}{\partial p})\end{aligned} \tag{4.22}$$

Using the central difference formula for the first derivative with respect to p, we obtain

$$\left(\frac{F(x,n)}{\hbar k\kappa}\frac{\partial h(x,p,n)}{\partial p}+\frac{F(x,n-1)}{\hbar k\kappa}\frac{\partial g(x,p,n-1)}{\partial p}\right)$$

$$=\frac{1}{2\Delta p}\{\frac{F(x,n)}{\hbar k\kappa}[h(x,p+1,n)-h(x,p-1,n)]$$

$$+\frac{F(x,n-1)}{\hbar k\kappa}[g(x,p+1,n-1)-g(x,p-1,n-1)]\}$$

Then Eq. (4.22) can be written as

$$h(x,p,n)=g(x,p,n-1)-\frac{\Delta t}{4\Delta p}\{\frac{F(x,n)}{\hbar k\kappa}[h(x,p+1,n)-h(x,p-1,n)]$$

$$+\frac{F(x,n-1)}{\hbar k\kappa}[g(x,p+1,n-1)-g(x,p-1,n-1)]\} \tag{4.23}$$

For example,

$$-\frac{\Delta t}{4\Delta p}\frac{F(x,n)}{\hbar k\kappa}h(x,p-1,n)+h(x,p,n)+\frac{\Delta t}{4\Delta p}\frac{F(x,n)}{\hbar k\kappa}h(x,p+1,n)$$

$$=\frac{\Delta t}{4\Delta p}\frac{F(x,n-1)}{\hbar k\kappa}g(x,p-1,n-1)+g(x,p,n-1)-\frac{\Delta t}{4\Delta p}\frac{F(x,n-1)}{\hbar k\kappa}g(x,p+1,n-1) \tag{4.24}$$

Eq. (4.24) is of the tridiagonal form, and so can be solved by Thomas' algorithm [4.36-4.37]. In this section, the case of full step Δt in Eq. (4.20) is discussed. For the term of half step $\Delta t/2$ in Eq. (4.19), the method is same.

4.4.4 Fourier transform of operation functions

For Eq. (4.20), it can also be shown as following after the function of Fourier transform:

$$h(x,p,n)=\mathcal{F}^{-1}\mathcal{F}\{h(x,p,n)\}=\mathcal{F}^{-1}\mathcal{F}\{\exp(-c_1 p\Delta t\frac{\partial}{\partial x})g(x,p,n)\} \tag{4.25}$$

The Fourier transform is

$$\mathcal{F}[e^{\frac{\partial}{\partial x}}f(x)]=\int_{-\infty}^{+\infty}[1+\frac{\partial}{\partial x}+\frac{1}{2!}\frac{\partial}{\partial x}\cdot\frac{\partial}{\partial x}+...]f(x)e^{-ikx}dx \tag{4.26}$$

,

in which the second term can be solved as

$$\int_{-\infty}^{+\infty}\frac{\partial}{\partial x}f(x)e^{-ikx}dx=f(x)e^{-ikx}dx\Big|_{-\infty}^{+\infty}-\int_{-\infty}^{+\infty}f(x)\frac{\partial}{\partial x}e^{-ikx}dx$$

$$=ik\int_{-\infty}^{+\infty}f(x)e^{-ikx}dx=ik\mathcal{F}[f(x)] \tag{4.27}$$

and the third term is

$$\int_{-\infty}^{+\infty}\frac{\partial}{\partial x}(\frac{\partial}{\partial x}f(x))e^{-ikx}dx=\frac{\partial}{\partial x}f(x)e^{-ikx}dx\Big|_{-\infty}^{+\infty}-\int_{-\infty}^{+\infty}\frac{\partial}{\partial x}f(x)\frac{\partial}{\partial x}e^{-ikx}dx$$

$$=ik\int_{-\infty}^{+\infty}\frac{\partial}{\partial x}f(x)e^{-ikx}dx=(ik)^2\mathcal{F}[f(x)] \tag{4.28}$$

According to Eq. (4.27) and Eq. (4.28), the Eq. (4.26) can be written as

$$\mathcal{F}[e^{\frac{\partial}{\partial x}}f(x)]=\int_{-\infty}^{+\infty}[1+ik-\frac{1}{2!}(ik)^2+...]f(x)e^{-ikx}dx=e^{ik}\mathcal{F}[f(x)] \tag{4.29}$$

Then Eq. (4.25) can be rewritten as

$$h(x,p,n)=\mathcal{F}^{-1}\mathcal{F}\{h(x,p,n)\}=\mathcal{F}^{-1}\{\exp(-ic_1p\Delta tk)\mathcal{F}[h(x,p,n)]\}$$

,

where $x=k'\cdot dx$, $dk=(2\pi/dx)/K=2\pi/(2L/K)/K=\pi/L$.

4.5 Direct Solution Method

In this section, another method is used to solve the collisionless Boltzmann equation directly.

The normalized collisionless Boltzmann equation Eq. (4.12) can be written as

$$\frac{\partial f(x,p,t)}{\partial t}+c_1p\frac{\partial}{\partial x}f(x,p,t)+\frac{F(x,t)}{\hbar k\kappa}\frac{\partial}{\partial p}f(x,p,t)=0 \tag{4.30}$$

,

where p is the momentum, which is related to the velocity.

Usingthe split step method as described in Ref. 4.45, we can get

$$\frac{\partial f(x,p,t)}{\partial t}+c_1p\frac{\partial}{\partial x}f(x,p,t)=0 \tag{4.31}$$

$$\frac{\partial f(x,p,t)}{\partial t}+\frac{F(x,t)}{\hbar k\kappa}\frac{\partial}{\partial p}f(x,p,t)=0 \tag{4.32}$$

The solution for Eq. (4.31) and Eq. (4.32) will be described separately in the following:

For Eq. (4.32), when the separated process with time step size Δt is considered, the integration from t_n to t_{n+1}can be written as

$$\int_{t_n}^{t_{n+1}}\frac{\partial f(x,p,t)}{\partial t}dt=\exp[\int_{t_n}^{t_{n+1}}\frac{F(x,t)}{\hbar k\kappa}\frac{\partial f(x,p,t)}{\partial p}dt] \tag{4.33}$$

.

With the central-difference method, if the time stepsize Δt is small enough, Eq. (4.33) can be expressed as

$$f(x,p,n+1)-f(x,p,n)=-\int_{t_n}^{t_{n+1}}\frac{F(x,t)}{\hbar k\kappa}\frac{\partial f(x,p,t)}{\partial p}dt$$

$$\approx-\frac{\Delta t}{2}\{\frac{F(x,n+1)}{\hbar k\kappa}\frac{\partial f(x,p,n+1)}{\partial p}+\frac{F(x,n)}{\hbar k\kappa}\frac{\partial f(x,p,n)}{\partial p}\} \tag{4.34}$$

Then we can get

$$\frac{F(x,n+1)}{\hbar k\kappa}\frac{\partial f(x,p,n+1)}{\partial p}+\frac{2}{\Delta t}f(x,p,n+1)=\frac{2}{\Delta t}f(x,p,n)-\frac{F(x,n)}{\hbar k\kappa}\frac{\partial f(x,p,n)}{\partial p} \tag{4.35}$$

If $F(x, n+1)=0$, Eq. (4.35) can be written as

$$\frac{2}{\Delta t}f(x,p,n+1)=\frac{2}{\Delta t}f(x,p,n)-\frac{F(x,n)}{\hbar k\kappa}\frac{\partial f(x,p,n)}{\partial p} \tag{4.36}$$

If $F(x, n+1)\neq 0$, the second derivative and the first derivative for Eq. (4.35) can be written as

$$\frac{F(x,n+1)}{\hbar k\kappa}\frac{\partial^3 f(x,p,n+1)}{\partial p^3}+\frac{2}{\Delta t}\frac{\partial^2 f(x,p,n+1)}{\partial p^2}=$$
$$\frac{2}{\Delta t}\frac{\partial^2 f(x,p,n)}{\partial p^2}-\frac{F(x,n)}{\hbar k\kappa}\frac{\partial^3 f(x,p,n)}{\partial p^3} \tag{4.37}$$

and

$$\frac{F(x,n+1)}{\hbar k\kappa}\frac{\partial^2 f(x,p,n+1)}{\partial p^2}+\frac{2}{\Delta t}\frac{\partial f(x,p,n+1)}{\partial p}=\frac{2}{\Delta t}\frac{\partial f(x,p,n)}{\partial p}-\frac{F(x,n)}{\hbar k\kappa}\frac{\partial^2 f(x,p,n)}{\partial p^2} \tag{4.38}$$

Putting Eq. (4.38) into Eq. (4.37), we can get

$$\left(\frac{F(x,n+1)}{\hbar k\kappa}\right)^2\frac{\partial^3 f(x,p,n+1)}{\partial p^3}-\left(\frac{2}{\Delta t}\right)^2\frac{\partial f(x,p,n+1)}{\partial p}=-\left(\frac{2}{\Delta t}\right)^2\frac{\partial f(x,p,n)}{\partial p}$$

$$+\frac{2}{\Delta t}\frac{F(x,n)}{\hbar k\kappa}\frac{\partial^2 f(x,p,n)}{\partial p^2}+\frac{2}{\Delta t}\frac{F(x,n+1)}{\hbar k\kappa}\frac{\partial^2 f(x,p,n)}{\partial p^2}-\frac{F(x,n)}{\hbar k\kappa}\frac{F(x,n+1)}{\hbar k\kappa}\frac{\partial^3 f(x,p,n)}{\partial p^3}$$

then

$$\frac{\partial^3 f(x,p,n+1)}{\partial p^3}-\left(\frac{2}{\Delta t}\right)^2\frac{1}{\left(\frac{F(x,n+1)}{\hbar k\kappa}\right)^2}\frac{\partial f(x,p,n+1)}{\partial p}$$

$$=-\left(\frac{2}{\Delta t}\right)^2\frac{1}{\left(\frac{F(x,n+1)}{\hbar k\kappa}\right)^2}\frac{\partial f(x,p,n)}{\partial p}+\frac{2}{\Delta t}\frac{\frac{F(x,n)}{\hbar k\kappa}}{[\frac{F(x,n+1)}{\hbar k\kappa}]^2}\frac{\partial^2 f(x,p,n)}{\partial p^2}$$

$$+\frac{2}{\Delta t}\frac{1}{\dfrac{F(x,n+1)}{\hbar k\kappa}}\frac{\partial^2 f(x,p,n)}{\partial p^2}-\frac{\dfrac{F(x,n)}{\hbar k\kappa}}{\dfrac{F(x,n+1)}{\hbar k\kappa}}\frac{\partial^3 f(x,p,n)}{\partial p^3}. \tag{4.39}$$

If we set

$$g_{jn}(x)=\left(\frac{2}{\Delta t}\right)^2\frac{1}{\left(\dfrac{F(x,n+1)}{\hbar k\kappa}\right)^2}\frac{\partial f(x,p,n)}{\partial p}-\frac{2}{\Delta t}\frac{\dfrac{F(x,n)}{\hbar k\kappa}}{\left(\dfrac{F(x,n+1)}{\hbar k\kappa}\right)^2}\frac{\partial^2 f(x,p,n)}{\partial p^2}$$

$$-\frac{2}{\Delta t}\frac{1}{\dfrac{F(x,n+1)}{\hbar k\kappa}}\frac{\partial^2 f(x,p,n)}{\partial p^2}+\frac{\dfrac{F(x,n)}{\hbar k\kappa}}{\dfrac{F(x,n+1)}{\hbar k\kappa}}\frac{\partial^3 f(x,p,n)}{\partial p^3} \tag{4.40}$$

Eq. (4.39) can be shown as

$$\frac{\partial^3 f(x,p,n+1)}{\partial p^3}=\left(\frac{2}{\Delta t}\right)^2\frac{1}{\left(\dfrac{F(x,n+1)}{\hbar k\kappa}\right)^2}\frac{\partial f(x,p,n+1)}{\partial p}-g_{jn}(x) \tag{4.41}$$

Using central-difference formulas of order $o(\Delta v^4)$ [4.38], the first, second and third differential of momentum p for the distribution function can be displayed as

$$\frac{\partial f(x,p,n)}{\partial p}=\frac{-f(x,p+2\Delta p,n)+8f(x,p+\Delta p,n)-8f(x,p-\Delta p,n)+f(x,p-2\Delta p,n)}{12\Delta p}$$

$$\frac{\partial^2 f(x,p,n)}{\partial p^2}=\frac{-f(x,p+2\Delta p,n)+16f(x,p+\Delta p,n)-30f(x,p,n)+16f(x,p-\Delta p,n)-f(x,p-2\Delta p,n)}{12\Delta p^2}$$

$$\frac{\partial^3 f(x,p,n)}{\partial p^3}=\frac{-f(x,p+3\Delta p,n)+8f(x,p+2\Delta p,n)-13f(x,p+\Delta p,n)+13f(x,p-\Delta p,n)-8f(x,p-2\Delta p,n)+f(x,p+3\Delta p,n)}{8\Delta p^3} \tag{4.42}$$

On the other hand, the distribution function $f(x, p, n)$ can also be expanded with momentum p using a Taylor expansion as follow:

$$f(x,p_{j+1},t_n)=f(x,p_j,t_n)+\frac{\partial f(x,p_j,t_n)}{\partial p}\Delta p+\frac{1}{2}\frac{\partial^2 f(x,p_j,t_n)}{\partial p^2}\Delta p^2$$
$$+\frac{1}{6}\frac{\partial^3 f(x,p_j,t_n)}{\partial p^3}\Delta p^3+o(\Delta p^4) \tag{4.43}$$

$$f(x,p_{j-1},t_n)=f(x,p_j,t_n)-\frac{\partial f(x,p_j,t_n)}{\partial p}\Delta p+\frac{1}{2}\frac{\partial^2 f(x,p_j,t_n)}{\partial p^2}\Delta p^2$$
$$-\frac{1}{6}\frac{\partial^3 f(x,p_j,t_n)}{\partial p^3}\Delta p^3+o(\Delta p^4) \tag{4.44}$$

Calculating the difference between Eq. (4.43) and Eq. (4.44), we can get

$$f(x,p_{j+1},t_n)-f(x,p_{j-1},t_n)=2\frac{\partial f(x,p_j,t_n)}{\partial p}\Delta p$$
$$+\frac{1}{3}\frac{\partial^3 f(x,p_j,t_n)}{\partial p^3}\Delta p^3+o(\Delta p^5)$$
$$\frac{\partial f(x,p_j,t_n)}{\partial p}=\frac{f(x,p_{j+1},t_n)-f(x,p_{j-1},t_n)}{2\Delta p}-\frac{1}{6}\frac{\partial^3 f(x,p_j,t_n)}{\partial p^3}\Delta p^2-o(\Delta p^4) \tag{4.45}$$

Put Eq. (4.41) into Eq. (4.45) and replace t_n by t_{n+1}, we can get

$$\frac{\partial f(x,p_j,n+1)}{\partial p}\{1+\frac{1}{6}\{[\frac{2}{\Delta t\dfrac{F(x,n+1)}{\hbar k\kappa}}]^2\}=\frac{f(x,p_{j+1},n+1)-f(x,p_{j-1},n+1)}{2\Delta p}+\frac{1}{6}g_{jn}(x)\Delta p^2 \tag{4.46}$$

If we set

$$c(x,n)=1+\frac{1}{6}\{[\frac{2\Delta p}{\Delta t\dfrac{F(x,n+1)}{\hbar k\kappa}}]^2 \tag{4.47}$$

Eq. (4.46) can be written as

$$\frac{\partial f(x,p_j,n+1)}{\partial p}=\frac{f(x,p_{j+1},n+1)-f(x,p_{j-1},n+1)}{2\Delta pc(x,n)}+\frac{1}{6}\frac{g_{jn}(x)}{c(x,n)}\Delta p^2 \tag{4.48}$$

Substituting Eq. (4.48) into Eq. (4.35), we can get

$$\frac{F(x,n+1)}{\hbar k\kappa}[\frac{f(x,p_{j+1},n+1)-f(x,p_{j-1},n+1)}{2\Delta pc(x,n)}+\frac{1}{6}\frac{g_{jn}(x)}{c(x,n)}\Delta p^2]+\frac{2}{\Delta t}f(x,p_j,n+1)$$
$$=\frac{2}{\Delta t}f(x,p_j,n)-\frac{F(x,n)}{\hbar k\kappa}\frac{\partial f(x,p_j,n)}{\partial p} \tag{4.49}$$

Then Eq. (4.32) can be transformed and numerically solved using

$$\frac{F(x,n+1)}{\hbar k\kappa}\frac{f(x,p_{j+1},n+1)-f(x,p_{j-1},n+1)}{2\Delta pc(x,n)}+\frac{2}{\Delta t}f(x,p_j,n+1)$$
$$=\frac{2}{\Delta t}f(x,p_j,n)-\frac{F(x,n)}{\hbar k\kappa}\frac{\partial f(x,p_j,n)}{\partial p}-\frac{F(x,n+1)}{\hbar k\kappa}\frac{g_{jn}(x)}{6c(x,n)}\Delta p^2=G(x,n) \tag{4.50}$$

A similar method will be used to transform and numerically solve Eq. (4.31) and the process is shown in the following.

$$\frac{\partial f(x,p,t)}{\partial t}+c_1 p\frac{\partial}{\partial x}f(x,p,t)=0 \tag{4.31}$$

First, Eq. (4.31) is integrated from t_n to t_{n+1} with time step size of $\Delta t = t_{n+1}-t_n$,

$$\int_{t_n}^{t_{n+1}}\frac{\partial f(x,p,t)}{\partial t}dt=-\int_{t_n}^{t_{n+1}}c_1 p\frac{\partial f(x,p,t)}{\partial x}dt=0 \tag{4.51}$$

With the central-difference method and the condition of a small time stepsize Δt, Eq. (4.51) can be integrated as

$$c_1 p\frac{\partial f(x,p,n+1)}{\partial x}+\frac{2}{\Delta t}f(x,p,n+1)=\frac{2}{\Delta t}f(x,p,n)-c_1 p\frac{\partial f(x,p,n)}{\partial x}. \tag{4.52}$$

If p=0, Eq. (4.52) can be written as

$$\frac{2}{\Delta t}f(x,0,n+1)=\frac{2}{\Delta t}f(x,0,n)\ . \tag{4.53}$$

If $p\neq 0$, the second derivative and the first derivative for Eq. (4.52) can be written as

$$c_1 p\frac{\partial^3 f(x,p,n+1)}{\partial x^3}+\frac{2}{\Delta t}\frac{\partial^2 f(x,p,n+1)}{\partial x^2}=\frac{2}{\Delta t}\frac{\partial^2 f(x,p,n)}{\partial x^2}-c_1 p\frac{\partial^3 f(x,p,n)}{\partial x^3} \tag{4.54}$$

and

$$c_1 p\frac{\partial^2 f(x,p,n+1)}{\partial x^2}+\frac{2}{\Delta t}\frac{\partial f(x,p,n+1)}{\partial x}=\frac{2}{\Delta t}\frac{\partial f(x,p,n)}{\partial x}-c_1 p\frac{\partial^2 f(x,p,n)}{\partial x^2}. \tag{4.55}$$

Putting Eq. (4.55) into Eq. (4.54) and following the deforming process as

$$c_1 p\frac{\partial^3 f(x,p,n+1)}{\partial x^3}+\frac{2}{\Delta t}\frac{1}{c_1 p}\Big[-\frac{2}{\Delta t}\frac{\partial f(x,p,n+1)}{\partial x}+\frac{2}{\Delta t}\frac{\partial f(x,p,n)}{\partial x}$$

$$-c_1 p\frac{\partial^2 f(x,p,n)}{\partial x^2}\Big]=\frac{2}{\Delta t}\frac{\partial^2 f(x,p,n)}{\partial x^2}-c_1 p\frac{\partial^3 f(x,p,n)}{\partial x^3}$$

$$(c_1 p)^2\frac{\partial^3 f(x,p,n+1)}{\partial x^3}-\left(\frac{2}{\Delta t}\right)^2\frac{\partial f(x,p,n+1)}{\partial x}=-\left(\frac{2}{\Delta t}\right)^2\frac{\partial f(x,p,n)}{\partial x}$$

$$+\frac{2}{\Delta t}c_1 p\frac{\partial^2 f(x,p,n)}{\partial x^2}+\frac{2}{\Delta t}c_1 p\frac{\partial^2 f(x,p,n)}{\partial x^2}-(c_1 p)^2\frac{\partial^3 f(x,p,n)}{\partial x^3}$$

we can get

$$\frac{\partial^3 f(x,p,n+1)}{\partial x^3}-\left(\frac{2}{\Delta t}\right)^2\frac{1}{(c_1 p)^2}\frac{\partial f(x,p,n+1)}{\partial x}=-\left(\frac{2}{\Delta t}\right)^2\frac{1}{(c_1 p)^2}\frac{\partial f(x,p,n)}{\partial x}$$

$$+\frac{4}{\Delta t}\frac{1}{c_1 p}\frac{\partial^2 f(x,p,n)}{\partial x^2}-\frac{\partial^3 f(x,p,n)}{\partial x^3} \tag{4.56}$$

If we set

$$r_{kn}(p)=\left(\frac{2}{\Delta t}\right)^2\frac{1}{(c_1 p)^2}\frac{\partial f(x,p,n)}{\partial x}-\frac{4}{\Delta t}\frac{1}{c_1 p}\frac{\partial^2 f(x,p,n)}{\partial x^2}+\frac{\partial^3 f(x,p,n)}{\partial x^3} \tag{4.57}$$

Eq. (4.56) can be rewritten as

$$\frac{\partial^3 f(x,p,n+1)}{\partial x^3}=\left(\frac{2}{\Delta t}\right)^2\frac{1}{(c_1 p)^2}\frac{\partial f(x,p,n+1)}{\partial x}-r_{kn}(p) \tag{4.58}$$

Using central-difference formulas of order $o(\Delta v^4)$, the first, second and third differential of position x for the distribution function can be displayed as

$$\begin{aligned}
\frac{\partial f(x,p,n)}{\partial x}&=\frac{\begin{array}{l}-f(x+2\Delta x,p,n)+8f(x+\Delta x,p,n)\\ -8f(x-\Delta x,p,n)+f(x-2\Delta x,p,n)\end{array}}{12\Delta x}\\
\frac{\partial^2 f(x,p,n)}{\partial x^2}&=\frac{\begin{array}{l}-f(x+2\Delta x,p,n)+16f(x+\Delta x,p,n)-30f(x,p,n)\\ +16f(x-\Delta x,p,n)-f(x-2\Delta x,p,n)\end{array}}{12\Delta x^2}\\
\frac{\partial^3 f(x,p,n)}{\partial x^3}&=\frac{\begin{array}{l}-f(x+3\Delta x,p,n)+8f(x+2\Delta x,p,n)-13f(x+\Delta x,p,n)\\ +13f(x-\Delta x,p,n)-8f(x-2\Delta x,p,n)+f(x+3\Delta x,p,n)\end{array}}{8\Delta x^3}
\end{aligned} \tag{4.59}$$

On the other hand, the distribution function $f(x, p, n)$ can also be expanded with position x using Taylor expansion as shown in the followings

$$\begin{aligned}
f(x_{k+1},p,t_n)&=f(x_k,p,t_n)+\frac{\partial f(x_k,p,t_n)}{\partial x}\Delta x+\frac{1}{2}\frac{\partial^2 f(x_k,p,t_n)}{\partial x^2}\Delta x^2\\
&+\frac{1}{6}\frac{\partial^3 f(x_k,p,t_n)}{\partial x^3}\Delta x^3+o(\Delta x^4)
\end{aligned} \tag{4.60}$$

$$\begin{aligned}
f(x_{k-1},p,t_n)&=f(x_k,p,t_n)-\frac{\partial f(x_k,p,t_n)}{\partial x}\Delta x+\frac{1}{2}\frac{\partial^2 f(x_k,p,t_n)}{\partial x^2}\Delta x^2\\
&-\frac{1}{6}\frac{\partial^3 f(x_k,p,t_n)}{\partial x^3}\Delta x^3+o(\Delta x^4)
\end{aligned} \tag{4.61}$$

Calculating the difference between Eq. (4.60) and Eq. (4.61), we can get

$$\begin{aligned}
f(x_{k+1},p,t_n)-f(x_{k-1},p,t_n)&=2\frac{\partial f(x_k,p,t_n)}{\partial x}\Delta x+\frac{1}{3}\frac{\partial^3 f(x_k,p,t_n)}{\partial x^3}\Delta x^3+o(\Delta x^5)\\
\frac{\partial f(x_k,p,t_n)}{\partial x}&=\frac{f(x_{k+1},p,t_n)-f(x_{k-1},p,t_n)}{2\Delta x}-\frac{1}{6}\frac{\partial^3 f(x_k,p,t_n)}{\partial x^3}\Delta x^2-o(\Delta x^4)
\end{aligned} \tag{4.62}$$

Put Eq. (4.58) into Eq. (4.62) and replace t_n by t_{n+1}, we can get

$$\frac{\partial f(x_k,p,n+1)}{\partial x}\{1+\frac{1}{6}[\frac{2\Delta x}{\Delta t c_1 p}]^2\}=\frac{f(x_{k+1},p,n+1)-f(x_{k-1},p,n+1)}{2\Delta x}+\frac{1}{6}r_{kn}(p)\Delta x^2 \tag{4.63}$$

If we set

$$q(p,n) = 1 + \frac{1}{6}[\frac{2\Delta x}{\Delta t c_1 p}]^2 \tag{4.64}$$

Eq. (4.63) can be written as

$$\frac{\partial f(x_k, p, n+1)}{\partial x} = \frac{f(x_{k+1}, p, n+1) - f(x_{k-1}, p, n+1)}{2\Delta x q(p,n)} + \frac{1}{6}\frac{r_{kn}(p)}{q(p,n)}\Delta x^2 \tag{4.65}$$

Substituting Eq. (4.65) into Eq. (4.52), we get

$$c_1 p[\frac{f(x_{k+1}, p, n+1) - f(x_{k-1}, p, n+1)}{2\Delta x q(p,n)} + \frac{1}{6}\frac{r_{kn}(p)}{q(p,n)}\Delta x^2] + \frac{2}{\Delta t} f(x_k, p, n+1) =$$

$$\frac{2}{\Delta t} f(x_k, p, n) - c_1 p \frac{\partial f(x_k, p, n)}{\partial x}$$

$$c_1 p \frac{f(x_{k+1}, p, n+1) - f(x_{k-1}, p, n+1)}{2\Delta x q(p,n)} + \frac{2}{\Delta t} f(x_k, p, n+1)$$

$$= \frac{2}{\Delta t} f(x_k, p, n) - c_1 p \frac{\partial f(x_k, p, n)}{\partial x} - c_1 p \frac{1}{6}\frac{r_{kn}(p)}{q(p,n)}\Delta x^2 = R(p,n)$$

Then Eq. (4.31) can be transformed and numerically solved by

$$c_1 p \frac{f(x_{k+1}, p, n+1)}{2\Delta x q(p,n)} + \frac{2}{\Delta t} f(x_k, p, n+1) - c_1 p \frac{f(x_{k-1}, p, n+1)}{2\Delta x q(p,n)} = R(p,n) \tag{4.66}$$

4.6 Numerical equations of the Statistical Model

We have introduced two numerical methods in section 4.4 and 4.5 to simulate the distribution variation of the ensemble of particles in the cavity based on one-dimensional Boltzmann Equation.

In section 4.4, the distribution function $f(x, p, T)$ for the normalized collisionless Boltzmann equation Eq. (4.30) could be obtained after the numerical procedure. In section 4.5, the equations are

$$\frac{F(x_k, n+1)}{\hbar k \kappa}\frac{f(x_k, p_{j+1}, n+1)}{2\Delta p c(p,n)} + \frac{2}{\Delta t} f(x_k, p_j, n+1) - \frac{F(x_k, n+1)}{\hbar k \kappa}\frac{f(x_k, p_{j-1}, n+1)}{2\Delta p c(x,n)} = G(x,n)$$

$$G(x,n) = \frac{2}{\Delta t} f(x, p_j, n) - \frac{F(x,n)}{\hbar k \kappa}\frac{\partial f(x, p_j, n)}{\partial p} - \frac{F(x,n+1)}{\hbar k \kappa}\frac{g_{jn}(x)}{6c(x,n)}\Delta p^2 \tag{4.50}$$

$$c_1 p \frac{f(x_{k+1}, p_j, n+1)}{2\Delta x q(p,n)} + \frac{2}{\Delta t} f(x_k, p_j, n+1) - c_1 p \frac{f(x_{k-1}, p_j, n+1)}{2\Delta x q(p,n)} = R(p,n)$$

$$R(p,n)=\frac{2}{\Delta t}f(x_k,p,n)-c_1 p\frac{\partial f(x_k,p,n)}{\partial x}-c_1 p\frac{1}{6}\frac{r_{kn}(p)}{q(p,n)}\Delta x^2 \tag{4.66}$$

The Thomas' algorithm can be applied to solve the above tridiagonal equations [4.36-4.37].

According to the discussion in section 4.3.3, the term $N\iint f(x,p,t)dv\cos^2(x)dx$ in Eq. (4.7) can be replaced with $N\sum_{i=1}^{Nx}\sum_{j=1}^{Np}f(x_i,p_j,t)\cos^2(x_i)$, the subscripts i,j stand for the position and the momentum in the coordinates as shown in Fig. 4.2.

Then Eq. (4.7) can be written as

$$\dot{\alpha}=[i\Delta_c-1]\alpha-[\Gamma_0+iU_0]\alpha N\sum_{i=1}^{Nx}\sum_{j=1}^{Nv}f(x_i,p_j,t)\cos^2(x_i)-\eta_{eff}N\sum_{i=1}^{Nx}\sum_{j=1}^{Nv}f(x_i,p_j,t)\cos(x_i)+\xi_\alpha$$

$$=[i\Delta_c-1]\alpha-iU_0N\alpha\sum_{i=1}^{Nx}\sum_{k=1}^{Np}f(x_i,p_j,t)\cos^2(x_i)-\eta_{eff}N\sum_{i=1}^{Nx}\sum_{k=1}^{Np}f(x_i,p_j,t)\cos(x_i)+\xi_\alpha \tag{4.67}$$

And Eq. (4.8) becomes

$$\frac{F(x,t)}{\hbar k\kappa}=U_0(|\alpha|^2-\frac{1}{2})N\sum_{k=1}^{Np}f(x,p_k,t)\sin(2x)-i(\eta_{eff}^*\alpha-\eta_{eff}\alpha^*)N\sum_{k=1}^{Np}f(x,p_k,t)\sin(2x) \tag{4.68}$$

4.7 Boundary Conditions

When we consider the numerical simulation of the statistical model, the boundary of the momentum and position are limited by the size of velocity and space. Therefore we need to discuss the boundary conditions for the numerical solutions for the normalized collisionless Boltzmann equation.

As analysed in chapter 3, there are three types of movements of the particles in the optical cavity:

1. The particles with lower initial momentum could be slowed and trapped within a small range along the cavity axis during the build up of the intracavity field;

2. The particles with higher initial momentum could be trapped ultimately by a stronger intracavity field within a relatively longer range along the cavity axis;

3. The particles with high initial momentum could not be trapped by the intracavity field. It can be treated as lost particle and neglected when it moves out of the cavity.

4.7.1 Boundary Condition of Momentum

According to the distribution correlation of the collisionless Boltzmann Equation, we can set one equation to solve Eq. (4.67) as

$$f(x_k, p_{j+1}, n+1) = e_j^{x,n} f(x_k, p_j, n+1) + d_{j+1}^{x,n}.$$

The above equation can be transform to

$$\frac{f(x_k, p_{j+1}, n+1) - d_{j+1}^{x,n}}{e_j^{x,n}} = f(x_k, p_j, n+1) \tag{4.69}$$

and

$$\frac{f(x_k, p_j, n+1) - d_j^{x,n}}{e_{j-1}^{x,n}} = f(x_k, p_{j-1}, n+1) \tag{4.70}$$

When we know the initial distribution of the momentum at a certain time, we can try to solve the dynamic equations in the follow way:

Putting Eq. (4.69) and Eq. (4.70) into Eq. (4.67), we can get

$$\begin{aligned} &\frac{F(x_k, n+1)}{\hbar k \kappa} \frac{1}{2\Delta pc(x,n)} [e_j^{x,n} f(x_k, p_j, n+1) + d_{j+1}^{x,n}] + \frac{2}{\Delta t} f(x_k, p_j, n+1) \\ &- \frac{F(x_k, n+1)}{\hbar k \kappa} \frac{1}{2\Delta pc(x,n)} [\frac{f(x_k, p_j, n+1) - d_j^{x,n}}{e_{j-1}^{x,n}}] = G(x,n) \end{aligned} \tag{4.71}$$

For Eq. (4.71), there are two variable parameters which satisfied with

$$\frac{F(x_k, n+1)}{\hbar k \kappa} \frac{1}{2\Delta pc(x,n)} e_j^{x,n} + \frac{2}{\Delta t} - \frac{F(x_k, n+1)}{\hbar k \kappa} \frac{1}{2\Delta pc(x,n)} \frac{1}{e_{j-1}^{x,n}} = 0 \tag{4.72}$$

$$\frac{F(x_k, n+1)}{\hbar k \kappa} \frac{1}{2\Delta pc(x,n)} d_{j+1}^{x,n} + \frac{F(x_k, n+1)}{\hbar k \kappa} \frac{1}{2\Delta pc(x,n)} \frac{d_j^{x,n}}{e_{j-1}^{x,n}} = G(x,n). \tag{4.73}$$

In Eq. (4.72) and (4.73), we should have a boundary condition as $f(x, p_j, n+1) \to 0$ when $|p| \to \infty$. In our model, the boundary is required to set as large as possible. Therefore the condition is $f(x, p_j, n+1) \to 0$ when $|p| \to p_{\lim}$. j=0 is a boundary. Then we can set $\frac{1}{e_0^{x,n}} = 0$, $\frac{d_1^{x,n}}{e_0^{x,n}} = 0$ and we also have $f(x, p_0, n+1) = 0$.

From Eq. (4.72), we can get $e_j^{x,n}$ from $e_{j-1}^{x,n}$ since the initial condition $\frac{1}{e_{j-1}^{x,n}} = 0$.

Then from Eq. (4.73), we can get $d_{j+1}^{x,n}$ from $\frac{d_j^{x,n}}{e_{j-1}^{x,n}}$ since the initial condition $\frac{d_1^{x,n}}{e_0^{x,n}} = 0$.

4.7.2 Boundary Condition of Position

For Eq. (4.68), the similar way can be used to get the boundary conditions of the position. First we set an equation as

$$f(x_{k+1}, p_j, n+1) = u_k^{p,n} f(x_k, p_j, n+1) + v_{k+1}^{p,n}$$
$$\frac{f(x_{k+1}, p_j, n+1) - d_{k+1}^{p,n}}{u_k^{p,n}} = f(x_k, p_j, n+1) \tag{4.74}$$

and

$$\frac{f(x_k, p_j, n+1) - v_k^{p,n}}{u_{k-1}^{p,n}} = f(x_{k-1}, p_j, n+1)\,. \tag{4.75}$$

Putting Eq. (4.74) and Eq. (4.75) into Eq. (4.68), then we can get

$$\begin{aligned} &c_1 p \frac{1}{2\Delta x q(p,n)}[u_k^{p,n} f(x_k, p_j, n+1) + v_{k+1}^{p,n}] + \frac{2}{\Delta t} f(x_k, p_j, n+1) \\ &- c_1 p \frac{1}{2\Delta x q(p,n)} \frac{f(x_k, p_j, n+1) - v_k^{p,n}}{u_{k-1}^{p,n}} = R(p,n) \end{aligned}\,. \tag{4.76}$$

Eq. (4.76) can also be written as

$$c_1 p \frac{1}{2\Delta x q(p,n)} u_k^{p,n} + \frac{2}{\Delta t} - c_1 p \frac{1}{2\Delta x q(p,n)} \frac{1}{u_{k-1}^{p,n}} = 0 \tag{4.77}$$

$$c_1 p \frac{1}{2\Delta x q(p,n)} v_{k+1}^{p,n} + c_1 p \frac{1}{2\Delta x q(p,n)} \frac{v_k^{p,n}}{u_{k-1}^{p,n}} = R(p,n)\,. \tag{4.78}$$

The case of theboundary condition for the position x is a little complex.

There are periodic boundary conditions for the x when we use the collisionless Boltzmann Equation method to do the simulation. Theoretically, the force due to the position of the particle is periodic and the boundary range can be set as 1 period, i.e. $kx=2\pi$. When the particles reach the boundary, they are treated as moving into the start of next period.

However, there are some differences when we are doing the numerical simulation.

Firstly, the third type particles with higher momentum could not be trapped and can be treated as “fly away particles” and neglected.

Secondly, in the numerical algorithm the space is segmented with a certain step size. Due to the limitation of the amount of the calculation of the computer, the step size could not be small enough to reach the limitation of a theoretical value. Then the

movement of particles with high momentum at the boundary could have some errors which lead to instability and invalidate the numerical simulation model.

Therefore, we consider two cases to deal with these situations.

When we analyse the dynamic characteristic of an ensemble, the initial momentum is relative small. Nearly all the particles could be slowed down and trapped in a small space. The boundary condition can be set as $f(x_i, p, n+1) \to 0$ when $|x| \to x_{\lim}$.

When we try to simulate a dynamic process of an ensemble, the initial momentum is relatively high. The particles are easier to fly away due to weak interaction force to the intracavity field. Therefore we consider the case of adding a Super Gaussian potential along the cavity axis as discussed in section 2.3.5, which can trap and rebound the particles back in to the potential. The particles with momentum higher than the depth of the potential could be treated as the third type of particles and neglected. The boundary condition is also set as $f(x_i, p, n+1) \to 0$ when $|x| \to x_{\lim}$.

4.8 Conclusion

In this chapter, we develop the numerical method to simulate the case of a large ensemble of particles. T. Grießer/H. Ritsch and co-workers derive a corresponding Vlasov type equation by using the constancy of the distribution along the characteristics, i.e. particle trajectories, and Fourier expansion of the distribution [4.39]. In our numerical equation in section 4.6, the noises of the field and of the force on the particles are both considered. According to the scaling law discussed in section 3.5.6, the pump frequency detuning Δ_a should be large enough to avoid the effect of defect particles which cause the noise effect of Γ_0 is very small and could be been neglected.

In chapter 5, we firstly test the validity of our statistical model and the numerical algorithm in section 5.2. Then we study the dynamic characteristic of a large ensemble of molecules in a cavity based on our model.

4.9 References

[4.1] P. Horak, G. Hechenblaikner, K. M. Gheri, H. Stecher, and H. Ritsch, *Cavity-Induced Atom Cooling in the Strong Coupling Regime*, Physical Review Letters, **79**, 4974-4977 (1997).

[4.2] P. Maunz, T. Puppe, I. Schuster, N. Syassen, P. W. H. Pinkse, and G. Rempe, *Cavity cooling of a single atom*, Nature, 428, 50-52 (2004).

[4.3] J. D. Weinstein, R. deCarvalho, T. Guillet, B. Friedrich, and J. M. Doyle, *Magnetic trapping of calcium monohydridemolecules atmillikelvin temperatures*, Nature (London), **395**, 148-150 (1998).

[4.4] J. M. Doyle, B. Friedrich, Jinha Kim, and David Patterson, *Buffer-gas loading of atoms and molecules into a magnetic trap*, Phys. Rev. A, **52**, R2515-2518 (1995).

[4.5] H. L. Bethlem, G. Berden, F. M. H. Crompvoets, R. T. Jongma, A. J. A. van Roij, and G. Meijer, *Electrostatic trapping of ammonia molecules*, Nature, 406, 491-494 (2000).

[4.6] M. R. Tarbutt, H. L. Bethlem,J. J. Hudson, V. L. Ryabov, V. A. Ryzhov, B. E. Sauer, G. Meijer, and E. A. Hinds, *Slowing Heavy, Ground-State Molecules using an Alternating Gradient Decelerator*, Physical Review Letters, **92**, 173002-1-4 (2004).

[4.7] P. Domokos and H. Ritsch, *Collective Cooling and Self-Organization of Atoms in a Cavity*, Physical Review Letters, 89, 253003-1-4 (2002).

[4.8] H. W. Chan, A. T. Black, and V. Vuletic, *Observation of Collective-Emission-Induced Cooling of Atoms in an Optical Cavity*, Physical Review Letters, 90, 063003-1-4 (2003).

[4.9] J. K. Asboth, P. Domokos, H. Ritsch, and A. Vukics, *Self-organization of atoms in a cavity field: Threshold, bistability, and scaling laws*, Physical Review A, 72, 053417-1-12 (2005).

[4.10] W. Lu, Y. Zhao and P. F. Barker, *Cooling Molecules in Optical Cavities*, Physical Review A, **76**, 013417-1-4 (2007).

[4.11] B. L. Lev, A. Vukics, E. R. Hudson, B. C. Sawyer, P. Domokos, H. Ritsch, and J. Ye, *Prospects for the Cavity-assisted Laser Cooling of Molecules*, Physical Review A, **77**, 023402-1-13 (2008).

[4.12] J. H. Grinstead1 and P. F. Barker, *Coherent Rayleigh Scattering*, Physical Review Letters, **85**, 1222-1225 (2000).

[4.13] X.G. Pan, M. N. Shneider, and R. B. Miles, *Coherent Rayleigh-Brillouin Scattering*, Physical Review Letters, **89**, 183001-1-4 (2002).

[4.14] P. Ryytty and M. Kaivola, *Pulsed Standing-Wave Mirror for Neutral Atoms and Molecules*, Physical Review Letters, **84**, 5074-5077 (2000).

[4.15] G. Dong, W. Lu, and P. F. Barker, *Collisionless Boltzmann equation with an external periodic traveling force: Analytical solution and application to molecular optics*, Physical Review E, **68**, 016607-1-9 (2003).

[4.16] G. Dong, W. Lu, and P. F. Barker, *Decelerating and bunching molecules with pulsed traveling optical lattices*, Physical Review A, **69**, 013409-1-4 (2004).

[4.17] P. F. Barker and M. N. Shneider, *Optical microlinear accelerator for molecules and atoms*, Physical Review A, **64**, 033408-1-9 (2001).

[4.18] P. F. Barker and M. N. Shneider, *Slowing molecules by optical microlinear deceleration*, Physical Review A, **66**, 065402-1-4 (2002).

[4.19] B. Friedrich, *Slowing of supersonically cooled atoms and molecules by time-varying nonresonant induced dipole forces*, Physical Review A, 61, 025403-1-4 (2000).

[4.20] R. Fulton, A. I. Bishop, and P. F. Barker, *Optical Stark Decelerator for Molecules*, Physical Review Letters, **93**, 243004-1-4 (2004).

[4.21] J. J. Larsen, H. Sakai, C. P. Safvan, I. Wendt-Larsen, and H. Stapelfeldt, *Aligning molecules with intense nonresonant laser fields*, Journal of Chemical Physics, 111, 7774-7781 (1999).

[4.22] H. Sakai, A. Tarasevitch, J. Danilov, H. Stapelfeldt, R. W. Yip, C. Ellert, E. Constant, and P. B. Corkum, *Optical deflection of molecules*, Physical Review A, 57, 2794-2801 (1998).

[4.23] H. Stapelfeldt, H. Sakai, E. Constant, and P. B. Corkum, *Deflection of Neutral Molecules using the Nonresonant Dipole Force*, Physical Review Letters, **79**, 2787-2790 (1997).

[4.24] P. Ryytty and M. Kaivola, *Reflection of thermal atoms by a pulsed standing wave*, The European Physical Journal D, **12**, 415-423 (2000).

[4.25] D. Herschbach, *Chemical physics: Molecular clouds, clusters, and corrals*, Reviews of Modern Physics, 71, S411-S418 (1999).

[4.26] G. Scoles, D Bassi, and U. Buck, *Atomic and Molecular Beam Methods*, Oxford University Press, New York (1988).

[4.27] K. Huang, *Statistical Mechanics*, Wiley, New York (1987).

[4.28] C. Cercignani, *The Boltzmann Equation and Its Applications*, Springer-Verlag, New York (1988).

[4.29] J. L. Lebowitz and E. W. Montroll, *Nonequilibrium Phenomena I: The Boltzmann Equation*, North-Holland, Amsterdam (1983).

[4.30] P. R. Garabedian, *Partial Differential Equations*, Wiley, New York (1964).

[4.31] F. Sharipov, W. Marques, and G. M. Kremer, *Free molecular sound propagation*, Journal of the Acoustical Society of America, 112, 395-401 (2002).

[4.32] R. Heather, H. Metiu, *An efficient procedure for calculating the evolution of the wave function by fast Fourier transform methods for systems with spatially extended wave function and localized potential*, The Journal of Chemical Physics, 86, 5009-5017 (1987).

[4.33] M. B. Giles and W. T. Thompkins, *Propagation and Stability of Wavelike Solutions of Finite Difference Equations with Variable Coefficients*, Journal of Computational Physics, 58, 349-360 (1985).

[4.34] G. H. Weiss and A. A. Maradudin, *The Baker-Hausdorff Formula and a Problem in Crystal Physics*, Journal of Mathematical Physics, 3, 771-777 (1962).

[4.35] O. V. Sinkin, R. Holzlohner, J. Zweck, and C. R. Menyuk,*Optimization of the Split-Step Fourier Method in Modeling Optical-Fiber Communications Systems*, Journal of Lightwave Technoligy, 21, 61-68 (2003).

[4.36] D. Britz, *Modifed Thomas Algorithm for the Digital Simulation of the Catalytic EC' Mechanism Under Cottrellian Conditions*, International Journal of Electrochemical Science, 1, 1-11 (2006).

[4.37] T. R. Bewley, *Numerical Methods in Science and Engineering*, http://casimpkinsjr.radiantdolphinpress.com/pages/cogsci109/handouts/Numerical_methods_in_sci_and_eng.pdf.

[4.38] J. H. Mathews and K. K. Fink, *Numerical Methods Using Matlab, Upper Saddle River*, New Jersey, USA (2004).

[4.39] T. Grießer, H. Ritsch, M. Hemmerling, and G.R.M. Robb, *A Vlasov approach to bunching and selfordering of particles in optical resonators*, The European Physical Journal D, 58, 349-368 (2010).

[4.40] S. Deachapunya, P. J. Fagan, A. G. Major, E. Reiger, H. Ritsch, A. Stefanov, H. Ulbricht, and M. Arndt, *Slow beams of massive molecules*, The European Physical Journal D, 46, 307–313 (2008).

[4.41] Thomas Salzburger and Helmut Ritsch, *Collective transverse cavity cooling of a dense molecular beam*, New Journal of Physics, 11, 055025-1-22 (2009).

[4.42] P. Horak and H. Ritsch, *Scaling properties of cavity-enhanced atom cooling*, Physical Review A, 64, 033422-1-7 (2001).

[4.43] D. Nagy, J. K. Asboth, P. Domokos and H. Ritsch, *Self-organization of a laser-driven cold gas in a ring cavity*, Europhysics Letter, 74, 254-260 (2006).

[4.44] H. Yee, R. Beam, and R. Warming, *Stable Boundary Approximations for a Class of Implicit Schemes for the One-Dimensional Inviscid Equations of Gas Dynamics*, AIAA-81-1009-CF, AIAA Computational Fluid Dynamics Conference, Palo Alto (1981).

[4.45] Akil Narayan and Andreas Klöckner, *Deterministic Methods for the Boltzmann Equation*. http://mathema.tician.de/dl/academic/talks/boltzmann-notes.pdf.

Chapter 5

Cooling and trapping of a Molecular Cloud

5.1 Introduction

In chapter 2 and 3, we studied the centre-of-mass motion of N two-level particles in an optical cavity pumped by a laser field that is transverse to the cavity axis based on a discrete model which is so-called a multi-particle model.

In chapter 4, we developed a new statistical model based on the collisionless Boltzmann equation which can simulate the movement of a huge of particles.

In this chapter, we want to explore the scaling laws with a view to the self-organization and cooling of a large ensemble of species. Firstly, we show a good agreement between the theory and numerical simulations based on the comparison results of the discrete model and the statistical model. Then we show that the scaling laws we obtain differ from the current ones which is introduced at chapter 3 in the case when a large ensemble of species are involved. Finally, we study the cooling of a CN molecular cloud of the density $10^{13}/cm^3$, with an initial temperature at 10 mK in an optical cavity. We find that more than a third of the molecules are stably trapped by the intracavity field and the final temperature is below 1mK.

5.2 Comparing Between Statistical Model and Discrete Model

To validate the statistical model discussed in chapter 4, we choose same initial distribution conditions to do the simulation with two models (discrete and statistical) firstly. We still choosing CN as the object particles.

5.2.1 The distribution of position and velocity

Before the simulation, we need consider the ranges, numbers and resolutions of the space x and momentum p. The initial particle distribution is Gaussian, placed in the central region of the cavity which means the position is uniform distribution and the velocity is normal.

From the results of discrete model with small initial conditions, we set the space of position x as [-6π, 6π), and the space of momentum p as [-51.2, 51.2], which equal to the velocity as [-1.97, 1.97] (m/s). We set the nod number as N_x=2048, N_v=2048, then the resolution dx=12π/2048, dv=0.05.

According to the scaling laws $|\eta_{thr}|^2 \propto \frac{\Delta_a^2 \kappa^2}{g^2 N}$ in chapter 3, we choose the parameters of N=1000, κ=20MHz, g=0.866κ, η=300κ, $\Delta_a = -1000 \times \sqrt{5}\kappa$, γ=0. In this case, the cavity parameters are L=1.5mm, waist w_o≈5μm, finesse F=3.1×10^4.

Fig. 5.1 gives the evolution of position and velocity with the statistical model. Fig. 5.2 gives those with the discrete model. These two models have same initial conditions. The initial momentum of 1000 molecules obeys normal distribution with a mean of 0 and a standard deviation of 1. The position is uniform distribution in the space of [-π/2 π/2].

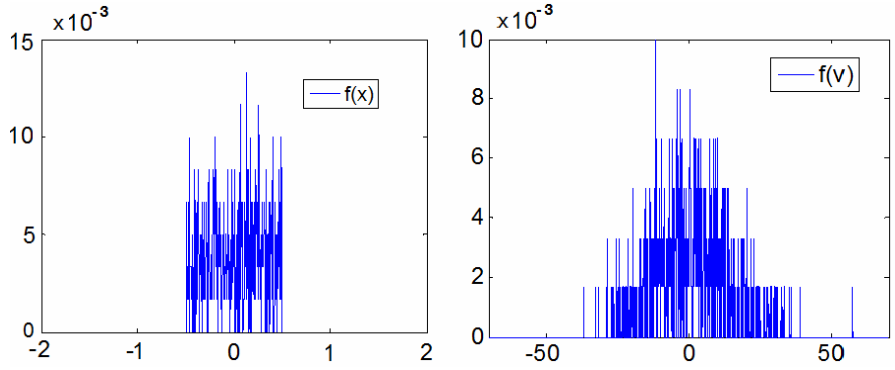

(a) Initial distribution of position *f*(*x*) (π) and velocity *f*(*v*)

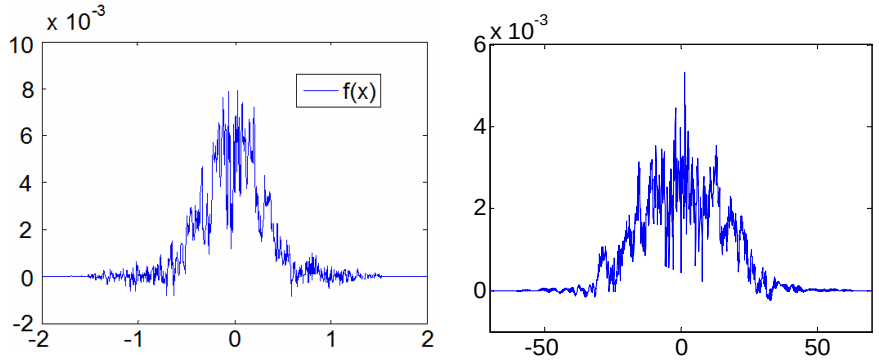

(b) *f*(*x*) (π) and *f*(*v*) after 500steps

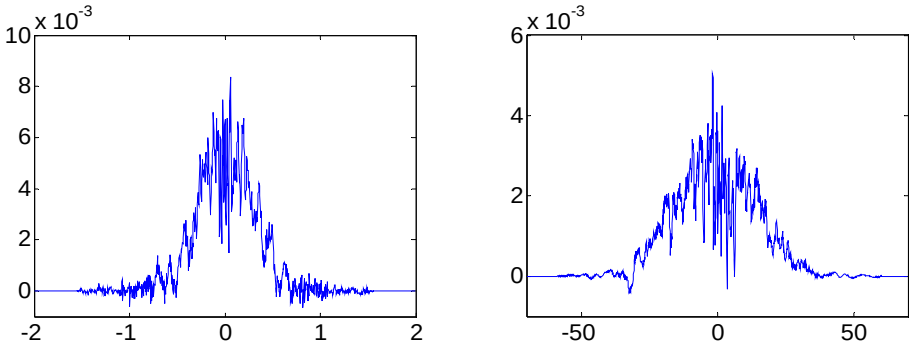

(c) $f(x)$ (π) and $f(v)$ after 1000steps

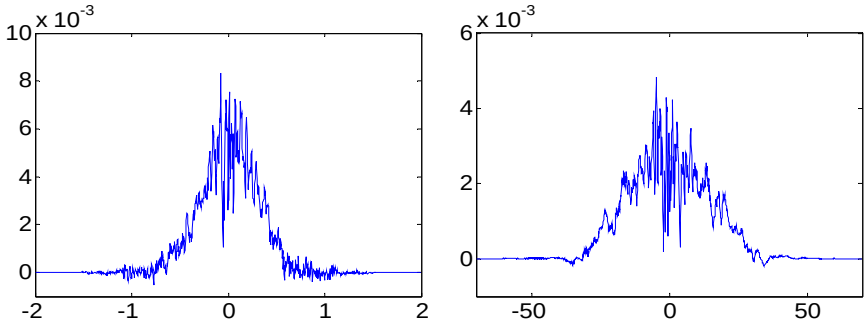

(d) $f(x)$ (π) and $f(v)$ after 2000steps

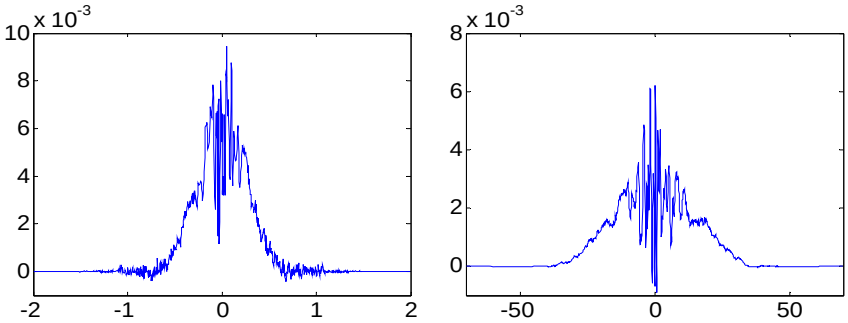

(e) $f(x)$ (π) and $f(v)$ after 10000steps

Fig. 5.1 Evolution of position and velocity with the statistical model

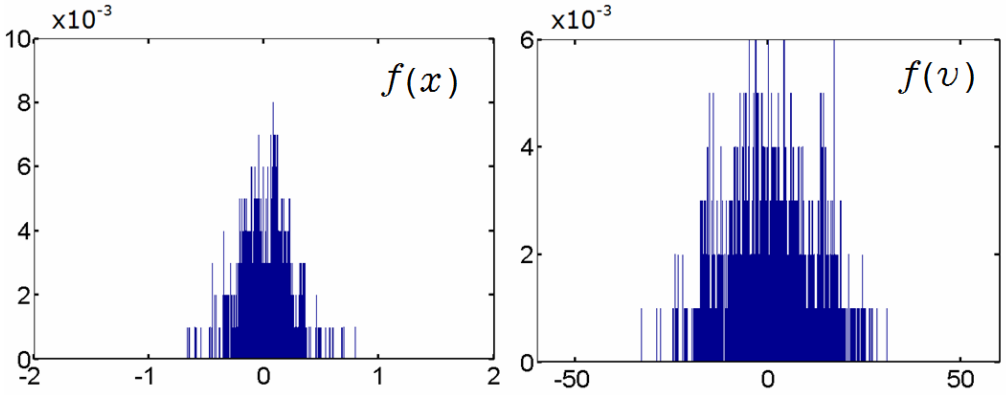

(a) Distribution of position $f(x)$ (π) and velocity $f(v)$ after 500steps with the discrete model

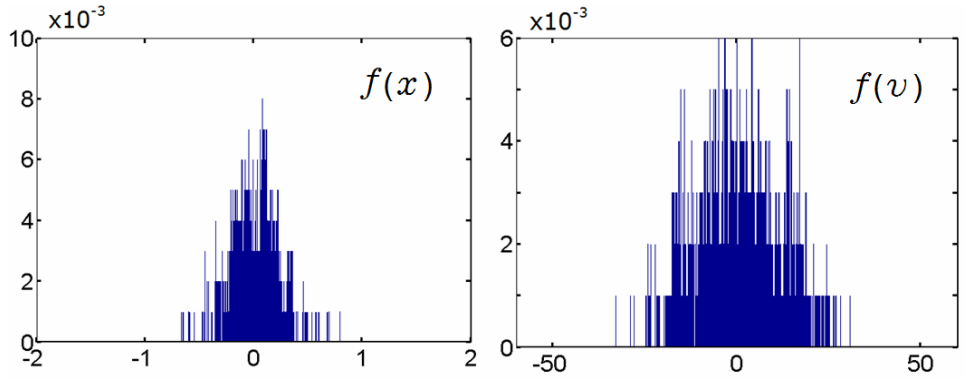

(b) *f*(*x*) and *f*(*v*) after 1000steps

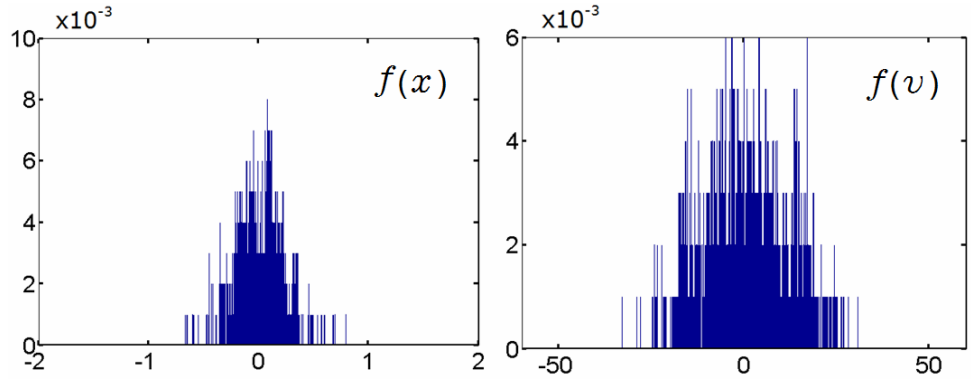

(c) *f*(*x*) and *f*(*v*) after 10000steps

Fig. 5.2 Evolution of position and velocity with the discrete model

The simulation results of steady states are similar. However, there are some negative values of $f(x)$ and $f(v)$ in the case of statistical model due to calculate error caused by the lack of particles. Next we will increase the number of the particles and make a comparison in detail.

5.2.2 Comparison between statistical and many-particle models

Now according the scaling laws, we choose the following parameters as N=2000, κ=20MHz, g=0.866κ, η=300κ, $\Delta_a = -1000\times\sqrt{10}\kappa = -3160\kappa$, γ=0. In this case, the cavity parameters are still L=1.5mm, waist w_o≈5μm, finesse F=3.1×10^4.

As shown in Fig. 5.3, the simulation results after 0.05ms of two models (discrete and statistical) with same initial conditions are similar.

The plot on the up shows the initial and final momentum distributions whereas that on the down gives the position distribution. The parameters used are N=2000, κ=20M*Hz*, g=0.866κ, η=300κ, Δ_A=-3160κ.

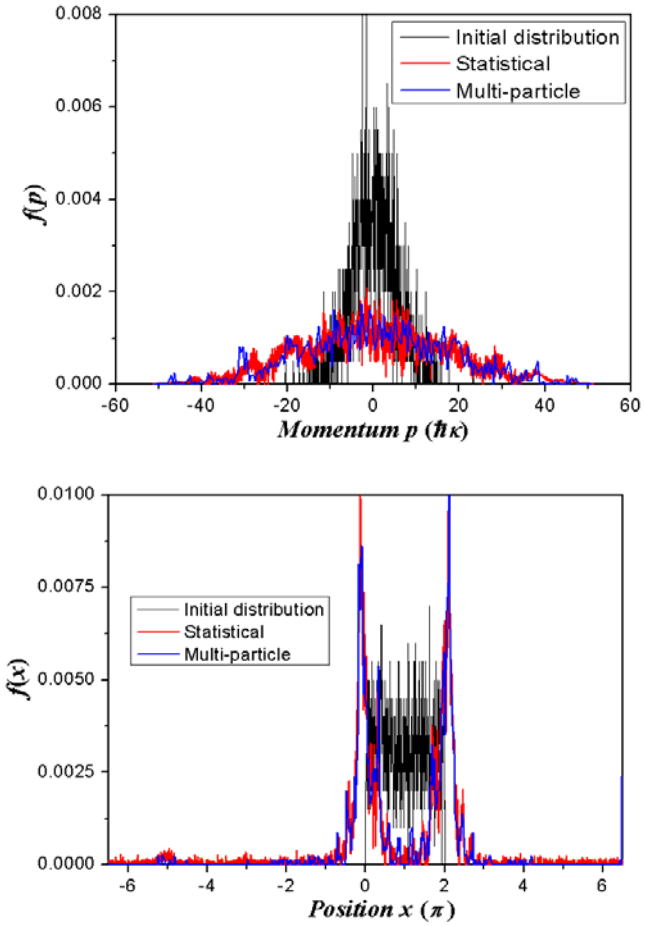

Fig. 5.3 Comparison of the results between the statistical and discrete models.

Fig. 5.4 show the dynamic comparison of the photon number ($|\alpha|^2$), spreading parameter (k^2x^2) and defect between the statistical and the discrete models. The left of each figure shows the first 40 steps in unit of κ and the right shows a period of 0.05ms.

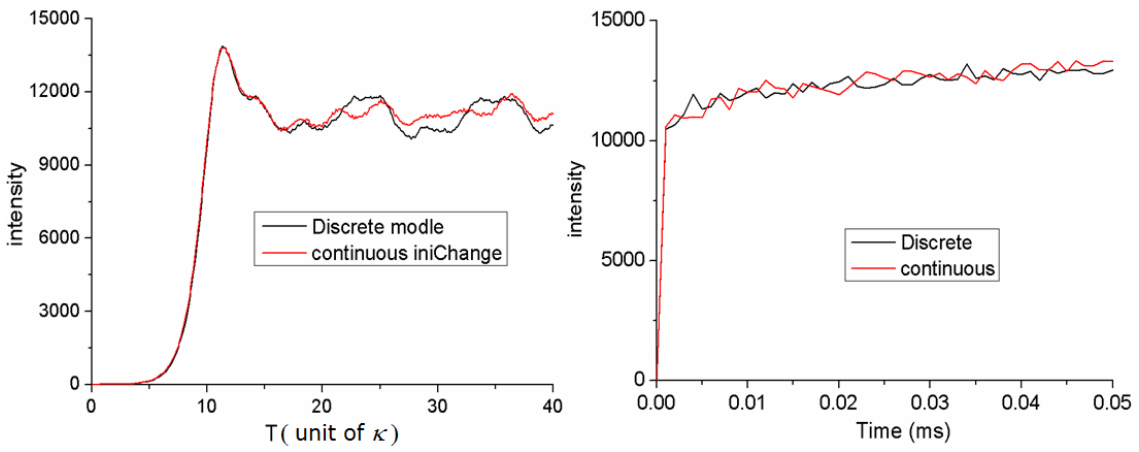

(a) Evolution plot of the intra-cavity field intensity (photon number $|\alpha|^2$) between the discrete model and the statistical model (continuous model).

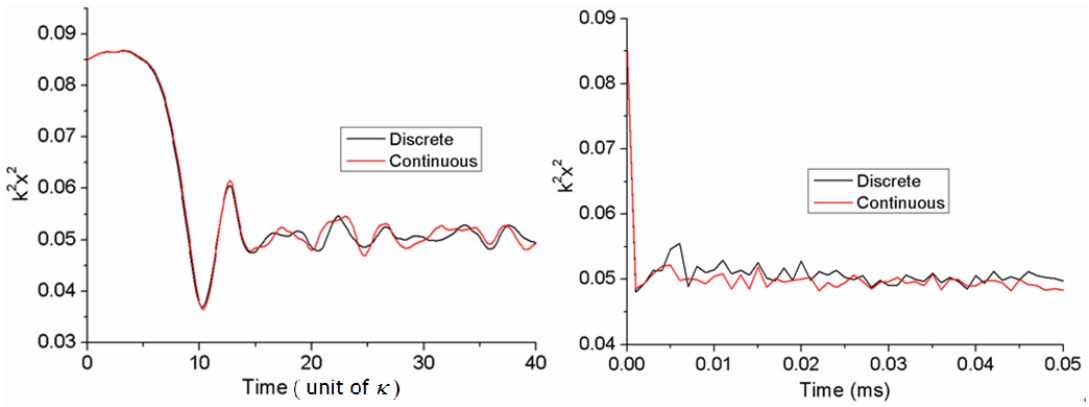

(b) Evolution plot of the spreading parameter (k^2x^2) between the discrete model and the statistical model (continuous model).

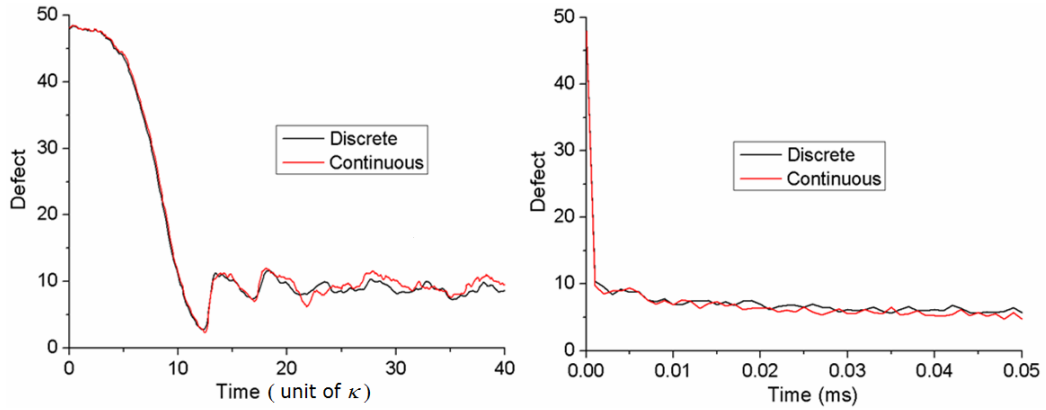

(c) Evolution plot of the defect (percentage) between the discrete model and the statistical model (continuous model).

Fig. 5.4 Comparison of the photon number ($|\alpha|^2$), spreading parameter (k^2x^2)and defect between the statistical and the discrete models. The left of each figure shows the first 40 steps in the unit of κ and the right shows a period of 0.05ms.

Fig. 5.1 to 5.4 have shown a remarkable agreement of the distributions, photon number ($|\alpha|^2$), spreading parameter (k^2x^2) and defect between the statistical and the discrete models. The discrete model can exactly work out the status of each particle in the cavity. However, it is limit to a maximum particle number N~10^4. The statistical model requires the continuity of the distribution, which means it work well with a large number of particles. The results indicate that particles as few as 2000 can be well described by the statistical model. However, the ranges of position and velocity are limited by the resolution and the grid number.

5.3 Simulation of Experiments

5.3.1 Cavity parameters

Now we investigate cavity cooling and trapping molecules in a realistic experimental environment. We still choose CN molecules as the object. For the experiment conditions, the cavity length could be $L\approx1.5$mm with a waist of $w_o\approx50\mu$m. The finesse usually is less than F~$10^{3\text{-}4}$ when the wavelength is near ultraviolet. Now we need make a check for those parameters according to the details in chapter 3.

For the finesse, we got

$$F=\frac{\nu_{FSR}}{\Delta\nu}=\frac{\frac{c}{2L}}{\Delta\nu}=\frac{\lambda}{2L}Q=\frac{\pi\sqrt{R}}{1-R}\approx\frac{\pi}{1-R}\ , \tag{5.1}$$

where R is the reflectivity.

Then we can get

$$1-R=\frac{\pi}{F}\geq3.14\times10^{-4} \tag{5.2}$$

which means the maximum reflectivity of the mirrors of the cavity is 0.999686.

Then the cavity linewidth

$$\kappa=\frac{c\delta}{L}=\frac{c(1-R)}{L}=\frac{3\times10^{8}\times3.14\times10^{-4}}{1.5\times10^{-3}}=62.8MHz \tag{5.3}$$

and the coefficient $c_1=\hbar k^2/(m\kappa)$ should be 1/100. The coefficient c_2 in the statistical model will also change.

To obtain higher coupling strength, we choose the waist $w_o\approx25\mu$m. We consider the transition of the CN B-X, whose transitions' dipole moment is

$$d^2=2.954\times10^{-60}(\mathrm{C^2m^2}) \tag{5.4}$$

The effective mode volume is

$$V_{eff}=\frac{\pi w_0^2L}{4}\approx7.4\times10^{-13}(m^3)\ . \tag{5.5}$$

The coupling constant

$$g^2=\frac{2d^2\omega_c}{\pi\varepsilon_0\hbar(5w_0)^2L}=\frac{1}{25}g_{old}^2\ , \tag{5.6}$$

therefore

$$g=\frac{1}{5}g_{old}=17.32/5(MHz)\approx0.055\kappa\ .$$

The pump intensity is

$$I = P/A = \frac{|\eta|^2 \hbar \omega_p c}{V} A/A = \frac{|\eta|^2 \hbar \omega_p c}{V}, \tag{5.7}$$

where A is the pump area. As a rectangle,

$$A = 2w_o L \approx 2\times 25\times 10^{-6}\times 1.5\times 10^{-3} = 7.5\times 10^{-8} m^2 .$$

If the power of the pump is around 15mW which is checked from internet [5.14],

$$I = \frac{15\times 10^{-3}}{7.5\times 10^{-8}} = 2\times 10^5 W/m^2 = \frac{\eta^2 \times 1.0546\times 10^{-34}(J\cdot s)\times 4.864413\times 10^{15}(Hz)\times 3\times 10^8 (m/s)}{7.4\times 10^{-13}(m^3)}$$

then under these conditions, $\eta \approx 32$.

5.3.2 Molecular parameters

We consider the density of the molecular cloud to be $2\times 10^{14}/\text{cm}^3$. If we assume that the full length in the cavity is available, the cylindrical volume is $1.5\text{mm}\times 25^2 \mu m^2 \times \pi$, and the maximum number N is

$$(2\times 10^{14})\times 10^6 \times 1.5\times 10^{-3}\times \pi \times 25^2 \times 10^{-12} = 6\times 10^8 .$$

The actual density is smaller if the full cavity volume is considered.

According to our scaling $|\eta_{thr}|^2 \propto \frac{\Delta_a^2 \kappa^2}{g^2 N}$ and the conditions discussed in section 3.5, we set the parameters as below:

g changes from 0.866κ to 0.055κ, which decreases by 16 times; η decreases from 300 to 32; N increases from 2000 to 6×10^8, which increases by 3×10^5 times.

Following the scaling, the Δ_a^2 could be $3\times 10^5/(300/32)^2/16^2 = 12$ times larger. Therefore the molecules are considered to be pumped transversely by a laser source with a large frequency detuning.

$$\Delta_a = -1000\times \sqrt{10}\times \sqrt{12}\kappa = -1.1\times 10^4 \kappa = 690.8\text{GHz} .$$

Hence $\Gamma_0 \approx 6\times 10^{-12} << U_0$, which means $\Gamma_0 \to 0$.

From our simulation, we found if we increase η to η=64, the self-organization of this huge number of molecules can be built up rapidly according to the parameter of defect. This means the power of the pump will be 4 times higher, as 60mW.

The temperature of the molecules has the relationship to the momentum as

$$\frac{k_B T}{\hbar\kappa} = \left\langle c_1 (\frac{p}{\hbar k})^2 \right\rangle = \left\langle c_1 p_n^2 \right\rangle . \tag{5.8}$$

According to our setting conditions, the coefficient c_1=1/100, and the cooling limit $\hbar\kappa \approx 0.48(mK)$. We set the initial temperature of the molecular cloud is about 1mK, i.e. $\left\langle p_n^2 \right\rangle = \frac{k_B T}{c_1 \hbar\kappa} = 200$, the half width of the momentum Gaussian distribution should be larger than $3\sigma \approx 3\times\sqrt{200} \approx 42.5$ to contain near all molecules. In the simulation, we choose the momentum range as [-102.4, 102.4].

5.3.3 Dynamics of a large ensemble of CN molecules

The simulation results are shown in the Fig. 5.5 and 5.6. The figures of intracavity field intensity, spreading parameter k^2x^2 and the defect shows the self-organization evolution of the ensemble of molecule.

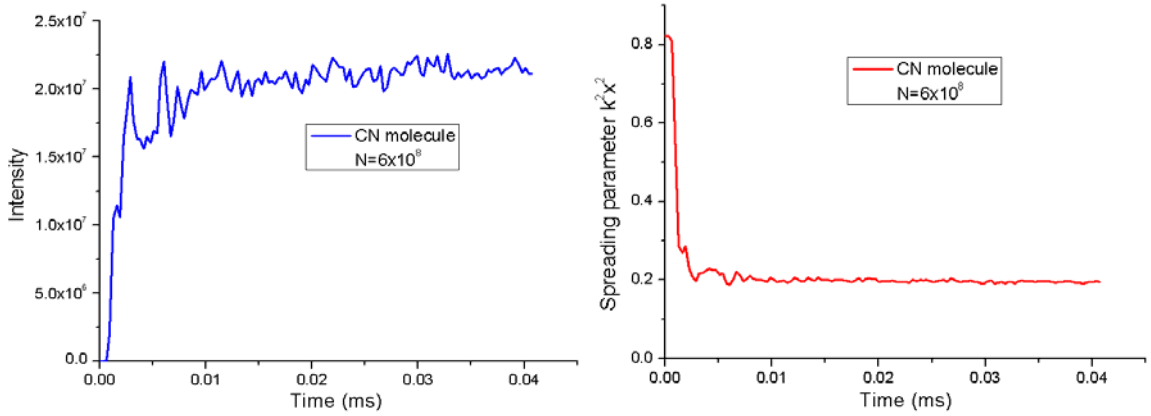

(a) **(b)**

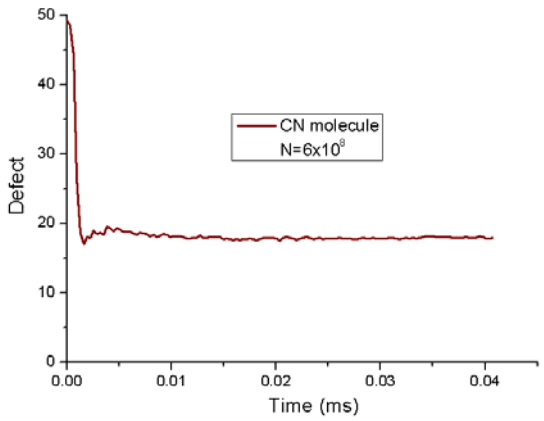

(c)

Fig. 5.5 Evolution plot of the intensity (a), spreading parameter (b) and defect with the statistical model. The parameters are setting as introduced in section 5.3.

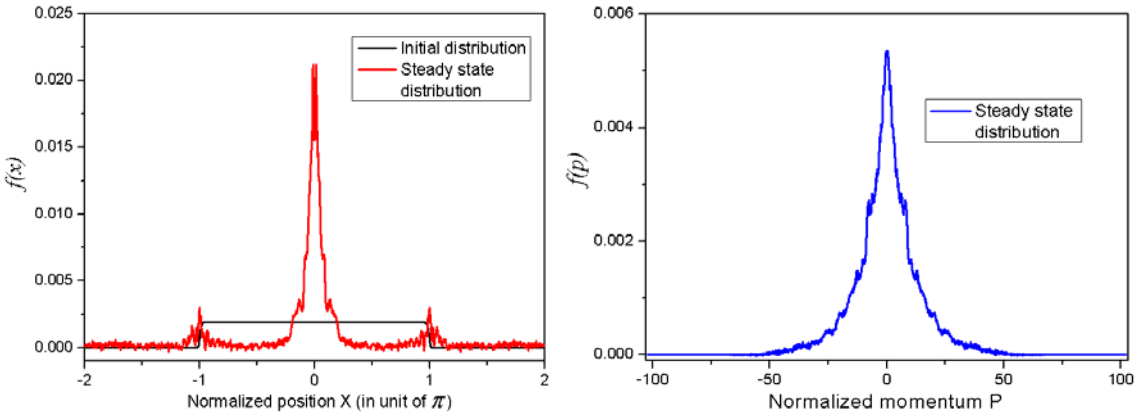

Fig. 5.6 The distribution of position (left) and velocity (right) of molecules in steady state

5.4 Scaling Laws for a large ensemble of Molecules

5.4.1 The limit of the small number scaling laws

In chapter 3, we have discussed the scaling laws in the case of smaller particle number and some conditions such as $U_0N<<1$. For a huge number of particles, we need analysis in detail.

We still start from the one-dimensional mathematical model as shown in Fig.5.7, which is introduced in chapter 3.

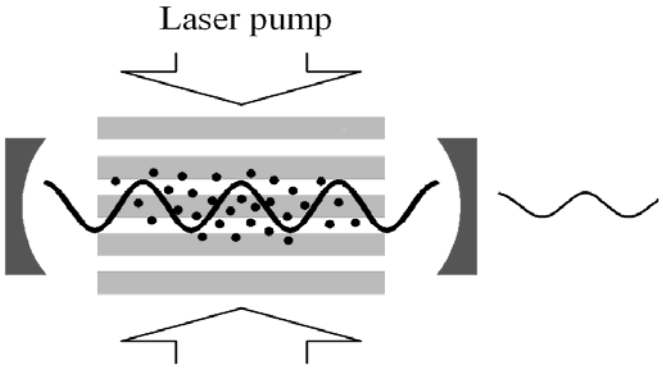

Fig. 5.7 Schematic representation of the perpendicular pump case

The equations of motion in the semi-classical limit are given by

$$\dot{\alpha} = [i\Delta_c - \kappa]\alpha - [\Gamma_0 + iU_0]\sum_j \cos^2(kx_j)\alpha - \eta_{eff}\sum_j \cos^2(kx_j) + \xi_\alpha \tag{5.9}$$

$$\dot{p}_j = \hbar k U_0(|\alpha|^2 - \frac{1}{2})\sin(2kx_j) + i\hbar k(\eta_{eff}^*\alpha - \eta_{eff}\alpha^*)\sin(kx_j) + \xi_{pj} \tag{5.10}$$

$$\dot{x}_j = p_j / m \quad (j=1, 2, \ldots, N) \tag{5.11}$$

where $\alpha(t)$ is the amplitude of the intracavity field, $x(t)$, $p(t)$ and t are particle position, momentum and the time.

The parameters

$$U_0 = \frac{\Delta_A g^2}{\gamma^2 + \Delta_a^2},\ \Gamma_0 = \frac{\gamma g^2}{\gamma^2 + \Delta_a^2},\ \eta_{eff} = \frac{\eta g}{-i\Delta_a + \gamma} \tag{5.12}$$

describe the dispersion and absorption of the particles and the effective external pumping respectively, $\Delta_c = \omega - \omega_c$ and $\Delta_a = \omega - \omega_a$ are the pump-cavity and pump-particle detuning. We restrict our investigation to the case of large detuning $|\Delta_a| >> \gamma, \kappa, g$, for which Γ_0 can be neglected.

Eq.(5.9～5.11) include a set of noise terms that are defined as

$$\left\langle \xi_\alpha^* \xi_\alpha \right\rangle = \kappa + \Gamma_0 \sum_{j=1}^{N} \cos^2(kx_j) \tag{5.13a}$$

$$\left\langle \xi_{pj}^* \xi_\alpha \right\rangle = -i\hbar k \Gamma_0 \alpha \sin(kx_j)\cos(kx_j) \tag{5.13b}$$

$$\left\langle \xi_{pj} \xi_{pj} \right\rangle = 2\hbar^2 \Gamma_0 k^2 \overline{u^2} \left|\cos(kx_j)\alpha + \eta / g\right|^2 + 2\hbar^2 k^2 \Gamma_0 |\alpha|^2 \sin^2(kx_j) \tag{5.13c}$$

We have investigated the pump threshold for the build-up of the intracavity field, which also marks the onset of self-organization (localization) of particles in space. Particles are initially uniformly distributed in space with statistical fluctuations. When the external pump is applied to them, the intracavity field emerges through a scattering process benefiting from the statistical fluctuations. The intracavity field then produces a periodic potential well along the cavity direction, which in turn localizes the particles around $kx = 2n\pi$ and $(2n+1)\pi$ positions.

According to Eq. (5.9), if we want to keep the intracavity intensity stable or higher, the pump photon must be larger than the reduction of the intensity.

For

$$|\alpha|^2 = \frac{|\eta_{eff}|^2 \left|\sum_j \cos(x_j)\right|^2}{\left|[i\Delta_c - 1] - [\Gamma_0 + iU_0]\sum_j \cos^2(x_j)\right|^2}, \tag{5.14}$$

if we want $|\alpha|^2 \geq 1$, we need

$$\left|\eta_{eff}\right|^2\left|\sum_j \cos(x_j)\right|^2 \geq \left|\left\{[-1-\Gamma_0\sum_j \cos^2(x_j)]+i[\Delta_c - U_0\sum_j \cos^2(x_j)]\right\}\right|^2 \tag{5.15}$$

We can neglect the term of Γ_0 in Eq. (5.15). When we simulate the threshold, we can choose the turning point where the intensity $|\alpha|^2$ is above 1, the spreading parameter k^2x^2 is around $\pi^2/12 \approx 0.83$, the defect particle number could be δN, the effective pump $\eta_{eff} \approx \frac{i\eta g}{\Delta_a}$, and the potential depth $U_0 \approx \frac{g^2}{\Delta_a}$.

So Eq. (5.15) can be written as

$$\frac{\eta^2 g^2}{\Delta_a^2}\left|\delta N(1-k^2x^2/2+k^4x^4/(4!))\right|^2 \geq \{1+[-1+U_0(N-\sum_j \cos^2(x_j))]^2\}. \tag{5.16}$$

With the proximities,

$$\frac{\eta^2 g^2}{\Delta_a^2}\left|\delta N(1-k^2x^2/2)\right|^2 \geq \{1+[-1+U_0N(1-\cos^2(x_j)]^2\},$$

Eq. (5.16) can be transformed into

$$\frac{\eta^2 g^2}{\Delta_a^2}[\delta N(1-k^2x^2/2)]^2 \geq \{1+[-1+U_0Nk^2x^2]^2\}.$$

Then we can get the relationship between the threshold and the defect as

$$\eta \geq \frac{\Delta_a}{\delta N(1-k^2x^2/2)g}\sqrt{1+[-1+\frac{g^2}{\Delta_a}Nk^2x^2]^2} \tag{5.17}$$

When U_0N<<1,

$$\eta \geq \frac{\Delta_a}{\delta N(1-k^2x^2/2)g}\sqrt{2}.$$

The defect number δN could be set as $\sqrt{N}$, which is the scaling law in chapter 3. However, if we set N=5000, the defect $= (N/2-\sqrt{N}/2)/N \times 100\% \approx 49.3\%$, the scaling law does not work.

5.4.2 Scaling laws for a large number molecule

In this section, we try to find a more applicable scaling law for the case of a very large number of particles based on the previous analysis.

From Eq. (5.10), the potential is given by

$$U \approx \hbar[U_0(|\alpha|^2-\frac{1}{2})\cos^2(kx)+\frac{2\eta g}{\Delta_a}\alpha_r\cos(kx)] \tag{5.18}$$

where α_r is the real part of the intracavity field amplitude.

The intracavity field amplitude (and its real part) can be estimated under the steady state solution of Eq. (5.9),

$$|\alpha|^2 = \frac{|\eta_{eff}|^2 \left| \sum_j \overline{\cos(kx_j)} \right|^2}{\left| [i\Delta_c - \kappa] - U_0 \sum_j \overline{\cos^2(kx_j)} \right|^2} \tag{5.19}$$

and

$$\overline{\dot{\alpha}_r} \approx -\kappa \overline{\alpha_r} - [\Delta_c - U_0 \sum_{j=1}^{m} \overline{\cos^2(kx_j)}]\alpha_i = 0 \tag{5.20a}$$

$$\overline{\dot{\alpha}_i} = [\Delta_c - U_0 \sum_{j=1}^{m} \overline{\cos^2(kx_j)}]\overline{\alpha_r} - \kappa \overline{\alpha_i} - \eta_{eff} \sum_{j=1}^{m} \overline{\cos(kx_j)} = 0 \tag{5.20b}$$

The relations $\sum \cos(kx_j) \approx 2\delta N / \pi$ and $\sum \cos^2(kx_j) \approx N/2$ hold well in the vicinity of the threshold, where δN is the deviation from the uniform distribution, for example, $(N - \delta N)/2$ species around $kx = 2n\pi$ and $(N + \delta N)/2$ around $(2n+1)\pi$.

Since $\eta >> |\alpha|$ in the vicinity of the threshold, we can neglect the first term in Eq. (5.18). The amplitude of the potential wells is therefore $U_{amp} \approx 2\hbar\eta g \alpha_r / \Delta_a$. Particles around the $(2n+1)\pi$ positions and with energy

$$\frac{p^2}{2m} \le \overline{U} \equiv \frac{2}{\pi} U_{amp} \tag{5.21}$$

can be trapped by the potential. Here $\overline{U}$ is mean value of the potential U around the $(2n+1)\pi$ positions. Eq. (5.21) gives the maximum momentum that can be trapped

$$p_{trap} = \sqrt{2m\overline{U}} \approx \sqrt{m\hbar\kappa} \frac{4}{\pi} \left(\frac{\eta g}{\Delta_a \kappa} \right) \sqrt{\delta N} \sqrt{(1 - \frac{N}{2}\frac{U_0}{\kappa})} / \sqrt{1 + [-1 + \frac{N}{2}\frac{U_0}{\kappa}]^2} \tag{5.22}$$

If the initial momentum distribution of the particles is Gaussian, the number of trapped particles is given by

$$\delta N = \frac{1}{2} N \int_{-p_{trap}}^{P_{trap}} \frac{1}{\sigma\sqrt{2\pi}} \exp(-\frac{p^2}{2\sigma^2}) dp \approx \frac{p_{trap} N}{\sigma\sqrt{2\pi}} \tag{5.23}$$

The factor ½ in the above results from the fact that only those molecules around the $(2n+1)\pi$ positions can be possibly trapped.

By substituting Eq. (5.22) to Eq. (5.23), we have

$$\delta N \approx N^2 \frac{8}{\pi^3}\frac{m\hbar\kappa}{\sigma^2}\left(\frac{\eta g}{\Delta_a \kappa}\right)^2 (1-\frac{N}{2}\frac{U_0}{\kappa})/\{1+[-1+\frac{N}{2}\frac{U_0}{\kappa}]^2\} \tag{5.24}$$

The deviation δN thus depends on the external pump as well as other parameters of the system.

We note that the value given by Eq. (5.24) in the vicinity of the threshold is significantly larger than that of statistical fluctuations, $\delta N = \sqrt{N}$, when a large number of particles are placed in the cavity. We have verified this through extensive numerical simulations. Now we go back to the threshold condition, $\Delta E = k_B T/2$. The trap depth is twice the amplitude of the potential produced by the intracavity field [5.1], we have therefore

$$\hbar\kappa \frac{8}{\pi}\left(\frac{\eta g}{\Delta_a \kappa}\right)^2 \delta N(1-\frac{N}{2}\frac{U_0}{\kappa})/\{1+[-1+\frac{N}{2}\frac{U_0}{\kappa}]^2\} = \frac{1}{2}k_B T \tag{5.25}$$

By substituting Eq.(5.24) to Eq.(5.25), we obtain a threshold of

$$\eta_{thr} = \frac{\pi\sqrt[4]{2}}{4}\sqrt{\frac{k_B T}{\hbar\kappa}}\frac{\Delta_a}{\sqrt{N}g}\sqrt{\{1+[-1+\frac{N}{2}\frac{U_0}{\kappa}]^2\}/(1-\frac{N}{2}\frac{U_0}{\kappa})} \tag{5.26}$$

We briefly discuss this expression. When the collective dispersion width is much smaller than cavity line width, $U_0 N << \kappa$, Eq. (5.26) is simplified to

$$\eta_{thr} = \frac{\pi\sqrt[4]{8}}{4}\sqrt{\frac{k_B T}{\hbar\kappa}}\frac{\Delta_a}{\sqrt{N}g} \tag{5.27}$$

Eq.(5.27) has the same scaling as that obtained under the mean-field approximation in terms of the system parameters Δ_a, N and g [5.1]. We note that there was a different scaling law derived in the same paper based on the statistical fluctuation consideration using the same threshold criterion as ours, $\Delta E = k_B T/2$. The reason for the difference is that they applied the simple finite-size fluctuation relation , $\delta N = \sqrt{N}$ to Eq. (5.25), whereas we derive a new expression Eq. (5.24).

The physics behind the building-up of the intracavity field is therefore different between the two approaches. In a certain sense, our approach unifies the scaling laws obtained by the statistical and mean-field models in the $U_0 N << \kappa$ limit. When $U_0 N/\kappa$ is not negligible, the scaling given by Eq. (5.26) deviates from that of Eq. (5.27). Generally speaking, the pump threshold η_{thr} increases faster than $\Delta_a/(\sqrt{N}g)$. This will be discussed further when compared to numerical results.

Now we compare the numerically computed scaling laws to the analytic expression Eq. (5.26). By substituting Eq. (5.26) to Eq. (5.24), we obtain the value of the population deviation at the threshold, $\delta N_{thr} = 22.5\%$, for the parameter set used in Fig. 5.8. The defects at threshold, given as $(N - \delta N_{thr})/2N$, are 38.8%. We have observed numerically that this value of defects corresponds indeed to the beginning of a sustaining intracavity field. We thus use this value to determine the pump threshold by averaging the defect of steady state in our simulations.

Fig. 5.8 shows η_{thr} vs. N while $\Delta_a/(\sqrt{N}g)$ is kept as a constant. This ratio keeps as a constant for up to N=1000, confirming the scaling given by Eq. (5.27) for $U_0 N/\kappa$. When the molecular number increases further from this value, this relation breaks and the curve follows the trend as described by Eq. (5.26). The numerical results fit the analysis quite well in terms of the fact that the latter is derived using the steady state solutions and involving various approximations.

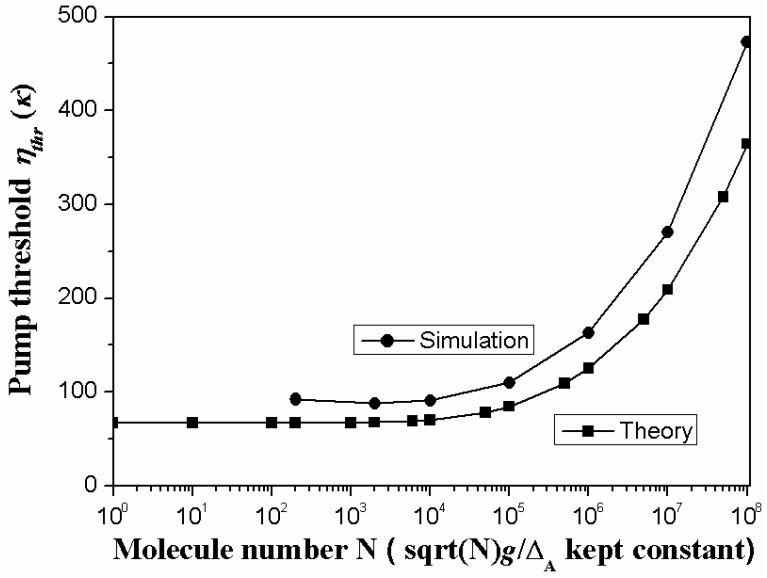

Fig. 5.8 The scaling law for the pump in terms of the system parameters with the statistical model.

A good agreement is obtained between the analysis and simulation. The parameters used in both theory and simulation are g=0.866κ, $\Delta_a = -1000\kappa$, κ=20MHz. The ratios $\Delta_a/(\sqrt{N}g) = -81.7$, and $\sqrt{k_B T/\hbar\kappa} = 1$.

We note that stable defects have been shown to appear when molecular number $N > N_{thr} = \kappa/|U_0|$ and they can destroy spatial self-organization [5.1-5.2]. Since

$U_0 \approx g^2/\Delta_A$, to avoid stable defects, one must increase the detuning Δ_a with the molecular number proportionally. This indicates that if a large ensemble of molecules is to be cooled in an optical cavity, a strong far off resonant pump should be utilized.

5.5 Trapping and Cooling of a Molecular Cloud

The above sections deal with a general case of spatial self-organization of an ultra cold ensemble in an optical cavity. Here we will study the cooling and trapping effects of a large ensemble of species with a temperature much higher than the cavity cooling temperature limit.

As an example we consider CN molecules, pumped by a far detuned optical beam. As studied in our earlier work, the molecules can be approximated as a three-level system under far detuned pumping [5.2].

The statistical model gives us an effective tool to simulate a large CN ensemble. Fig. 5.8(a) shows the time evolution of the intracavity field intensity and the temperature of the CN cloud. The results can be divided into three time zones.

In the first, a small window from the beginning, the intracavity field fluctuates but has no sustained build-up, whereas the temperature stays at the initial value at around 11 mK. This region corresponds to a spreading process of the molecules from their initial position along the axis direction. No molecular localisation has observed. The duration of this region depends on the cavity length and the initial position of the molecules.

The second region begins when a molecular group with the fastest velocity escapes as they reach the cavity mirrors. The intracavity field intensity then rapidly builds up while the temperature drops sharply. A rapid spatial self-organization of the remaining molecules is confirmed by the measurement of the spreading parameter (Fig. 5.8(b)), from initial uniform distribution ($k^2x^2 \approx 0.83$) to localization ($k^2x^2 \approx 0.28$). The molecules continue to escape until the full build-up of the intracavity field occurs. This marks the beginning of the third region. Around 35% of the molecules are stably trapped in the cavity by the potential produced by the intracavity field intensity (Fig. 5.8(b)). The temperature is now reduced to just below 1 mK. Molecules are further cooled in this region as the cavity non-adiabatic cooling process continues, but in a much slower scale. In general, the final temperature of the molecular cloud and the percentage number of trapped molecules depend on the pump intensity.

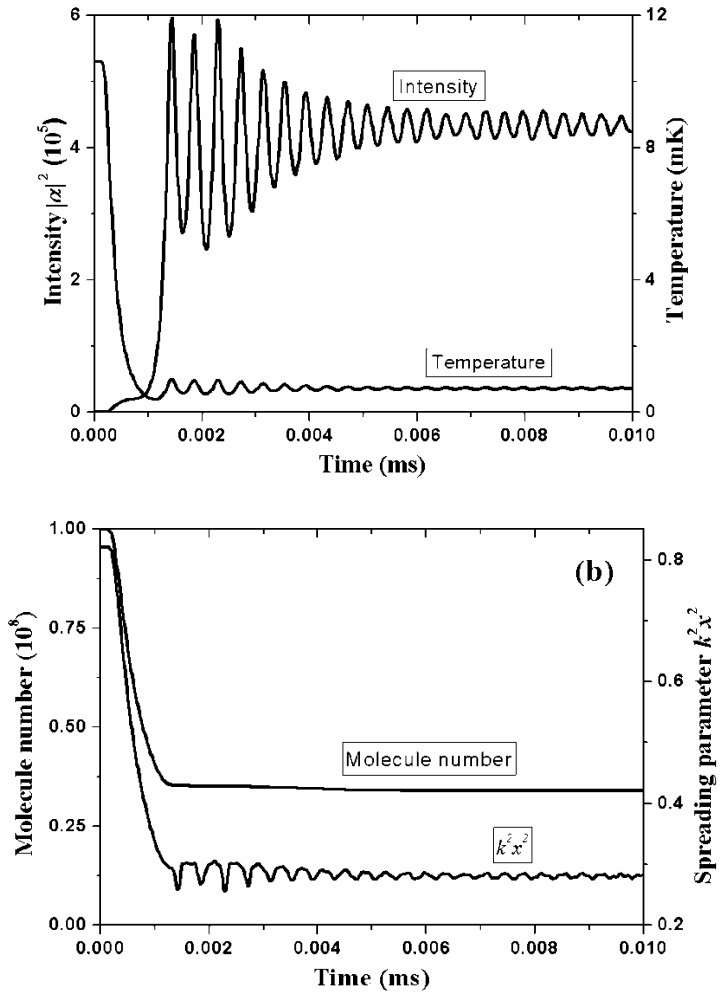

Fig. 5.8 Cavity cooling of a large ensemble of CN molecules with statistical model.

The parameters are set as g=0.055κ, Δ_A =-1.1×10$^4\kappa$. N=10^8, η=380κ and κ=62.8MHz. They corresponds to a CN cloud of 3×10^{13}/cm^3 in an optical cavity of length L=1.5mm, waist w_o=25μm, and finesse F=10^4 with pump in 2×10^3 W/cm^2.

5.6 From Near Resonant to Far Off Resonant (FOR) Cooling

5.6.1 Conditions for Far Off Resonant Cooling

When $\Delta_A = \omega_p - \omega_A >> \kappa$, U_0, Γ_0 and the noise terms →0. We need to consider the polarizability of the particle α_e [5.3-5.6]. The U_0 of far off resonant case is U_0=$\frac{\alpha_e \omega_p}{2\varepsilon_0 V_{eff}}$. The pump photons are scattered into the cavity by the particles.

The dynamics of the intensity and amplitude in the cavity obey

$$\frac{dE^2}{dt} = P - 2\kappa E^2 \tag{5.28}$$

and

$$\frac{dE}{dt} = E_{eff} - \kappa E \tag{5.29}$$

We can normalize the above two equations by $\frac{|\alpha|^2 \hbar\omega_p}{\varepsilon_0 V_{eff}} = |E|^2$ and get

$$\frac{d\alpha^2}{dt} = n_p - 2\kappa\alpha^2 \tag{5.30}$$

and

$$\frac{d\alpha}{dt} = \eta_{effn} - \kappa\alpha \tag{5.31}$$

where n_p is the scattered photon number rate, for example, the corresponding averaged free-space scattering rate

$\Gamma_{sc} = k^3 d^2 / 6\pi\varepsilon_0 \hbar$.

The induced dipole

d=$Re(\alpha)Est$.

We assume it is the steady state $\frac{d\alpha^2}{dt}, \frac{d\alpha}{dt} \to 0$. We get $\alpha = \sqrt{\frac{n_p}{2\kappa}}$ from Eq. (5.30), and get

$$\eta_{effn} = \kappa\alpha = \sqrt{\frac{\kappa n_p}{2}} = \sqrt{\frac{\kappa\Gamma_{sc}}{2}} \tag{5.32}$$

.

5.6.2 FOR Case

We can put the normalized effective pump $\eta_{eff} = \frac{\eta_{effn}}{\kappa} = \sqrt{\frac{\Gamma_{sc}}{2\kappa}}$ into the Eq. (5.28) and Eq. (5.29). Then the formulas of the far off resonant model are

$$\dot{\alpha} = [i\Delta_c - 1]\alpha - iU_0 \sum_j \cos^2(x_{nj})\alpha - \eta_{eff} \sum_j \cos^2(x_{nj}) \tag{5.33}$$

$$\dot{p}_{nj} = U_0(|\alpha|^2 - \frac{1}{2})\sin(2x_{nj}) - i(\eta_{eff} * \alpha - \eta_{eff}\alpha^*)\sin(x_{nj}) + \xi_{pj} \tag{5.34}$$

$$\dot{x}_{nj} = p_{nj} \cdot (\hbar k^2 / (m\kappa)) \qquad (j=1\ldots N) \tag{5.35}$$

$$\eta_{eff}=\sqrt{\frac{\Gamma_{sc}}{2\kappa}}=\sqrt{\frac{k^3}{6\pi\varepsilon_0\hbar\kappa}}d=\sqrt{\frac{k^3}{6\pi\varepsilon_0\hbar\kappa}}\mathrm{Re}(\alpha_e)E_p=\sqrt{\frac{k^3}{6\pi\varepsilon_0\hbar\kappa}}\mathrm{Re}(\alpha_e)\sqrt{\frac{\hbar\omega_p}{\varepsilon_0 V_{eff}}}|\eta|$$

$$=\sqrt{\frac{k^3}{6\pi\varepsilon_0\hbar}}\sqrt{\frac{\hbar\omega_p}{\varepsilon_0 V_{eff}}}\mathrm{Re}(\alpha_e)\frac{|\eta|}{\kappa} \tag{5.36}$$

The pump intensity

$$I=P/A=c\varepsilon_0\left|\varepsilon_p\right|^2\cdot A/A=\frac{|\eta|^2\hbar\omega_p c}{V_{eff}} \tag{5.37}$$

5.6.3 The parameters of CN and Rb_2 molecules

For comparison, we choose Rb_2 molecules and use the same cavity as the CN's [5.7-5.11], whose length is L=1.5mm, waist is w_0=10μm. The effective mode volume is $V_{eff}\approx1.178\times10^{-13}(m^3)$, pump area is $A=3\times10^{-8}(m^2)$. The finesse is F~$10^{3\text{-}4}$, which means the max reflectivity of the mirrors of the cavity is 0.999686. Then the linewidth of the cavity is κ=62.8M*Hz*.

	CN	Rb_2
Polarizability volume (cm^3)	3.061	79
Polarizability ($C^2m^2J^{-1}$)	3.4×10^{-40}	87.75×10^{-40}
Pump wavelength (nm)	1060	1060
Mass (u)	29	171
$\hbar k^2/m\kappa$	1/32	1/4920
U_0 (Hz)	0.29	7.48
$U_0(\kappa)$	-4.65×10^{-9}	-1.2×10^{-7}
$\eta_{eff}(\eta)$	1.4×10^{-9}	3.6×10^{-8}

According to the above parameters, if the pump power for Rb_2 is setting as P=15W, the pump strength of the mathematics equation is equal to η=794.4.

The polarizability volume of CN is 3.061(cm^3), Rb_2 is 79 (cm^3). Then the potential depth parameter of Rb_2 $U_{Rb2}=U_{CN}\times79/3.061=-3.781\times10^{-8}(\kappa)$.

Ⅰ. About the dipole polarizability

The polarizability $\alpha_e = 4\pi\varepsilon_0 a^3$ can be described as polarizability volume a^3, where $4\pi\varepsilon_0 \approx 1.113\times10^{-10}(As/(Vm))$, and its atom unit is $e^2a^2E_h^{-1}$, i.e.

1a.u.=1.6488×10^{-41}c^{2}m^{2}J^{-1}.

Ⅱ. Pump setting

The pump wavelength we can set as $\lambda_p = 1060nm$, $k_p = 5.93\times10^6 Hz$, $\omega_p = 1.77\times10^{15} Hz$. The pump intensity I can be set up to 10^{12}W/cm^2.

The polarizability volume of CN molecule is $3.061(\mathring{A}^3)$, $\alpha_{CN} = 3.4\times10^{-40}\left(\mathrm{C^2m^2J^{-1}}\right)$.

For Rb_2, $\alpha_{Rb} = 79(cm^3) = 87.75\times10^{-40}\left(\mathrm{C^2m^2J^{-1}}\right)$. M=85.4678×2u=171u.

If we think the cavity length l=3cm, waist width w_0=10μm, $V_{eff} = \dfrac{\pi w_0^2 l}{4} = 2.3562\times10^{-12}\,\mathrm{m}^3$. The finesse of cavity is $F = \dfrac{\pi}{1-R} = 10^4$, $\delta = 1-R = 3.14\times10^{-4}$, $\kappa = \dfrac{c\delta}{l} 3.14MHz$.

The maximum pump is

$\eta = 2\times10^6\kappa$.

$U_0 = \dfrac{\alpha_e\omega_p}{2\varepsilon_0 V_{eff}} = 0.372245Hz \approx 1.2\times10^{-7}\kappa$.

$\eta_{eff} = 3.6\times10^{-8}\dfrac{|\eta|}{\kappa}$.

5.7 Conclusions and Remarks

The cavity cooling concept was first proposed a decade ago and was confirmed through an experiment. However, little experimental progress has been made in extending cavity cooling from single particle to a dense cloud and from atoms to molecules, while optical manipulations of molecules using strong far off resonant lattices have been demonstrated in experiments [5.12]. The main activity in cavity cooling is so far still theoretical [5.13]. Lack of further progress may come from several factors. The realization of cavity cooling for a large molecular cloud is more complicated than conventional laser cooling, which makes it difficult to provide an accurate prediction on the operation conditions for experiments. The purpose of our

present work is to address the key issue of the scaling law of pump threshold for the onset of cavity cooling for a large ensemble of particles. We have shown a new scaling law applicable to a large ensemble. The statistical model we have developed offers an effective tool for extending cavity cooling to a molecular ensemble of any numbers. We have applied it for cooling of a dense CN molecular cloud. The agreement between the analysis and simulation is very good, which provides a platform for further theoretical and experimental studies.

5.8 References

[5.1] J. K. Asboth, P. Domokos, H. Ritsch and A. Vukics, *Self-organization of atom in a cavity field: Threshold, bistability, and scaling laws,* Physical Review A, 72, 053417-1-12 (2005).

[5.2] W. Lu and Y. Zhao, P. F. Baker, *Cooling molecules in optical cavities*, Physical Review A, 76, 013417-1-6 (2007).

[5.3] A. Hinchliffe, B. Nikolaidi and H. J. Soscun Machado, *Density Functional Studies of the Dipole Polarizabilities of Substituted Stilbene, Azoarene and Related Push-Pull Molecules*, International Journal of Molecular Sciences, 5, 224-238 (2004).

[5.4] J. D. Miller, R. A. Cline, and D. J. Heinzen, *Far-off-resonance optical trapping of atoms*, Physical Review A, 47, R4567-R4570 (1993).

[5.5] T. A. Savard, K. M. O Hara, and J. E. Thomas, *Laser-noise-induced Heating in Far-Off-Resonance Optical Traps*, Physical Review A, 56, R0195-R1098 (1997).

[5.6] V. Vuletic´ and S. Chu, *Laser cooling of atoms, ions or molecules by coherent scattering,* Physical Review Letters, 84, 3787-3790 (2000).

[5.7] A. Fioretti, J. Lozeille, C. A. Massa, M. Mazzoni, C. Gabbanini, *An optical trap for cold rubidium molecules*, Optics Communications 243, 203-208 (2004).

[5.8] S. J. Park, S. W. Suh, Y. S. Lee, and G. H. Jeungy, *Theoretical Study of the Electronic States of the Rb_2 Molecule, Journal of Molecular Spectroscopy*, 207, 129-135 (2001).

[5.9] K. D. Bayes, *A Study of the CN Emission from Active Nitrogen Flames*, Canadian Journal of Chemistry, 39, 1074-1085 (1961).

[5.10] R. F. Gutterres, J. Verges, and C. Amiot, *The BaI $X^2\Sigma^+$ and $B^2\Sigma^+$ Electronic States Through $B^2\Sigma^+$-$X^2\Sigma^+$ and $C^2\Sigma^+$- $X^2\Sigma^+$ Band Systems Analysis*, Journal of Molecular Spectroscopy, 196, 29-44 (1999).

[5.11] H. Ito, K. Suzuki, T. Kondow, and K. Kuchitsu, *Electronic transition moment for the emission of CN. Analysis of dependence on the internuclear distance*, Journal of Chemical Physics, 94, 5353-5359 (1991).

[5.12] R. Fulton, A. I. Bishop, M. N. Shneider and P. F. Barker, *Controlling the motion of cold molecules with deep periodic optical potentials,* Naural Physics, 2, 465-468 (2006).

[5.13] B. L. Lev, A. Vukics, E. R. Hudson, B. C. Sawyer, P. Domokos, H. Ritsch, and J. Ye, *Prospects for the Cavity-assisted Laser Cooling of Molecules*, Physical Review A, **77**, 023402-1-13 (2008).

[5.14] N. Aubert, T. Georges, C. Chauzat, R. L. Bras, and Patrice Feron, *Power control of a low noise CW Diode-Pumped Solid-State UV laser*, CLEO/Europe - IQEC (2007).

Chapter 6

Discussion and Conclusion

6.1 Introduction

This thesis aims to research a general cooling method that will be applicable to wide range of molecular and atomic species and other particles. Firstly we introduced the application of cold molecule and the techniques for creating cold molecules. The general model of cavity cooling from atoms to molecules and the dynamics of a particle in a single cavity mode were discussed. Then we studied the self-organization and scaling laws of many molecules in the cavity with a transverse pump. For simulate a huge of molecules, we proposed the statistical model and validate it with comparison of simulation. Then we discussed the scaling laws in the case when a large ensemble of species is involved. Finally, we studied the cooling of a CN molecular cloud and the case of far off resonant.

6.2 Extension of present model of cavity cooling of atoms to molecules

We extend the existing cooling scheme for two-level atoms to an ensemble of two-level molecules in chapter 2. This investigation linked with the existing work in the subject and provided useful insight into the development of the general cooling method. While the extension of the work is conceptually straightforward, there are some important differences between atoms and molecules.

Compared with two-level atoms that are pumped typically at visible to infrared wavelengths, with 100 MHz-10 GHz detuning from the resonance transition, the pump frequency required for a rotational-vibrational transition of molecules is in the UV and

VUV regions for most molecules and we have to take into account the limited availability of laser sources and high finesse cavity optics in these frequency regions.

Also the dipole momentum strengths of molecules corresponding to these transitions are generally much weaker than those of well-studied atoms such as Rubidium, which will lead to significant differences in the operating conditions between the two.

6.3 Investigation of dynamical process leading to spatial self organisation of molecules

We investigated the spatial dynamics and self-organisation of molecules in the new parameter conditions different from those of atoms. Spatial organisation of atoms in an optical cavity has been studied in a recent theoretical work [6.1-6.5]. Both simulation and experiment have shown that spatial organisation leads to collective dynamics of atoms and a favourable scaling behaviour for cooling.

We further investigated the scaling of a number of molecules. Cavity cooling began with a single atom theory based on a two-level model and the scaling with atomic numbers is nontrivial [6.6]. In general, the effects on the refractive index by one atom may be destroyed by another in the cavity, which leads to the increase of cooling time with the increase of atomic numbers [6.7]. On the other hand, when atoms are lined up in space, i.e., in spatially organised state, a simpler scaling holds from a single particle to a large number while the cooling rate remains the same [6.8-6.9].

We studied the dynamics of two-level molecules in an optical cavity in order to understand the cavity cooling schemes in general and the applicability and efficiency of the scheme to cooling molecules. We studied the dynamics of an ensemble of CN molecules in a millimetre cavity of finesse 3.1×10^4; the transition $B^2\Sigma^+ \rightarrow X^2\Sigma^+$ with dipole decay rate 15.4 MHz was pumped at nearly resonance (50MHz) by a tuneable diode laser at 387.5 nm.

The simulation result shows a group of trapped CN molecules initially at 160 mK to be cooled to 1 mK on the time scale of 5 ms. Accompanying with the cooling processing is the spatial localisation (selforganisation) of the molecules initially distributed uniformly in space, as evident by the decreasing spreading parameter $\overline{x^2}$ in time. The self-organisation takes place at the pump power of 0.4 mW [6.9].

Since collective dynamics and scaling depend on the parameters of the system such as the dipole strength, the recoil frequency and the cavity configuration, we anticipate different behaviours between molecules and atoms. In the same time we are confident through the above preliminary work that collective cooling of molecules in the two-level interaction model will take place through spatial self-organisation in realistic conditions. The focus of this phase of programme is to qualify the system behaviour and compare with atomic systems. The results obtained will be important to the development of the general cooling method in the following parts of the programme.

6.4 Numerical simulation of the general cooling model

Numerical simulation plays an important role in studying a number of issues involved in the case that the analysis may not be possible due to the complexity of the problems. The numerical study is undertaken not only to put the analysis and model on test but also to address practical issues by providing useful guidelines in the design and implementation of experiments in the future.

In cavity cooling, the commonly discrete model, i.e. the many-particle model which can be represented quantum mechanically or semi-classically, comprises a set of equations of motion for each particle that is coupled to the same intracavity field [6.9-6.10]. This model has shown in good agreement with the former in recent extensive studies for temperatures high than the cavity cooling limit. However, it becomes impractical when a large ensemble is involved. Our understanding so far of cooling of an ensemble of particles is based on the scaling laws which are obtained using various approximations and has not yet been fully tested [6.10].

Therefore we developed a new statistical model based on the Boltzmann equation and studied two solution methods. The results of the theory and numerical simulations between discrete model and statistical model show a good agreement, which validated this new model.

6.5 Study of collective cooling of a large molecular ensemble

Based on the study and experience in the numerical treatments, including various noise sources, of field-many molecules interaction in optical lattices and more

recently field-atom/molecules coupling in optical cavities, we explored the scaling laws with a view to the self-organization and cooling of a large ensemble of species.

We study the cooling of a CN molecular cloud of the density $10^{13}/cm^3$, with an initial temperature at 10 mK in an optical cavity. We find that more than a third of the molecules are stably trapped by the intracavity field and the final temperature is below 1mK [6.11].

6.6 Further Study

Based on the above studies in this thesis, my workmate further investigated the deceleration of molecules in a supersonic beam by the optical field in a low-finesse cavity [6.18]. It has been discussed that the interplay of the optical pump with a supersonic molecular beam in an optical cavity can produce two dynamical effects: it segments the beam into a periodic density wave and generates an intracavity optical field via coherent Bragg-type scattering. The optical field is then switched dynamically with the travelingmolecules in each cycle of the cavity mode. The nonadiabatic nature of the cavity dynamics gives rise to a friction force, which slows most molecules to zero central velocity through many cycles.

The simulation results demonstrate that most molecules in the beam can be decelerated to zero central velocity by the intracavity optical field in a process analogous to electrostatic Stark deceleration. It shows that the rapid switching of the optical field for slowing the molecules is automatically generated by the cavity-induced dynamics, and ~1% of the molecules can be optically trapped at a few millikelvin in the same cavity.

6.7 Future Work

Here we will investigate the effect of initial molecular distributions on the dynamical process of self-organisation and cooling rate. We expect that tailored initial conditions will reduce the self-organisation time and therefore cool molecules more rapidly. We will further consider the effects of Langevin-type noise fluctuations on the molecular momentum and intracavity field amplitude, and study their influence on the temperature limit and phase-space density of cooled molecules. Simulation will also provide us with the information of molecular dynamics in the transverse space. We are

interested in molecular dynamics under both 1D and 2D confinement by counter-propagating pump beams in the transverse space and will study conditions for restricting phase randomisation in the transverse motion which may destroy collective dynamics.

We will simulate cooling in cm long cavities as well as in microcavities (~100 um) that have high finesse of 10^5. In relation to our experimental work, we will focus particularly on the possibility to cool $> 10^7$ molecules initially at ~10-100 mK to the temperature of 10-100 μ K in the order of 100 ms and to simultaneously trap the cooled molecules within the strong intracavity optical potential wells. This work may need more processing to the statistical model and re-normalization to the mathematical simulation.

It has been observed that the coupled atom-field dynamics in an optical cavity can lead to a friction force that damps atomic motion [6.1, 6.3]. This scheme is commonly called cavity cooling where dissipation takes place via cavity loss rather than by spontaneous emission. Cavity cooling avoids or reduces several problems of the laser-cooling scheme, such as photon re-absorption and recoil heating. Moreover, as there is no requirement in cavity cooling for a closed multilevel system, it is an attractive approach for creating ultracold molecules. A range of techniques is now capable of producing and trapping stable cold molecules at temperatures in the 10-100 mK range [6.12-6.15]. Cavity cooling appears to be a promising route towards further cooling a large range of species1 to the ultracold regime below 1 mK [6.4, 6.5, 6.9, 6.10, 6.16].

We have extensively studied the cooling scheme under cavity configuration, naturally we will ask whether cavity cooling using a strong far off-resonant laser source can bring about a new cooling scheme. A far off-resonant field means that its frequency is less than the half of the lowest electronic dipole transition frequency. The dipole force arising from the far off-resonant interaction therefore does not depend on the internal energy structures of molecules. We therefore anticipate that cavity cooling using a far off-resonant laser source can be a general cooling method that is applicable to any particles.

In the final task we will explore methods for enhanced cooling of an ensemble of molecules in an optical cavity. The development of such methods is particularly important to molecules in a far off-resonant field because the weak coupling may lead to

a longer cooling duration. In the case of a single particle in an optical cavity, a simple relation holds between the position of the particle and the cavity transmittance, which can provide a means to control the motion of the particle by using the transmitted intensity as a feedback signal to modulate the pump strength. T. Fischer and his group at Max-Planck have employed this approach to extend the trapping time of an atom by 30% [6.17]. Two new schemes for rapid cooling of a particle in an optical cavity have been studied [6.9]. The first one is a feedback scheme that uses the variations of transmitted intensity to modify the cavity length. The results show that this feedback leads to increased friction force to rapidly decelerate the particle up to 10 times over the conventional cavity cooling. In a second scheme, it can be predicted that more rapid cooling can be attained by using an external pump field that decays over time.

To extend the existing schemes from a single particle to an ensemble, we will take into account the self-organisation process of the ensemble and explore mechanisms to enhance the recoil force that organises the collective dynamics of the ensemble. We will investigate two methods to implement the time-dependent pump. We first use the transmittance of the cavity as a feedback signal to modulate a constant external pump in the transverse direction. Although the approach is similar to that used in the cooling of a single particle by the Max-Planck group [6.17], the pump into the cavity in the longitudinal and transverse directions gives a different scaling of the system and requires a thorough investigation. We will further introduce a time delay in the feedback loop to control the phase difference between the intracavity intensity and the cavity transmittance. This new system control parameter may provide an additional degree of freedom for the optimization of the recoil force in the presence of the feedback signal.

In the second approach we will investigate the use of a laser source that exponentially decays in time as the external pump from the transverse direction. While a decaying pump may not enhance the recoil force for self-organisation (not obvious from the system dynamics), when a molecular ensemble is organised in space they behave in many ways like a single particle and the decaying pump can cool the ensemble significantly faster as in the single particle case [6.9]. Therefore, the feedback scheme and the time-dependent pump approach may enhance the cooling process in the two different stages of molecular dynamics and in this sense they are complementary. We will finally explore the possibility of combining the two schemes to achieve the optimal condition for faster cooling.

6.8 Thesis Conclusion

The ability to cool and trap atoms has revolutionised atomic and ultra-cold physics. Molecular physics is currently undergoing a similar transformation as effective methods for manipulating the motion of molecules are being put in place.

Our work is a basic research with the potential for cross-disciplinary applications in physics, chemistry, material science, metrology and engineering and aims to research a general cooling method that will be applicable to wide range of molecular and atomic species and other particles.

We studied the dynamics of molecules in optical fields, focusing in particular on exploring the molecular self-organisation phenomena in optical cavities to cool molecular ensembles to sub-mK temperatures. The scheme complements well with our present experimental work on the deceleration and focusing of cold molecules and can extend our present capability to simultaneously cool and trap a large cold molecular ensemble.

It will contribute to the understanding of optical interaction with molecules, and will be of immediate interest to researchers in the field of atom and molecule optics. The ability to create cold, slow molecules and clusters will make significant impact on the basic research of molecular dynamics, collisions and cold chemistry, and high-resolution spectroscopy. The results of this research will be disseminated by presentation at both national and international conferences, and in refereed journals.

6.9 References

[6.1] P. Horak, G. Hechenblaikner, K. M. Gheri, H. Stecher, and H. Ritsch, *Cavity-Induced Atom Cooling in the Strong Coupling Regime*, Physical Review Letters, 79, 4974-4977 (1997).

[6.2] V. Vuletic and S. Chu, *Laser Cooling of Atoms, Ions, or Molecules by Coherent Scattering*, Physical Review Letters, 84, 3787-3790 (2000).

[6.3] P. Maunz, T. Puppe, I. Schuster, N. Syassen, P. W. H. Pinkse, and G. Rempe, *Cavity cooling of a single atom*, Nature, 428, 50-52 (2004).

[6.4] P. Domokos and H. Ritsch, *Collective Cooling and Self-Organization of Atoms in a Cavity*, Physical Review Letters, 89, 253003-1-4 (2002).

[6.5] H. W. Chan, A. T. Black, and V. Vuletic, *Observation of Collective-Emission-Induced Cooling of Atoms in an Optical Cavity*, Physical Review Letters, 90, 063003-1-4 (2003).

[6.6] J. K. Asboth, P. Domokos, and H. Ritsch, *Correlated Motion of Two Atoms Trapped in a Single-mode Cavity Field*, Physical Review A, 70, 013414-1-11 (2004).

[6.7] P. Domokos and H. Ritsch, *Mechanical effects of light in optical resonators*, Journal of the Optical Society of America B-Optical Physics, 20, 1098-1130 (2003).

[6.8] H. W. Chan, A. T. Black, and V. Vuletic, *Observation of Collective-Emission-Induced Cooling of Atoms in an Optical Cavity*, Physical Review Letters, 90, 063003-1-4 (2003).

[6.9] W. Lu and Y. Zhao, *Cooling molecules in optical cavities,* Physical Review A, 75, 013417-1-6 (2007).

[6.10] J. K. Asboth, P. Domokos, H. Ritsch, and A. Vukics, *Self-organization of atoms in a cavity field: Threshold, bistability, and scaling laws*,Physical Review A, 72, 053417-1-12 (2005).

[6.11] Y. Zhao, W. Lu, P. Barker and G. Dong, *Self-organisation and cooling of a large ensemble of particles in optical cavities*, Faraday Discuss, 142, 311-318 (2009).

[6.12] J. D. Weinstein, R. deCarvalho, T. Guillet, B. Friedrich, and J. M. Doyle, *Magnetic trapping of calcium monohydridemolecules atmillikelvin temperatures*, Nature (London)**395**, 148-150 (1998).

[6.13] J. M. Doyle, B. Friedrich, Jinha Kim, and David Patterson, *Buffer-gas loading of atoms and molecules into a magnetic trap*,Physical Review A,**52**, R2515-2518 (1995).

[6.14] H. L. Bethlem, G. Berden, F. M. H. Crompvoets, R. T. Jongma, A. J. A. van Roij, and G. Meijer, *Electrostatic trapping of ammonia molecules*, Nature, 406, 491-494 (2000).

[6.15] M. R. Tarbutt, H. L. Bethlem,J. J. Hudson, V. L. Ryabov, V. A. Ryzhov, B. E. Sauer, G. Meijer, and E. A. Hinds, *Slowing Heavy, Ground-State Molecules using an Alternating Gradient Decelerator*, Physical Review Letters,**92**, 173002-1-4 (2004).

[6.16] B. L. Lev, A. Vukics, E. R. Hudson, B. C. Sawyer, P. Domokos, H. Ritsch, and J. Ye,*Prospects for the Cavity-assisted Laser Cooling of Molecules*, Physical Review A, **77**, 023402-1-13 (2008).

[6.17] T. Fischer, P. Maunz, P. W. H. Pinkse, T. Puppe and G. Rempe, *Feedback on the motion of a single atom in an optical cavity*, Physical Review Letters, 88, 163002-1-4 (2002).

[6.18] Zhihao Lan, Yongkai Zhao, Peter F. Barker, Weiping Lu, *Deceleration of molecules in a supersonic beam by the optical field in a low-finesse cavity*, Physical Review A, 81, 013419-1-5 (2010).

Appendix A: Program of discrete model

```
% Program of discrete model %%MatLab%

global m pm;
global g0 kr da n c1;
xl=1;
lop=1;
m=60000;
% mi=1:m;
%   xi=(mi-15)*xl*2*pi;
% ps=ones(1,m)*14.4*3;

  xi=(rand(1,m)-0.5)*pi;
  ps=normrnd(0,sqrt(32),1,m);

icon=[0.1,0.1,ps,xi];
%load icon icon;   %for continue calculate

h=0.1;
dh=sqrt(h);
l=sqrt(3);
au=0.4;
%c1=207.5;
c1=32;
% D=20000;      % for CN t(actual-1loop)=D*h/(2*10^4) ms, if D=2000,
t-1loop=0.01ms
%                % for Rb t=D*h/10^4ms,  if D=1000, t-1loop=0.01ms
D=500;

g0=0.866
% kr=0.75;
kr=0
da=-1000*sqrt(5)
u0=g0^2*da/(da^2+kr^2)
r0=g0^2*kr/(da^2+kr^2)
dc=m*u0-1
n=300
%n=40/sqrt(2)

% g0=5
% kr=2
% da=-1000
% u0=g0^2*da/(da^2+kr^2)
% r0=g0^2*kr/(da^2+kr^2)
% dc=m*u0-1
% n=40

realt=zeros(lop+1,1);
%kx2=zeros(lop+1,1);  %stactic
```

```
eapp=zeros(lop+1,1);
eabs=zeros(lop+1,1);
%mdefect=zeros(lop+1,1);
%anal=zeros(lop+1,m);
ax=zeros(lop+1,m);

tt=zeros(D+1,1);
xx=zeros(D+1,m);
pp=zeros(D+1,m);
app=zeros(D+1,1);
anr=zeros(D+1,1);

ac=ones(1,2*(m+1));
ac=ac*(1e-12);
options=odeset('RelTol',1e-6,'Abstol',ac);
ani=zeros(D+1,1);

eabs(1)=icon(1)^2+icon(2)^2;
realt(1)=0;tstep=0.01;

for ii=1:m
ax(1,ii)=xi(1,ii)/(2*pi);
end

for vv=1:lop
%load icon icon;
tt(1)=0+(vv-1)*D*h;
anr(1)=icon(1);
ani(1)=icon(2);
pp(1,:)=icon(3:m+2);
xx(1,:)=icon(m+3:2*m+2);
%  for jj=1:m
%      if(abs(pp(1,jj))>100)
%          anal(1,jj)=m;
%      end
%  end

% for jj=1:m
%     if(abs(xx(1,jj))>100)
%         xx(1,jj)=(xx(1,jj)/(2*pi)-round(xx(1,jj)/(2*pi)))*2*pi;
%     end
% end

vv

for j=1:D

t1=(j-1)*h+(vv-1)*D*h;
t2=j*h+(vv-1)*D*h;
tscal=[t1 t2];
tt(j+1)=t2;

% sr1=(rand(1,1)-0.5)*2*l;
 sr2=(rand(1,1)-0.5)*2*l;
% si1=(rand(1,1)-0.5)*2*l;
 si2=(rand(1,1)-0.5)*2*l;

 sar=(rand(1,1)-0.5)*2*l;
 sai=(rand(1,1)-0.5)*2*l;

for jj=1:m
```

```
 sp1(jj)=(rand(1,1)-0.5)*2*l;
 sp2(jj)=(rand(1,1)-0.5)*2*l;
 ss(jj)=(rand(1,1)-0.5)*2*l;
 sr1(jj)=(rand(1,1)-0.5)*2*l;
 si1(jj)=(rand(1,1)-0.5)*2*l;
end

csx=0;
cx=0;
cxs=0;
 for jj=1:m
    cx=cx+cos(xx(j,jj))*sr1(jj);         % real part
    csx=csx+cos(xx(j,jj))*si1(jj);       % image part
    cxs=cxs+cos(xx(j,jj))*ss(jj);        % correlated
 end
sanr=(-sqrt(r0)/2*cx+sqrt(0.5)*sar-
ani(j)/(anr(j)^2+ani(j)^2)*sqrt(r0/2)*cxs)*dh;
sani=(sqrt(r0)/2*csx+sqrt(0.5)*sai+anr(j)/(anr(j)^2+ani(j)^2)*sqrt(r0/
2)*cxs)*dh;
for jj=1:m
spp(jj)=(sqrt(2*au*r0)*((anr(j)*cos(xx(j,jj))+n/g0)*sp1(jj)+sqrt(abs(a
ni(j)^2-0.5))*cos(xx(j,jj))*sp2(jj))-
sqrt(2*r0*(anr(j)^2+ani(j)^2))*sin(xx(j,jj))*ss(jj))*dh;
end

icon=[anr(j),ani(j),pp(j,:),xx(j,:)];
[t,Y]=ode113(@markm,tscal,icon,options);
%[t,Y]=ode45(@markm,tscal,icon,options);

[o,w]=size(Y);
%eabs=zeros(h,1);
 anr(j+1)=Y(o,1)+sanr;
 ani(j+1)=Y(o,2)+sani;
 for jj=1:m
 pp(j+1,jj)=Y(o,2+jj)+spp(jj);
 xx(j+1,jj)=Y(o,2+m+jj);
 end

% for jj=1:m
%     if(abs(xx(1,jj))>100)
%         xx(1,jj)=(xx(1,jj)/(2*pi)-round(xx(1,jj)/(2*pi)))*2*pi;
%     end
% end
end

neabs=anr.^2+ani.^2;
napp=mean(pp.^2/c1,2);
realt(vv+1)=realt(vv)+tstep;
% mapp(vv)=mean(app);
eabs(vv+1)=neabs(D+1,1);
eapp(vv+1)=napp(D+1,1);

for jj=1:m
     if(abs(pp(D+1,jj))>100)
         anal(vv,jj)=jj;
     end
 end
% rx=(xx/pi-round(xx/pi));
% kx2(vv)=mean(rx(D+1,:).^2),2);

rx=(xx(D+1,:)/pi-round(xx(D+1,:)/pi));
```

```
kx2(vv)=mean(rx.^2);

rx=xx(D+1,:)/pi;
rrx=round(abs(mod(rx,2)-1));
neven=0;
nodd=0;
nall=0;
%for ii=1:D+1
%     for jj=1:m
%         if(rrx(ii,jj)==1)
%             neven=neven+1;
%         elseif(rrx(ii,jj)==0)
%             nodd=nodd+1;
%         end
%         nall=nall+1;
%     end
%end
    for jj=1:m
        if(rrx(jj)==1)
            neven=neven+1;
        elseif(rrx(jj)==0)
            nodd=nodd+1;
        end
        nall=nall+1;
    end
if((nodd/nall)>0.5)
    mdefect(vv)=1-nodd/nall;
else
    mdefect(vv)=nodd/nall;
end

% ax=zeros(o,m);
for ii=1:m
ax(vv+1,ii)=xx(D+1,ii)/(2*pi);
end

 icon=[anr(j+1),ani(j+1),pp(j+1,:),xx(j+1,:)];
% save icon icon
end

%function of markm.m%

function dy=markm(t,y)
global m pm;                    % m atoms
global g0 kr da n c1;

% g0=0.866;                      % CN molecular
% kr=0.75;
% da=-1000;

%g0=5;                 % Rb molecular
%kr=2;
%da=-1000;
u0=g0^2*da/(da^2+kr^2);
r0=g0^2*kr/(da^2+kr^2);
dc=m*u0-1;
nr=n*g0*kr/(da^2+kr^2);
ni=n*g0*da/(da^2+kr^2);

%pm=2;               % max p0 of m atoms   used in standing wave added
```

```
dy=zeros(2*(m+1),1);

% w=100;                 % wx  width
% b=1;                  % Gaussian b=1 or Super-Gaussian b=12
% a=1;                  % depth scale

%dy(1)=(-1-r0*(cos(y(2*m+2)))^2)*(y(1))-(y(2))*(dc-
u0*(cos(y(2*m+2)))^2)+n;
%dy(2)=y(1)*(dc-u0*(cos(y(2*m+2)))^2)-y(2)*(1+r0*(cos(y(2*m+2)))^2);

yy1=0;
yy2=0;
for ii=1:m
% yy1=yy1-(y(1)*r0-y(2)*u0)*(cos(y(m+ii+2)))^2-nr*cos(y(m+ii+2));
% yy2=yy2-(y(1)*u0+y(2)*r0)*(cos(y(m+ii+2)))^2-ni*cos(y(m+ii+2));
yy1=yy1+(cos(y(m+ii+2)))^2;
yy2=yy2+cos(y(m+ii+2));
end

dy(1)=-y(1)-y(2)*dc-(y(1)*r0-y(2)*u0)*yy1-nr*yy2;
dy(2)=y(1)*dc-y(2)-(y(1)*u0+y(2)*r0)*yy1-ni*yy2;

%dy(3)=u0*((y(1))^2+(y(2))^2)*sin(2*(y(4)));    %p
for ii=1:m
dy(2+ii)=u0*((y(1))^2+(y(2))^2-0.5)*sin(2*(y(m+2+ii)))-2*(nr*y(2)-
ni*y(1))*sin(y(m+2+ii));               %p
%dy(2+ii)=u0*((y(1))^2+(y(2))^2)*sin(2*(y(m+2+ii)))-
a*b/w^(2*b)*pm^2*y(m+ii+2)^(2*b-1)*exp(-(y(m+ii+2)/w )^(2*b));    %add
the Gaussian mirror
%dy(2+ii)=u0*((y(1))^2+(y(2))^2)*sin(2*(y(m+2+ii)))-
a/4*pm^2*sin(y(m+2+ii)-pi/3);     % add a depth standing wave  xk/2
phase
%dy(2+ii)=u0*((y(1))^2+(y(2))^2)*sin(2*(y(m+2+ii)))-
a/4*pm^2*sin(y(m+2+ii));     % add the a depth standing wave  xk/2
%dy(2+ii)=(u0*((y(1))^2+(y(2))^2)-a/2*pm^2)*sin(2*(y(m+2+ii)));     %
add the a depth standing wave  xk
dy(m+2+ii)=y(ii+2)/c1;  %Rb 85  %x
%dy(m+2+ii)=y(ii+2)/32;  %CN  %x
End
```

Appendix B: Program of statistical model

```
C=================================================================
C  CCNSGCVTUN.F on 18/Jun/2008  using UN as U and N
C  This programme is test for the mothod of Boltzmann Equation and
C  discrete model. In this test, we calculate long time results.
C  An SG potential with waist wx and depth ga (hk) is added in this
C  model to enhance cooling effect
C  Fortran
C=================================================================
      IMPLICIT NONE
      INTEGER II,NX,NV,NT,NG,JJ,TT,KK,MM,NR,IIFALL
      INTEGER I,J,M,JS,JS0,I0,NN,IW,NSN,NXX
      INTEGER CNN,neven,nodd,tistart,tiend,avI
      INTEGER VN,XN,OUTVL,OUTVZ,OUTXL,OUTXZ
      INTEGER RN1,RN2,RN3,RN4,RN5,RN6,RN7,RN8
      PARAMETER (NX=1024,NV=2048)
      PARAMETER (NR=2,M=2000000,I0=0,JS0=200)
      PARAMETER (IW=21*NR+28)
      REAL*8 DT,TN,MTEM,PI,SI,PTEM,HTEM,VLI,TEMPER,realtime
      REAL*8 FS(0:NV-1,0:NX-1),FE(0:NV-1,0:NX-1),EX(0:NX-1)
      REAL*8 FORCE1(0:NX-1),FORCE2(0:NX-1),NAU,NPM
      REAL*8 L0,L1,XSCAL(0:NX-1),VSCAL(0:NV-1)
      DOUBLE PRECISION U,R,DC,P,T,T0,DH,au,g0,da,kr,conc,ga,wx
      DOUBLE PRECISION PM,PR,TOL,TEND,dw,TO,DX,DV,LIX,parat
      DOUBLE PRECISION AY(1:2),AF(1:2),AYO(1:2),FX(0:NX-1)
      DOUBLE PRECISION SA(NR),SS(NR),W(IW),AYS(NR)
      DOUBLE PRECISION eabs,app,timepm,irum,xlimit,lx
      DOUBLE PRECISION D02CJW,X01AAF,relx(0:NX-1),kx2,rtemx(0:NX-1)
      DOUBLE PRECISION xma,xmi,vma,vmi,G05CAF
      DOUBLE PRECISION xstart,xend,stdp,meanp,yy1,yy2,relxs(0:NX-1)
      DOUBLE PRECISION mdefect,peven,podd,xsumtem,xsumodd,xsumeven
      DOUBLE PRECISION wxPI,LIXPI,stdpconc,xstartPI,xendPI,tipm
      CHARACTER*8 name
      CHARACTER*2 numb
      INTRINSIC EXP,DBLE
      EXTERNAL C06FCF,C06GCF,X01AAF,G05CAF
      EXTERNAL D02CJF,D02CJX,FCN,D02CJW,FORCE,PROCESS
      COMMON /PAP/ U,R,DC,P,PM,PR,PI,conc,DT,DX,DV,NAU,NPM
      COMMON /FXSP/ FX
      COMMON /XSC/ XSCAL
      COMMON /VSC/ VSCAL
      COMMON /FORC/ FORCE1,FORCE2
      COMMON /yy/ yy1,yy2
      COMMON /GU/ ga,wx

      PI=X01AAF(0.0D0)
      lx=4.0D0*PI
      DX=lx/DBLE(NX)
      DV=0.1D0
```

```
      DT=0.1D0
      DH=SQRT(DT)
      NT=M
      RN1=5000
      RN2=10000
      RN3=20000
      RN4=50000
      RN5=100000
      RN6=300000
      RN7=500000
      RN8=1000000

C=====================================================================
C  Define the parameter of cavity model
g0,r(kr),da,U,R,DC,P(Pump),PR(effective
C  pump real), PM(image),conc(recoil parameter, for CN is 32), au(
C  recoil direction probability)
C=====================================================================
      name='CRbm6008'
      numb='11'
      U=-2.75D0*10.**(-7.)
      NAU=-165.0D0
      R=0.0D0
      DC=NAU-1.
      P=64.0D0
      PR=0.0D0
      PM=-5.0D0*P*10.**(-6.)
      NPM=-3000.0D0*P
      conc=100.0D0
      au=0.4D0
      ga=100.0D0
      wx=1.6*PI
      LIX=1.9*PI
      VLI=100.0D0
      parat=0.48D0
      TOL=10.0D0**(-12)
      meanp=0.0D0
c     stdp=SQRT(stdpconc*conc)
      stdp=30.0D0
      xstart=-PI
      xend=PI
      T=0.0D0
C     realtime=T*timepm
      IIFALL=0

      OPEN(9,FILE=name//'sgNUcd'//numb//'.txt',STATUS='unknown')
      WRITE(9,*) 'name, numb=',name,',',numb
      WRITE(9,*) 'U0=',U
      WRITE(9,*) 'U0N=',NAU
      WRITE(9,*) 'Pu=',P
      WRITE(9,*) 'PM=',PM
      WRITE(9,*) 'PR=',PR
      WRITE(9,*) 'NPM=',NPM
      WRITE(9,*) 'conc=',conc
      WRITE(9,*) 'au=',au
      WRITE(9,*) 'VLI=',VLI
      WRITE(9,*) 'ga=',ga
      WRITE(9,*) 'wx=',wxPI,'*PI=',wx
      WRITE(9,*) 'LIX=',LIXPI,'*PI=',LIX
      WRITE(9,*) 'meanp=',meanp
      WRITE(9,*) 'stdp=SQRT(',stdpconc,'*conc)=',stdp
```

```
      WRITE(9,*) 'xstart=',xstartPI,'*PI=',xstart
      WRITE(9,*) 'xend=',xendPI,'*PI=',xend
c     WRITE(9,*) 'timepm=1/',tipm,'=',timepm
      WRITE(9,*) 'RN1=',RN1,' RN2=',RN2,' RN3=',RN3,' RN4=',RN4
      WRITE(9,*) 'RN5=',RN5,' RN6=',RN6,' RN7=',RN7,' RN8=',RN8
      WRITE(9,*) 'lx=',lx,'  DX=',DX,'  NX=',NX,'  DV=',DV,'  NV=',NV
     *  ,'  DT=',DT
      CLOSE(9)

      DO 30 II=0,NX-1
      XSCAL(II)=DBLE(II-NX/2)*DX
30    CONTINUE
      DO 31 II=0,NV-1
      VSCAL(II)=DBLE(II-NV/2)*DV
31    CONTINUE

c     CALL G05ZAF('O')
c     CALL G05CBF(0)
c     CALL G05FDF(meanp,stdp,NA,rap)
c     CALL G05FAF(xstart,xend,NA,rax)

C=====================================================
C  INITIAL DISTRIBUTION FUNCTION
C=====================================================
c     OUTVL=0
c     OUTVZ=0
c     OUTXL=0
c     OUTXZ=0
c     DO 35 JJ=0,NV-1
c     DO 36 II=0,NX-1
c     FS(JJ,II)=0.0D0
c36   CONTINUE
c35   CONTINUE
c     DO 39 II=0,NA-1
c     PTEM=0.0D0
c     VN=NINT(rap(II)/DV)+NV/2
c     XN=NINT(rax(II)/DX)+NX/2
c     IF(VN.GT.NV-1) THEN
c     VN=NV-1
c     OUTVL=OUTVL+1
c     ENDIF
c     IF(VN.LT.0) THEN
c     VN=0
c     OUTVZ=OUTVZ+1
c     ENDIF
c     IF(XN.GT.NX-1) THEN
c     XN=NX-1
c     OUTVL=OUTVL+1
c     ENDIF
c     IF(XN.LT.0) THEN
c     XN=0
c     OUTXZ=OUTXZ+1
c     ENDIF
c     FS(VN,XN)=FS(VN,XN)+1.0/DBLE(NA)
c39   CONTINUE

c     DO 46 JJ=0,NV-1
c     DO 47 II=0,NX-1
c     IF (ABS(VSCAL(JJ)).GE.VLI .OR. ABS(XSCAL(II)).GT.LIX) THEN
cc    IF (ABS(VSCAL(JJ)).GE.VLI) THEN
c     FS(JJ,II)=0.0D0
```

```
c     ENDIF
c47   CONTINUE
c46   CONTINUE

c     OPEN(3,FILE='inVCNNU'//numb//'.txt',STATUS='unknown')
c     MTEM=0.0D0
c     TEMPER=0.0D0
c     DO 40 JJ=0,NV-1
c     PTEM=0.0D0
c     DO 41 II=0,NX-1
c           PTEM=PTEM+FS(JJ,II)
c           MTEM=MTEM+FS(JJ,II)
c41   CONTINUE
c     WRITE(3,*) VSCAL(JJ),PTEM
c     TEMPER=TEMPER+VSCAL(JJ)**2./conc*PTEM
c40   CONTINUE
c     CLOSE(3,STATUS='KEEP')

      DO 25 II=0,NX-1
      EX(II)=EXP(-((XSCAL(II)-(xend+xstart)/2.0)/PI)**100.0)
25    CONTINUE

      OPEN(3,FILE='inVCNNU'//numb//'.txt',STATUS='unknown')
      MTEM=0.0D0
      TEMPER=0.0D0
      DO 40 JJ=0,NV-1
      PTEM=0.0D0
      DO 41 II=0,NX-1
      FS(JJ,II)=EXP(-((VSCAL(JJ)-meanp)/stdp)**2.0D0/2.)/SQRT(2.*
     *  PI)/(xend-xstart)/stdp*EX(II)*DV*DX
      PTEM=PTEM+FS(JJ,II)
      MTEM=MTEM+FS(JJ,II)
41    CONTINUE
      WRITE(3,*) VSCAL(JJ),PTEM
      TEMPER=TEMPER+VSCAL(JJ)**2./conc*PTEM
40    CONTINUE
      CLOSE(3,STATUS='KEEP')

      peven=0.0D0
      podd=0.0D0
      xsumtem=0.0D0
      xsumodd=0.0D0
      xsumeven=0.0D0

      OPEN(4,FILE='inXCNNU'//numb//'.txt',STATUS='unknown')
      DO 37 II=0,NX-1
      PTEM=0.0D0
      DO 38 JJ=0,NV-1
      PTEM=PTEM+FS(JJ,II)
38    CONTINUE
      relx(II)=XSCAL(II)/PI-NINT(XSCAL(II)/PI)
      xsumtem=xsumtem+relx(II)**2.*PTEM
      relxs(II)=XSCAL(II)/PI
      rtemx(II)=ABS(ABS(MOD(relxs(II),2.))-1.)
      IF(NINT(rtemx(II)).EQ.1) THEN
      xsumeven=xsumeven+relx(II)**2.*PTEM
      peven=peven+PTEM
      ELSE
      xsumodd=xsumodd+relx(II)**2.*PTEM
      podd=podd+PTEM
      ENDIF
```

```
      WRITE(4,*) XSCAL(II),PTEM
37    CONTINUE
      CLOSE(4,STATUS='KEEP')

      IF(podd.GE.0.5D0) THEN
      mdefect=(1.-podd)*100.
      ELSE
      mdefect=podd*100.
      ENDIF

C================================================
C  CALCULATE THE FORCE ON T=0
C  AY(1) is the real part of field, AY(2) image.
C  FORCE1(NX) is the force on start time
C================================================
      OPEN(9,FILE='CNNUda'//numb//'.txt',STATUS='unknown')
      AYS(1)= 0.1D0
      AYS(2)= 0.1D0
      AY(1)=AYS(1)
      AY(2)=AYS(2)
      JS=0
      HTEM=AY(1)**2+AY(2)**2
      WRITE(9,*) realtime,HTEM,TEMPER,MTEM,xsumtem,mdefect
      CLOSE(9)
C=====================================================================
C  MAIN LOOP
C=====================================================================
      DO 100 TT=1,NT
      CALL FORCE(AY,FORCE1)

C=================================================================
C  CALCULATE THE FIELD AFTER DT using variable step ODE method
C=================================================================
      DO 50 II=0,NX-1
      PTEM=0.0D0
      DO 51 JJ=0,NV-1
      PTEM=PTEM+FS(JJ,II)
51    CONTINUE
      FX(II)=PTEM
50    CONTINUE

      DO 52 II=1,NR
      irum=G05CAF(irum)
      SS(II)=(irum-0.5D0)*2.*SQRT(3.)
      SA(II)=SS(II)*(0.5**0.5)*DH
52    CONTINUE

C     T=TO
      TEND=T+DT
C     CALL FCN(T,AY,AF)
      CALL D02CJF(T,TEND,NR,AY,FCN,TOL,'Default',D02CJX,D02CJW,
     *  W,IIFALL)

C     AYO(1)=AY(1)+SA(1)
C     AYO(2)=AY(2)+SA(2)
      AYO(1)=AY(1)
      AYO(2)=AY(2)

C=================================================================
C  CALCULATE THE TEMP FORCE2 (AFTER DT)
C=================================================================
```

```
      CALL FORCE(AYO,FORCE2)

      CALL PROCESS(FS,FE)
      MTEM=0.0D0
      TEMPER=0.0D0
      DO 120 JJ=0,NV-1
      PTEM=0.0D0
      DO 121 II=0,NX-1
      IF (ABS(VSCAL(JJ)).LT.VLI .AND. ABS(XSCAL(II)).LE.LIX) THEN
      FS(JJ,II)=FE(JJ,II)
      ELSE
      FS(JJ,II)=0.0D0
      ENDIF
      PTEM=PTEM+FS(JJ,II)
      MTEM=MTEM+FS(JJ,II)
121   CONTINUE
      TEMPER=TEMPER+VSCAL(JJ)**2./conc*PTEM
120   CONTINUE

        JS=JS+1
        IF(JS.EQ.JS0) THEN
      peven=0.0D0
      podd=0.0D0
      xsumtem=0.0D0
      xsumodd=0.0D0
      xsumeven=0.0D0
      DO 127 II=0,NX-1
      PTEM=0.0D0
      DO 128 JJ=0,NV-1
      PTEM=PTEM+FE(JJ,II)
128   CONTINUE
      relx(II)=XSCAL(II)/PI-NINT(XSCAL(II)/PI)
      xsumtem=xsumtem+relx(II)**2.*PTEM
      relxs(II)=XSCAL(II)/PI
      rtemx(II)=ABS(ABS(MOD(relxs(II),2.))-1.)
      IF(NINT(rtemx(II)).EQ.1) THEN
      xsumeven=xsumeven+relx(II)**2.*PTEM
      peven=peven+PTEM
      ELSE
      xsumodd=xsumodd+relx(II)**2.*PTEM
      podd=podd+PTEM
      ENDIF
127   CONTINUE

      IF(podd.GE.0.5D0) THEN
      mdefect=(1.-podd)*100.
      ELSE
      mdefect=podd*100.
      ENDIF

      realtime=T*timepm
      HTEM=AYO(1)**2+AYO(2)**2
      OPEN(9,FILE='CNNUda'//numb//'.txt',STATUS='old',ACCESS=
     *  'APPEND')
      WRITE(9,*) realtime,HTEM,TEMPER,MTEM,xsumtem,mdefect
      CLOSE(9)
      JS=0
      ENDIF

      IF(TT.EQ.RN1) THEN
      OPEN(7,FILE='cnNUFX'//numb//'-1.txt',STATUS='unknown')
```

```
      DO 258 II=0,NX-1
      PTEM=0.0D0
      DO 259 JJ=0,NV-1
      PTEM=PTEM+FE(JJ,II)
259   CONTINUE
      WRITE(7,*) XSCAL(II),PTEM
258   CONTINUE
      CLOSE(7,STATUS='KEEP')

      OPEN(8,FILE='cnNUFV'//numb//'-1.txt',STATUS='unknown')
      DO 453 JJ=0,NV-1
      PTEM=0.0D0
      DO 454 II=0,NX-1
      PTEM=PTEM+FE(JJ,II)
454   CONTINUE
      WRITE(8,*) VSCAL(JJ),PTEM
453   CONTINUE
      CLOSE(8,STATUS='KEEP')
      ENDIF

      IF(TT.EQ.RN2) THEN
      OPEN(7,FILE='cnNUFX'//numb//'-2.txt',STATUS='unknown')
      DO 260 II=0,NX-1
      PTEM=0.0D0
      DO 261 JJ=0,NV-1
      PTEM=PTEM+FE(JJ,II)
261   CONTINUE
      WRITE(7,*) XSCAL(II),PTEM
260   CONTINUE
      CLOSE(7,STATUS='KEEP')
      OPEN(8,FILE='cnNUFV'//numb//'-2.txt',STATUS='unknown')
      DO 456 JJ=0,NV-1
      PTEM=0.0D0
      DO 455 II=0,NX-1
      PTEM=PTEM+FE(JJ,II)
455   CONTINUE
      WRITE(8,*) VSCAL(JJ),PTEM
456   CONTINUE
      CLOSE(8,STATUS='KEEP')
      ENDIF

      IF(TT.EQ.RN3) THEN
      OPEN(7,FILE='cnNUFX'//numb//'-3.txt',STATUS='unknown')
      DO 262 II=0,NX-1
      PTEM=0.0D0
      DO 263 JJ=0,NV-1
      PTEM=PTEM+FE(JJ,II)
263   CONTINUE
      WRITE(7,*) XSCAL(II),PTEM
262   CONTINUE
      CLOSE(7,STATUS='KEEP')

      OPEN(8,FILE='cnNUFV'//numb//'-3.txt',STATUS='unknown')
      DO 457 JJ=0,NV-1
      PTEM=0.0D0
      DO 458 II=0,NX-1
      PTEM=PTEM+FE(JJ,II)
458   CONTINUE
      WRITE(8,*) VSCAL(JJ),PTEM
457   CONTINUE
      CLOSE(8,STATUS='KEEP')
```

```
      ENDIF

      IF(TT.EQ.RN4) THEN
      OPEN(7,FILE='cnNUFX'//numb//'-4.txt',STATUS='unknown')
      DO 264 II=0,NX-1
      PTEM=0.0D0
      DO 265 JJ=0,NV-1
      PTEM=PTEM+FE(JJ,II)
265   CONTINUE
      WRITE(7,*) XSCAL(II),PTEM
264   CONTINUE
      CLOSE(7,STATUS='KEEP')

      OPEN(8,FILE='cnNUFV'//numb//'-4.txt',STATUS='unknown')
      DO 459 JJ=0,NV-1
      PTEM=0.0D0
      DO 460 II=0,NX-1
      PTEM=PTEM+FE(JJ,II)
460   CONTINUE
      WRITE(8,*) VSCAL(JJ),PTEM
459   CONTINUE
      CLOSE(8,STATUS='KEEP')
      ENDIF

      IF(TT.EQ.RN5) THEN
      OPEN(7,FILE='cnNUFX'//numb//'-5.txt',STATUS='unknown')
      DO 266 II=0,NX-1
      PTEM=0.0D0
      DO 267 JJ=0,NV-1
      PTEM=PTEM+FE(JJ,II)
267   CONTINUE
      WRITE(7,*) XSCAL(II),PTEM
266   CONTINUE
      CLOSE(7,STATUS='KEEP')

      OPEN(8,FILE='cnNUFV'//numb//'-5.txt',STATUS='unknown')
      DO 461 JJ=0,NV-1
      PTEM=0.0D0
      DO 462 II=0,NX-1
      PTEM=PTEM+FE(JJ,II)
462   CONTINUE
      WRITE(8,*) VSCAL(JJ),PTEM
461   CONTINUE
      CLOSE(8,STATUS='KEEP')
      ENDIF

      IF(TT.EQ.RN6) THEN
      OPEN(7,FILE='cnNUFX'//numb//'-6.txt',STATUS='unknown')
      DO 268 II=0,NX-1
      PTEM=0.0D0
      DO 269 JJ=0,NV-1
      PTEM=PTEM+FE(JJ,II)
269   CONTINUE
      WRITE(7,*) XSCAL(II),PTEM
268   CONTINUE
      CLOSE(7,STATUS='KEEP')

      OPEN(8,FILE='cnNUFV'//numb//'-6.txt',STATUS='unknown')
      DO 463 JJ=0,NV-1
      PTEM=0.0D0
      DO 464 II=0,NX-1
```

```
      PTEM=PTEM+FE(JJ,II)
464   CONTINUE
      WRITE(8,*) VSCAL(JJ),PTEM
463   CONTINUE
      CLOSE(8,STATUS='KEEP')
      ENDIF

      IF(TT.EQ.RN7) THEN
      OPEN(7,FILE='cnNUFX'//numb//'-7.txt',STATUS='unknown')
      DO 270 II=0,NX-1
      PTEM=0.0D0
      DO 271 JJ=0,NV-1
      PTEM=PTEM+FE(JJ,II)
271   CONTINUE
      WRITE(7,*) XSCAL(II),PTEM
270   CONTINUE
      CLOSE(7,STATUS='KEEP')

      OPEN(8,FILE='cnNUFV'//numb//'-7.txt',STATUS='unknown')
      DO 465 JJ=0,NV-1
      PTEM=0.0D0
      DO 466 II=0,NX-1
      PTEM=PTEM+FE(JJ,II)
466   CONTINUE
      WRITE(8,*) VSCAL(JJ),PTEM
465   CONTINUE
      CLOSE(8,STATUS='KEEP')

C     OPEN(8,FILE='cnNUFXV'//numb//'-7.txt',STATUS='unknown')
C     DO 280 II=0,NX-1
C     DO 281 JJ=0,NV-1
C     WRITE(8,*) FE(JJ,II)
C281  CONTINUE
C280  CONTINUE
C     CLOSE(8,STATUS='KEEP')
      ENDIF

100   CONTINUE

      OPEN(7,FILE='CNNUFXd'//numb//'.txt',STATUS='unknown')
      DO 256 II=0,NX-1
      PTEM=0.0D0
      DO 257 JJ=0,NV-1
      PTEM=PTEM+FE(JJ,II)
257   CONTINUE
      WRITE(7,*) XSCAL(II),PTEM
256   CONTINUE
      CLOSE(7,STATUS='KEEP')

      OPEN(8,FILE='CNNUFVd'//numb//'.txt',STATUS='unknown')
      DO 451 JJ=0,NV-1
      PTEM=0.0D0
      DO 452 II=0,NX-1
      PTEM=PTEM+FE(JJ,II)
452   CONTINUE
      WRITE(8,*) VSCAL(JJ),PTEM
451   CONTINUE
      CLOSE(8,STATUS='KEEP')

c     OPEN(10,FILE='FXVdistr1411.txt',STATUS='unknown')
c     DO 456 II=0,NX-1
```

```
c     DO 457 JJ=0,NV-1
c     WRITE(10,*) FE(JJ,II)
c457  CONTINUE
c456  CONTINUE
c     CLOSE(7,STATUS='KEEP')

      END

C=====================================================================
C       Ordinary differential equations (ODE)
C       dAY(i)/dt=AF(i)=.....................
        SUBROUTINE FCN(XXX,AY,AF)
      IMPLICIT NONE
        INTEGER  III,NR,NX
      PARAMETER (NX=1024)
      COMMON /PAP/ U,R,DC,P,PM,PR,PI,conc,DT,DX,DV,NAU,NPM
      DOUBLE PRECISION U,R,DC,P,PM,PR,PI,conc,DX,DV,XSCAL(0:NX-1),NAU
      DOUBLE PRECISION XXX,AY(1:2),AF(1:2),yy1,yy2,FX(0:NX-1),DT,NPM
      COMMON /FXSP/ FX
      COMMON /XSC/ XSCAL
      COMMON /yy/ yy1,yy2

      yy1=0.0D0
      yy2=0.0D0

      DO 180 III=0,NX-1
c     yy1=yy1+FX(III)*DBLE(NAA)*DX*DV*DCOS(XSCAL(III))**2.
c     yy2=yy2+FX(III)*DBLE(NAA)*DX*DV*DCOS(XSCAL(III))
      yy1=yy1+FX(III)*DCOS(XSCAL(III))**2.
      yy2=yy2+FX(III)*DCOS(XSCAL(III))
180   CONTINUE

      AF(1)= -AY(1)-AY(2)*DC+AY(2)*NAU*yy1
      AF(2)= AY(1)*DC-AY(2)-AY(1)*NAU*yy1-NPM*yy2

        RETURN
        END

C=====================================================================
C       the dipole force
C=====================================================================
        SUBROUTINE FORCE(AY,FO)
      IMPLICIT NONE
      INTEGER III,NX
      PARAMETER (NX=1024)
      COMMON /PAP/ U,R,DC,P,PM,PR,PI,conc,DT,DX,DV,NAU,NPM
      DOUBLE PRECISION U,R,DC,P,PM,PR,PI,conc,DT,DX,DV,ga,wx
      DOUBLE PRECISION AY(1:2),XSCAL(0:NX-1),FO(0:NX-1),NAU,NPM
      COMMON /XSC/ XSCAL
      COMMON /GU/ ga,wx

      DO 160 III=0,NX-1
        FO(III)= U*(AY(1)**2.+AY(2)**2.-0.5)*DSIN(2.*XSCAL(III))
     *  -2.*(PR*AY(2)-PM*AY(1))*DSIN(XSCAL(III))-ga*12.*XSCAL(III)*
     *  *23./(wx**24.)*EXP(-(XSCAL(III)/wx)**24.)
160   CONTINUE

      RETURN
      END

C=====================================================================
```

```
C       the subroutine of process
C=================================================================
        SUBROUTINE PROCESS(FS,FE)
      IMPLICIT NONE
      INTEGER II,NX,NV,IFALL,JJ,KK,MM
      PARAMETER (NX=1024,NV=2048)
      COMMON /PAP/ U,R,DC,P,PM,PR,PI,conc,DT,DX,DV,NAU,NPM
      DOUBLE PRECISION U,R,DC,P,PM,PR,PI,conc,DX,DV,DT,G05CAF
      DOUBLE PRECISION FS(0:NV-1,0:NX-1),FE(0:NV-1,0:NX-1),NAU,NPM
      DOUBLE PRECISION YY(0:NX-1),WORK(NX),X0(0:NX-1),Y0(0:NX-1)
      REAL*8 H(0:NV-1,0:NX-1),G(0:NV-1,0:NX-1),X(0:NX-1),Y(0:NX-1)
      REAL*8 A(1:NV),B(1:NV),C(1:NV),XX(0:NX-1),XSCAL(0:NX-1)
      REAL*8 D(1:NV),BP(1:NV),DP(1:NV),MTEM,PTEM,HTEM
      REAL*8 FORCE1(0:NX-1),FORCE2(0:NX-1),VSCAL(0:NV-1),FX(0:NX-1)
      COMPLEX*16 Q
      INTRINSIC EXP,DBLE
      EXTERNAL C06FCF,C06GCF,G05CAF
      COMMON /FXSP/ FX
      COMMON /XSC/ XSCAL
      COMMON /VSC/ VSCAL
      COMMON /FORC/ FORCE1,FORCE2
C=================================================================
C  from f(x,v,t) to g(k,m,t) FFT TRANSFORM
C=================================================================
C     OPEN(114,FILE='GVdistr.txt',STATUS='unknown')

      DO 60 JJ=0,NV-1
      PTEM=0.0D0
      DO 61 II=0,NX-1
      X(II)=FS(JJ,II)
      X0(II)=X(II)
      Y(II)=0.0D0
      Y0(II)=Y(II)
61    CONTINUE

      IFALL=0

      CALL C06FCF(X,Y,NX,WORK,IFALL)

      DO 62 II=0,NX/2
      Q=CMPLX(X(II),Y(II))*CMPLX(DCOS(-PI*VSCAL(JJ)*DT*DBLE(II)/conc
     *  /(DX*DBLE(NX))),DSIN(-PI*VSCAL(JJ)*DT*DBLE(II)/conc/
     *  (DX*DBLE(NX))))
      XX(II)=DREAL(Q)
      YY(II)=DIMAG(Q)
62    CONTINUE

      DO 63 II=NX/2+1,NX-1
      Q=CMPLX(X(II),Y(II))*CMPLX(DCOS(-PI*VSCAL(JJ)*DT*DBLE(II-NX)/
     *  conc/(DX*DBLE(NX))),DSIN(-PI*VSCAL(JJ)*DT*DBLE(II-NX)/conc
     *  /(DX*DBLE(NX))))
      XX(II)=DREAL(Q)
      YY(II)=DIMAG(Q)
63    CONTINUE

      IFALL=0

      CALL C06GCF(YY,NX,IFALL)
      CALL C06FCF(XX,YY,NX,WORK,IFALL)
      CALL C06GCF(YY,NX,IFALL)
```

```
      DO 64 II=0,NX-1
      G(JJ,II)=XX(II)
      PTEM=PTEM+G(JJ,II)
64    CONTINUE

60    CONTINUE

C=====================================================================
C  THOMAS ALGRITHM
C=====================================================================

      DO 101 KK=0,NX-1
      DO 102 MM=1,NV
      A(MM)=-DT*FORCE2(KK)/DV/4.0
      C(MM)=DT*FORCE2(KK)/DV/4.0
      B(MM)=1.0D0
102   CONTINUE
      A(1)=0.0D0
      C(NV)=0.0D0
      D(1)=G(0,KK)-DT*FORCE1(KK)*G(1,KK)/DV/4.0
      DO 103 MM=2,NV-1
      D(MM)=DT*FORCE1(KK)*G(MM-2,KK)/DV/4.0+G(MM-1,KK)-DT*FORCE1(KK)
     *  *G(MM,KK)/DV/4.0
103   CONTINUE
      D(NV)=DT*FORCE1(KK)*G(NV-2,KK)/DV/4.0+G(NV-1,KK)

      BP(1)=B(1)
      DP(1)=D(1)

      DO 105 MM=2,NV
      MTEM=A(MM)/BP(MM-1)
      BP(MM)=B(MM)-(MTEM*C(MM-1))
      DP(MM)=D(MM)-(MTEM*DP(MM-1))
105   CONTINUE

      H(NV-1,KK)=DP(NV)/BP(NV)

      DO 106 MM=NV-1,1,-1
      H(MM-1,KK)=(DP(MM)-C(MM)*H(MM,KK))/BP(MM)
106   CONTINUE
101   CONTINUE

      DO 110 JJ=0,NV-1
      HTEM=0.0D0
      DO 111 II=0,NX-1
      X(II)=H(JJ,II)
      Y(II)=0.0D0
      HTEM=HTEM+H(JJ,II)
111   CONTINUE

      IFALL=0

      CALL C06FCF(X,Y,NX,WORK,IFALL)

      DO 112 II=0,NX/2
      Q=CMPLX(X(II),Y(II))*CMPLX(DCOS(-PI*VSCAL(JJ)*DT*DBLE(II)/
     *  conc/(DX*DBLE(NX))),DSIN(-PI*VSCAL(JJ)*DT*DBLE(II)/
     *  conc/(DX*DBLE(NX))))
      XX(II)=DREAL(Q)
      YY(II)=DIMAG(Q)
112   CONTINUE
```

```
      DO 113 II=NX/2+1,NX-1
      Q=CMPLX(X(II),Y(II))*CMPLX(DCOS(-PI*VSCAL(JJ)*DT*DBLE(II-NX)
     *  /conc/(DX*DBLE(NX))),DSIN(-PI*VSCAL(JJ)*DT*DBLE(II-NX)/conc
     *  /(DX*DBLE(NX))))
      XX(II)=DREAL(Q)
      YY(II)=DIMAG(Q)
113   CONTINUE

      IFALL=0

      CALL C06GCF(YY,NX,IFALL)
      CALL C06FCF(XX,YY,NX,WORK,IFALL)
      CALL C06GCF(YY,NX,IFALL)

      PTEM=0.0D0
      DO 114 II=0,NX-1
      FE(JJ,II)=XX(II)
c     PTEM=PTEM+FE(JJ,II)
114   CONTINUE
110   CONTINUE

      RETURN
      END
```